The Dissertation Committee for Wenbin Lu
certifies that this is the approved version of the following dissertation:

The Radiation Mechanism of Fast Radio Bursts

Committee:

Pawan Kumar, Supervisor

J. Craig Wheeler

Ramesh Narayan

Miloš Milosavljević

Neal J. Evans II

The Radiation Mechanism of Fast Radio Bursts

by

Wenbin Lu

DISSERTATION

Presented to the Faculty of the Graduate School of

The University of Texas at Austin

in Partial Fulfillment

of the Requirements

for the Degree of

DOCTOR OF PHILOSOPHY

THE UNIVERSITY OF TEXAS AT AUSTIN

May 2018

Dedicated to my parents

Limei and Zhongxiao,

and wife Chunmei.

Acknowledgments

I would like to begin by thanking my advisor, Pawan Kumar. Looking back, only now I realize that I have learned so much from the numerous discussions over the blackboard in his office. I am grateful that I was given room to figure things out by myself, but Pawan was always there when I needed help. Although most of the ideas flying around were killed, I had very satisfactory feeling when, after a long while of back-and-forth debate, the physical arguments eventually became clear to both of us. Pawan always taught me to identify and think about big unsolved puzzles, and he encouraged me to devote a good fraction of my time to "risky" projects with no guaranteed rewarding. He also said that good theorists must forget about their wishful thinkings and look at each possibility in an unbiased way. Besides research, Pawan was supportive in many other aspects, like a father to me. It was mostly him who made Austin feel like home to me.

Thanks to my committee members, J. Craig Wheeler, Ramesh Narayan, Miloš Milosavljević, and Neal J. Evans for their guidance and advice. Discussions with Craig got me interested in the physics of superluminous supernovae. Thanks to Ramesh for hosting me at the Black Hole Initiative twice, for teaching me the basics of numerical simulations, and for encouraging me to undertake the project of using infalling stars to test the black hole event horizon. I

still remember going to CfA colloquia of unfamiliar topics with Ramesh, and he told me that one does not have to know everything, just listen and learn. Thanks to Miloš for the advice on career picking and for listening to my new (mostly dumb) ideas over coffee time. Neal was a great teacher. In his comprehensive course on the interstellar medium, I learned the interactions between radiation, magnetic field, gas, and dust.

Thanks to my collaborators over the years on various projects, Julian Krolik, Patrick Crumley, Rudy Santana, Mukul Bhattacharya, and Liang Dai. They are also good friends with me. Over numerous discussions, we often had (sometimes strong) disagreements but eventually converge on the clean physical picture. Thanks to Julian for his advice on scientific writing and for taking me and my wife to lunch at Johns Hopkins University. Patrick hosted me at Princeton University and gave me valuable advice on job applications. Thanks to Rudy for always going to lunch with me, for helping me know more about Austin, and for teaching me how to drive. Thanks to Mukul for his accompany. I remember that, over the lunch break at a conference in Mexico, we walked for two and a half hours to buy a dress for my wife. Thanks to Liang for hosting me at Institute for Advanced Study and for the interesting discussions about the propagation of radio waves through a gravitational lens and a plasma.

Thanks to my friends and colleagues in the UT Astronomy Department, who have made our department a great place to think and learn. I also want to thank my friends on the Texas Rock Climbing Team and our coach John

Myrick, who helped to make the five years in Austin an enjoyable time with lots of adventures.

I gratefully acknowledge funding by the Named Continuing Fellowship, the David Alan Benfield Memorial Fellowship, and the Frank Edmonds Memorial Fellowship at UT.

The Radiation Mechanism of Fast Radio Bursts

Wenbin Lu, Ph.D.
The University of Texas at Austin, 2018

Supervisor: Pawan Kumar

Recent observations show that fast radio bursts (FRBs) are energetic but probably non-catastrophic events occurring at cosmological distances. The properties of their progenitors are largely unknown in spite of many attempts to determine them using the event rate, duration and energetics. Understanding the radiation mechanism for FRBs should provide the missing insights regarding their progenitors, which is investigated in this thesis. The high brightness temperatures ($\gtrsim 10^{35}\,\mathrm{K}$) of FRBs mean that the emission process must be coherent. Two general classes of coherent radiation mechanisms are considered — maser and the antenna mechanism. We use the observed properties of the repeater FRB 121102 to constrain the plasma conditions needed for these two mechanisms. We have looked into a wide variety of maser mechanisms operating in either vacuum or plasma and find that none of them can explain the high luminosity of FRBs without invoking unrealistic or fine-tuned plasma conditions. The most favorable mechanism is antenna curvature

emission by coherent charge bunches where the burst is powered by magnetic reconnection near the surface of a magnetar ($B \gtrsim 10^{14}\,\mathrm{G}$). We show that the plasma in the twisted magnetosphere of a magnetar may be clumpy due to two-stream instability. When magnetic reconnection occurs, the pre-existing density clumps may provide charge bunches for the antenna mechanism to operate. This model should be applicable to all FRBs that have multiple outbursts like FRB 121102.

Table of Contents

List of Figures

Chapter 1

Introduction

The first fast radio burst (FRB) was reported about a decade ago from analyzing the archival data of the Parkes radio telescope [1]. This so-called "Lorimer burst" (FRB 010724) had a peak flux density of >30 Jy at 1.4 GHz and duration of ∼5 ms. The dispersion measure $DM = 375\,\mathrm{pc\,cm^{-3}}$, i.e. the column density of free electrons integrated along the line of sight, exceeds the contribution from the interstellar medium of the Milky Way by a factor of ∼10. Thus, it was inferred that FRBs are from cosmological distances ∼Gpc with DM dominated by the extremely dilute intergalactic medium (IGM). Indeed, no Hα filaments or H II regions that could explain the large DM were found in archival images [1, 2]. Follow-up observations for ∼100 hours did not find any more bursts at this location, which implies that it may be a catastrophic event such as coalescence of relativistic objects. However, this single event offered limited clue for understanding its nature. Later on, four more FRBs with similar properties as the "Lorimer burst" were discovered by the High Time Resolution Universe survey designed to detect such short timescale radio transients [3]. Thus, FRBs are established as a new type of astrophysical phenomenon. Since then, more FRBs have been discovered and their all-sky rate is estimated to be $\sim 10^3$ to $10^4\,\mathrm{d^{-1}}$ at ~ 1 GHz above ~ 1 Jy ms [3, 4, 5, 6].

The breakthrough came when one burst originally discovered by the Arecibo telescope, FRB 121102, was found to repeat [7, 8]. It not only showed that as least this FRB is not a catastrophic event but also allowed interferometric follow-up observations to determined the precise location to an accuracy of $\sim 3\,\mathrm{mas}$ [9, 10]. The location of this FRB is found to be in the star-forming region of a low-metallicity dwarf galaxy at redshift[1] $z = 0.193$ [12, 13], similar to the environment of hydrogen-poor superluminous supernovae and long gamma-ray bursts [14].

Confirmation of cosmological origin means that the bursts from FRB 121102 are quite energetic. If the FRB sources are isotropic (the effect of anisotropy will be included later on), then the luminosity is

$$L_{\rm iso} = 4\pi D_{\rm L}^2 \mathcal{S}_\nu \Delta\nu \simeq (1.2\times10^{42}\,{\rm erg\,s^{-1}})\frac{\mathcal{S}_\nu}{\rm Jy}\left(\frac{D_{\rm L}}{\rm Gpc}\right)^2 \Delta\nu_9, \tag{1.1}$$

where $\mathcal{S}$ is the flux density, $D_{\rm L}$ is the luminosity distance and $\Delta\nu = \Delta\nu_9\,\mathrm{GHz}$ is the width of the FRB spectrum. We define the apparent brightness temperature by using the maximum transverse area of the emitting region for a non-relativistic source $\pi(ct_{\rm FRB})^2$,

$$T_{\rm B} = \frac{\mathcal{S}_\nu D_{\rm A}^2}{2\pi t_{\rm FRB}^2 \nu^2 k_{\rm B}} \simeq (1.1\times10^{35}\,{\rm K})\,\frac{\mathcal{S}_\nu}{\rm Jy}\left(\frac{D_{\rm A}}{\rm Gpc}\right)^2 t_{{\rm FRB},-3}^{-2}\nu_9^{-2}, \tag{1.2}$$

where $t_{\rm FRB} = t_{{\rm FRB},-3}\,\mathrm{ms}$ is the burst duration, $\nu = \nu_9\,\mathrm{GHz}$ is the observational frequency, $D_{\rm A}$ is the angular-diameter distance, c is the speed of light in vacuum and $k_{\rm B}$ is the Boltzmann constant. Note that eq. (1.2) is only a lower

[1] Throughout this thesis, we assume *Planck* best-fit cosmology [11] and this redshift corresponds to luminosity distance 0.97 Gpc and angular-diameter distance 0.68 Gpc.

limit on the true brightness temperature, which is unknown. If the source is moving toward the Earth at Lorentz factor Γ, then the transverse area of the emitting region may be $\pi(\Gamma c t_{\rm FRB})^2$, and in this case the true brightness temperature in the lab frame is smaller than that in eq. (1.2) by a factor of Γ^2. From Lorentz transformation, the true brightness temperature in the source's comoving frame is even smaller by another factor of Γ. Still, for any reasonable Lorentz factor, a coherent radiation mechanism is required [15].

Although the DMs of the repeating bursts from FRB 121102 stay constant with time (within the measurement error $\sim 5\,{\rm pc\,cm^{-3}}$), their fluences/fluxes vary by a factor of $\sim 10^3$ and the durations vary from $\lesssim 1\,{\rm ms}$ to $\sim 10\,{\rm ms}$ [8, 16, 17]. The isotropic equivalent energy distribution function is a single power-law with ${\rm d}N/{\rm d}E_{\rm iso} \propto E_{\rm iso}^{-1.7}$ spanning $E_{\rm iso} \in (10^{37.3}, 10^{40})\,{\rm erg}$ with no evidence of a cut-off at either the low- or high-energy end [17]. None of these events show evidence of frequency-dependent asymmetric pulse broadening as observed in Galactic pulsars [8]. Thus, their durations are likely intrinsic, if the cosmological time dilation is neglected. We note that about half of the other (so-far) non-repeating FRBs show pulse broadening with width $W \propto \nu^{\sim -4}$, which is consistent with scattering by inhomogeneities of the circumstellar/interstellar medium in the host galaxy along the line of sight [18, 19, 20, 21]. The other half do not show any evidence of scattering broadening and their durations (from $\ll 1\,{\rm ms}$ to $\sim 10\,{\rm ms}$) are consistent with being intrinsic [22].

The distances of most FRBs and hence their luminosities are unknown.

Their DMs are too large to fit in the empirical scaling laws between DM and scattering broadening for Galactic pulsars. This suggests that a large fraction of the DMs may be due to the IGM whose contribution to scattering broadening is negligible at low redshifts [23, 20]. If the IGM contributes a large portion of the DMs, one can estimate the luminosity distances of known FRBs to be $D_{\rm L} \in (1,\ 10)$ Gpc, minimum[2] peak isotropic luminosities $L_{\rm iso,min} \in (10^{42.5}, 10^{44})\,{\rm erg\,s^{-1}}$, and minimum isotropic energies $E_{\rm iso,min} \in (10^{39.5}, 10^{42})\,{\rm erg}$ (see the FRB catalog by Petroff et al. [24]). It has been shown that the energy distribution function of FRB 121102 is so far consistent with being representative of all FRBs [25]. One can also see that those (so-far) non-repeating FRBs have much larger luminosities/energies than the events from the repeater. This is most likely a selection effect because FRB 121102 has better localization and can be observed by more sensitive telescopes. Very recently, a very bright burst from FRB 121102 was discovered by the Apertif Radio Transient System [26] with peak flux density $\mathcal{S}_\nu \sim 24\,{\rm Jy}$ and duration $\Delta t_{\rm FRB} \sim 1.3\,{\rm ms}$ [27], corresponding to isotropic luminosity $L_{\rm iso} \sim 2.6\times10^{43}\,{\rm erg\,s^{-1}}$, isotropic energy $E_{\rm iso} \sim 3\times10^{40}\,{\rm erg}$ and apparent brightness temperature $T_{\rm B} \sim 3\times10^{35}\,{\rm K}$. These energetics are comparable to the (so-far) non-repeaters, further suggesting that the repeater may not be a special member of the FRB family.

In this thesis, we mainly focus on the radiation mechanism of the repeater FRB 121102, although our analysis should be applicable to other re-

[2]Note that, except for FRB 121102 whose precise location is known, the reported peak fluxes from other FRBs are only lower limits inferred based on the assumption that they occurred at the nearest beam center, see Ref. [22].

peating FRBs as well. Our general guide line is that, any FRB model must explain not only the *typical* isotropic luminosity $L_{\rm iso} \sim 10^{43}\,{\rm erg\,s^{-1}}$, energy $E_{\rm iso} \sim 10^{40}\,{\rm erg}$, apparent brightness temperature $T_{\rm B} \sim 10^{35}\,K$ and duration $t_{\rm FRB} \sim 1\,{\rm ms}$ but also the large *variations* of these quantities at a given frequency ($\sim$GHz).

This thesis is organized as follows. In §2, we discuss the constraints on the nature of FRB progenitors from the event rate, duration and energy budget. In §3, we describe two general classes of coherent emission mechanisms — maser and the antenna mechanism. The goal of this thesis is to test each of these coherent emission mechanisms and see whether they are consistent with the basic properties of FRBs. In §4, we discuss various maser mechanisms operating inside the corotating magnetosphere of a neutron star. In §5, we discuss the possibility of maser emission powered by the dissipation of a relativistic outflow at large distances from the central object. Then in §6, we discuss the antenna mechanism. Conclusions are drawn at the end of each section. In §7, we discuss the differences between the mechanisms of FRBs and pulsar radio emission. A summary of the thesis is provided in §8. Throughout the thesis, the convention $Q = 10^n Q_n$ and CGS units are used.

Chapter 2

General considerations of FRB progenitors

We first summarize the general constraints on FRB progenitor models from the event rate, duration and energy budget. Then we review various FRB progenitor models proposed in the literature. We show that these lowest-order constraints (from the event rate, duration and energy) are not sufficient to prove or falsify many of these models. Thus, one is forced to take one step further and consider the radiation mechanisms and the required plasma conditions, which will be described in later sections.

2.0.1 Event rate, duration and energy budget

There may be two classes of FRBs: repeating and non-repeating. In the following, we provide order-of-magnitude estimates of the birth rate of FRB progenitors R_0 (in unit $\mathrm{Gpc^{-3}\,yr^{-1}}$) based on the repeating or non-repeating hypothesis. The all-sky detection rate above $\sim 1\,\mathrm{Jy\,ms}$ at $\sim 1.4\,\mathrm{GHz}$ is denoted as $R_{\rm det} = 10^{3.5} R_{\rm det,3.5}\,\mathrm{d^{-1}}$. A typical FRB with isotropic energy $E_{\rm iso} \simeq 10^{40} A^{-1}\,\mathrm{erg}$ within redshift $z \simeq 0.5$ (corresponding to an IGM DM of $\simeq 400\,\mathrm{pc\,cm^{-3}}$) will have fluence $\gtrsim A^{-1}\,\mathrm{Jy\,ms}$, where $A < 1$ is the attenuation factor due to the off-center position of the FRB in the beam of detection. The comoving volume out to this redshift is $V \simeq 30\,\mathrm{Gpc^3}$. We define a beaming

factor $f_{\rm b}$ for each burst as the solid angle of the radiation beaming cone divided by 4π.

If the majority of FRBs are non-repeating, then the birth rate of FRB progenitors R_0, averaged within $z \simeq 0.5$, can be estimated by the projected all-sky detection rate

$$R_0 \simeq \frac{(1+z)R_{\rm det}}{f_{\rm b}V} \simeq 6\times10^4 \frac{R_{\rm det,3.5}}{f_{\rm b}}\,{\rm Gpc^{-3}\,yr^{-1}}. \quad (2.1)$$

Note that we have assumed that all FRBs have similar isotropic energy of $\sim 10^{40}A^{-1}\,{\rm erg}$. There are potentially more undetected FRBs with much smaller energies $E_{\rm iso} \ll 10^{40}A^{-1}\,{\rm erg}$ (as seen from the repeater FRB 121102), so eq. (2.1) should be considered as a stringent lower limit. The volumetric rate of core-collapse supernovae (CCSNe) at $z \simeq 0.5$ is $R_{\rm CCSN} \simeq 3\times10^5\,{\rm Gpc^{-3}\,yr^{-1}}$ [28]. The beaming factors of FRBs are unknown, but all known examples of coherent radio emission (e.g. pulsar radio emission) show strong beaming see Ref [29] for a review. Therefore, a small beaming factor $f_{\rm b} \ll 1$ posts severe challenge to non-repeating FRB models that are based on black holes or neutron stars [30, 31, 32, 33, 34], because the progenitors' birth rate in this case is greater or at least comparable to the rate of CCSNe. This has been pointed out by Ref. [35].

A more natural way of explaining the high observed FRB rate is that they are from repeating sources. First, it is a fine-tuned coincidence that the first (and only) FRB found by Arecibo is from a new, repeating class, while all the other ∼30 FRBs belong to a different non-repeating class. Second,

the hypothesis that all FRBs are repeating with a similar energy distribution function as FRB 121102 is so far consistent with all observations [25]. In fact, if FRB 121102 had a location error similar to those found by the Parkes telescope, the true location may fall into the low-sensitivity gaps between beams during follow-up observations and perhaps none of the subsequent bursts could have been detected. Based on the assumption of a universal energy distribution function (i.e. the same repetition rate at any given isotropic energy), Ref. [25] derived that the ratio between the birth rate of FRB progenitors and CCSN rate is in the range $(10^{-5}, 10^{-3})(\tau_{\rm active}/30\,{\rm yr})^{-1}{\rm A}^{0.7}{\rm f}_{\rm b,tot}^{-1}$ with 3σ confidence, where $\tau_{\rm active}$ is the duration of the bursting activity per progenitor, $A < 1$ is the typical off-beam-center attenuation factor for Parkes FRBs, and $f_{\rm b,tot}$ is the total beaming factor (the combined solid angle of all bursts from the same progenitor divided by 4π). We note that this rate ratio is $\sim 2 \times 10^{-4}$ for hydrogen-poor superluminous supernovae [36] and $\sim 10^{-3}$ for gamma-ray bursts (GRBs, here we have assumed a typical GRB beaming factor of 10^{-2}, [37]). Thus, FRB progenitors may be rare objects in the Universe. We note that a similar conclusion was drawn by Ref. [38] and [17].

Although the existence of a (small) population of non-repeating FRBs cannot be ruled out, they are not the main focus of this thesis. Instead, we restrict ourselves solely to the repeater FRB 121102, which has accumulated a large amount of data from extensive observations. Hereafter, unless specially noted with "non-repeating", an "FRB" means one of the bursts from the repeating source FRB 121102, and "the (FRB) progenitor" means the central

object responsible for the many bursts from FRB 121102.

In the following, we consider general constraints on the progenitor from FRB durations and the total energy reservoir. And then, for the neutron-star (NS) progenitor model, we derive constraints on the basic properties of the NS such as surface B-field strength and rotation period.

Durations of FRBs are likely controlled by the dynamical time of the system. For instance, the free-fall time near the surface of a star of radius R and mass M is $t_{\rm ff} \sim (R^3/GM)^{1/2}$, which is $\sim 0.1\,{\rm ms}$ for a NS or stellar-mass black hole (BH). On the other hand, a white dwarf has free-fall time $t_{\rm ff} \sim 10\,{\rm s}$, which is much longer than FRB durations. Even the light-crossing time for a white dwarf $R/c \sim 30(R/10^9\,{\rm cm})\,{\rm ms}$ is too long to be consistent with FRB durations. The typical timescale for a sudden accretion of a block of gas is either given by the dynamical time at the mass feeding end or the viscous time of the accretion disk. For a binary system where an object is accreting mass from the compact/non-compact companion (e.g. as in the model of [39]), the dynamical timescale of the system is much longer than FRB durations.

There is also the possibility that the emitting plasma is moving towards the observer at Lorentz factor $\Gamma \gg 1$. Such a relativistic plasma can only be launched from relativistic compact object (a NS or BH). In this case, the plasma can dissipate its free energy via internal dissipations (e.g. magnetic reconnection or internal shocks) or external shocks (when the plasma interacts with the surrounding medium). The distance between the dissipation location and the center of the progenitor star can be much larger than $ct_{\rm FRB} = 3 \times$

$10^7 t_{\rm FRB,-3}\,{\rm cm}$ by a factor of $\sim 2\Gamma^2$. We conclude that the constraint from FRB durations leave NSs or BHs[1] as the most possible progenitors.

The repetition pattern of FRB 121102 is sporadic and non-Poissonic [42]. Adding up the isotropic equivalent energy of all the bursts detected by the Arecibo campaign ($4.3\times10^{39}\,{\rm erg}$ up to Feb. 2016, [16]) and then dividing it by the total on-source time 15.8 hr, we obtain a long-time averaged luminosity

$$\langle L_{\rm frb}\rangle_{\rm Arecibo} \simeq 8\times10^{34}(f_{\rm b,tot}/f_{\rm r})\,{\rm erg\,s^{-1}}, \tag{2.2}$$

where $f_{\rm r}$ is the radio emission efficiency and $f_{\rm b,tot}$ is the total beaming factor (the combined solid angle of all bursts, including those beamed away from the Earth, divided by 4π). Note that this is only a lower limit because bursts with much higher fluences than the observed ones require a long monitoring time and bursts with much lower fluences are not observable. The energy distribution function ${\rm d}N/{\rm d}E_{\rm iso} \propto E_{\rm iso}^{-1.7}$ implies that most of the energy is near the high-energy end $E_{\rm iso,max}$, which is currently unknown. For Very Large Array (VLA) observations at 3 GHz by Ref. [17], the total burst energy is $1.9\times10^{40}\,{\rm erg}$ and the total on-source time is $\sim 60\,{\rm hr}$, so the time-averaged luminosity is $\langle L_{\rm frb}\rangle_{\rm VLA} \simeq 9\times10^{34} f_{\rm r}^{-1} f_{\rm b,tot}\,{\rm erg\,s^{-1}}$. The same analysis with the Green Bank Telescope observations by Ref. [16] gives a similar result. In the following, we take $\langle L_{\rm frb}\rangle_{\rm Arecibo}$ as a lower limit and obtain the energy reservoir

[1] If one only considers FRB durations, intermediate-mass or supermassive BHs are viable progenitors because the outflow Lorentz factor Γ may be large and the dissipation region could be much smaller than the size of the causally-connected region $\sim R/\Gamma^2$ (such as in the model of [40, 41]). Our discussion is applicable to these high-mass progenitors as well.

required to supply the bursting activity for a duration $\tau_{\rm active}$

$$E_{\rm tot} \gtrsim (7.5\times10^{43}\,{\rm erg})\ (f_{\rm b,tot}/f_{\rm r})(\tau_{\rm active}/30\,{\rm yr}). \tag{2.3}$$

If FRBs are powered by accretion onto BHs, the minimum accretion rate is $\dot{M}_{\rm min} \gtrsim \langle L_{\rm frb}\rangle_{\rm Arecibo}/c^2 \sim 10^{-13}\,(f_{\rm b,tot}/f_{\rm r})\,{\rm M_\odot\,yr^{-1}}$, which can be satisfied by many known accreting systems. If FRBs are produced by magnetic dissipation in the magnetosphere of a NS and the B-field energy is not replenished by differential rotation on timescales $\ll \tau_{\rm active}$, the minimum surface B-field strength is given by $B_*^2R_*^3/6 \gtrsim E_{\rm tot}$ ($R_*\approx 10\,{\rm km}$ being the NS radius), i.e.

$$B_* \gtrsim (2.1\times10^{13}\,{\rm G})\ (f_{\rm b,tot}/f_{\rm r})^{1/2}(\tau_{\rm active}/30\,{\rm yr})^{1/2}. \tag{2.4}$$

FRB 121102 has been repeating since discovery in 2011 [7]. To avoid the chance of coincidence, the true active duration $\tau_{\rm active}\gg 6\,{\rm yr}$. The radiation efficiency $f_{\rm r}$ and (total) beaming factor $f_{\rm b,tot}$ are poorly constrained, but these two factors tend to cancel each other in a square root term in eq. (2.4), so we obtain a rough estimate of the surface B-field strength $B_*\gtrsim$a few$\times10^{13}\,{\rm G}$ in the NS progenitor scenario.

If the NS has radius $R_*\approx 10\,{\rm km}$, surface dipole B-field near the polar cap $B_*=10^{14}B_{*,14}\,{\rm G}$, and spin period $P=0.1P_{-1}\,{\rm s}$, the spin-down luminosity is [43]

$$L_{\rm sd}=\frac{6\pi^4B_*^2R_*^6}{P^4c^3}\simeq(2.2\times10^{39}\,{\rm erg\,s^{-1}})\ B_{*,14}^2P_{-1}^{-4}, \tag{2.5}$$

where we have assumed a magnetic inclination angle of 45° (not sensitive). The spin-down timescale is given by the total rotational energy divided by the

spin-down luminosity

$$t_{\rm sd} = \frac{2\pi^2 I_*/P^2}{L_{\rm sd}} \simeq (29\,{\rm yr})\ B_{*,14}^{-2} P_{-1}^2, \tag{2.6}$$

where $I_* \approx 10^{45}\,{\rm g\,cm^2}$ is the moment of inertia of the NS. The NS was born with a supernova remnant[2], which is currently expanding. Non-detection of a time derivative of DM from the repeater over the past ~ 6 yrs means that the age of the system $t_{\rm age} \gtrsim 30\,{\rm yr}$ [45, 46]. The absence of free-free absorption of GHz waves also gives a similar constraint on the age. The fact that the spin-down time must be longer than the age means $t_{\rm sd} \gtrsim 30\,{\rm yr}$, which constrains the current rotation period[3]

$$P \gtrsim 0.1 B_{*,14}\,{\rm s}. \tag{2.7}$$

We conclude from eqs. (2.4) and (2.7) that observations are consistent with a slowly rotating high-B NS as the FRB progenitor. On the other hand, a BH with a small accretion rate $\gtrsim 10^{-13}\,{\rm M_\odot\,yr^{-1}}$ is also possible.

2.0.2 No easy answer to the progenitor puzzle

From §2.1, we see that NS or BH progenitors can comfortably meet the requirements of short durations and relatively small energy budget. The

[2]If the NS is born in a "dark" stellar collapse without a supernova ejecta (e.g. [44]), then the constraint on the age is weaker $t_{\rm age} \gtrsim 6\,{\rm yr}$ and hence the lower limit on the spin period in eq. (2.7) will be weaker by a factor of $\sim$2.

[3]If the radiation has beaming angle $\Delta\theta$ and the beaming cone corotates with the NS, then the cone sweeps across the observer's line of sight in a time $\simeq 16 P_{-1}(\Delta\theta/1\,{\rm rad})$ ms. We take the conservative limit $\Delta\theta < 1\,{\rm rad}$ and then the longest burst from FRB 121102 ($\Delta t_{\rm FRB} \sim 8\,{\rm ms}$, assuming intrinsic) gives $P \gtrsim 50\,{\rm ms}$.

low progenitor birth rate simply requires a special subgroup of NSs or BHs. Many models that satisfy these constraints have been proposed in the literature (see a review by [47]). They fall into two general categories in terms of emission locations: (1) emission within the magnetosphere of NSs such as hyper-energetic giant pulses [48, 35, 49], emission accompanying magnetar flares [50, 2, 51], emission due to B-field disturbance by infalling gas/bodies [52, 53, 54], or small-scale magnetic reconnection events near the NS surface [55]; (2) emission from a relativistic outflow which is undergoing internal dissipation or interacting with the surrounding medium at large distances from the central object [56, 40, 46, 57, 58, 41].

We see that there is no easy answer to the progenitor puzzle, if one only considers the lowest-order constraints from FRB event rate, durations and energetics.

In this thesis, we take one step further and explore all possible coherent radiation mechanisms operating in the radio wavelengths. We carefully study the plasma conditions needed to reproduce the basic observational properties of FRBs. These aspects have not been considered in most of the previous works (except [55]), mainly because no consensus has been reached over the (coherent) pulsar radio emission mechanism, despite decades of hard work and debates (see the reviews by [59, 29]). However, FRBs are drastically different from normal pulsar radio emission in that they are much brighter (by a factor of $\sim 10^{10}$) and only last for a brief period of time. As we show later in §4, §5 and §6, much more stringent constraints can be put on the source plasma of

FRBs, and therefore most of the viable options for pulsar radio emission can actually be ruled out.

Chapter 3

Possible radiation mechanisms

There are generally two classes of coherent emission mechanisms: maser and the antenna mechanism [60]. The first one requires special particle distribution function (population inversion) so that incoming radiation from certain direction has negative absorption coefficient; an example is vacuum synchrotron maser which occurs in the direction near the edge of the γ^{-1} beaming cone around the momentum vector of the emitting particle [61]. The antenna mechanism involves phase-coordinated time-dependent currents; a widely discussed case under the conditions of the NS magnetosphere is curvature emission by charge bunches of size $\lesssim$ the wavelength of emission [62].

A special case of maser mechanism is collective plasma emission (hereafter plasma maser). In this process, plasma waves are excited and exponentially amplified by certain plasma instabilities and then the energy in plasma waves is transformed into escaping modes of electromagnetic (EM) radiation. For example, the most widely discussed pulsar radio emission mechanism describes that a fast beam of particles runs into a slowly-moving plasma, and the free energy associated with the relative motion is transferred to plasma waves due to an instability, and then these waves are converted to escaping

radio modes [29]. One important point, which will be useful later, is that in any plasma maser mechanism, the energy of the observed EM radiation comes from particles' kinetic energy.

If the emission region is at radius r from the center of the progenitor, the strength of the electromagnetic fields associated with FRB radiation in the source region is

$$E_{\perp\rm EM} \simeq B_{\perp\rm EM} \geq \sqrt{\frac{L_{\rm iso}}{r^2 c}} \simeq (1.8\times10^{10}\ {\rm G}) L_{\rm iso,43}^{1/2} r_6^{-1}, \tag{3.1}$$

where "$\perp$" means the fields are perpendicular to the line of sight and we have "$>$" when the local curvature of the emitting surface is smaller than r. This EM wave is very intense in that the dimensionless non-linearity parameter

$$a_0 = \frac{eE_{\perp\rm EM}}{m_{\rm e}\omega c} \geq 5.0\times10^7 L_{\rm iso,43}^{1/2} r_6^{-1} \nu_9^{-1}, \tag{3.2}$$

where $\omega = 2\pi\nu$ is the angular frequency. This means that free electrons along the line of sight at distance $r \lesssim 5\times10^{13}$ cm from the progenitor will be accelerated to relativistic speeds. In the regime of non-linear optics $a_0 \gg 1$, particles' effective mass and hence the effective plasma frequency depend on the wave amplitude [63].

On the other hand, in the case where the EM waves are generated in (and/or propagate through) a medium with strong B-field perpendicular to the wave electric field, the acceleration due to $E_{\perp\rm EM}$ only lasts for a gyration time $\omega_{\rm B}^{-1}$ [$\omega_{\rm B} = eB/(m_{\rm e}c)$], and hence the non-linearity parameter becomes $a_0 = E_{\perp\rm EM}/B$. As long as $E_{\perp\rm EM}/B \ll 1$, the propagation characteristics of

the wave can be treated by linear approximation. This will be the base of the discussion on plasma dispersion relation in §4.2.

To make our discussion as general as possible, in the following sections, we consider NSs or BHs as viable FRB progenitors and the emitting plasma could either be within the corotating magnetosphere of a NS or a relativistic outflow launched from a NS or BH. We discuss possible maser mechanisms in §4 and §5, and then the antenna mechanism is discussed in §6.

Chapter 4

Masers inside the neutron star magnetosphere

Based on the assumption that the source plasma is confined by the B-field of a NS, we first constrain the source location and the B-field strength in the source region from energetic requirements. And then in §4.1, we show that the traditional magnetosphere of a rotating NS or magnetar cannot provide enough particle kinetic energy to power FRBs. Then, under the assumption that some explosive process injects a large amount of particle kinetic energy in the magnetosphere, we derive the basic requirements on particles' distribution function for various maser mechanisms, including plasma maser (§4.2) and masers in vacuum (§4.3). Conclusions are drawn at the end of each subsection.

We assume that the B-field configuration at radius $r \gg R_*$ is dipolar

$$B(r) = B_*(r/R_*)^{-3} \simeq (10^{11}\ \mathrm{G}) B_{*,14} r_7^{-3}. \tag{4.1}$$

The energy density of the FRB EM waves at a distance r from the center of the star is given by

$$U_{\rm EM} = \frac{L_{\rm iso}}{4\pi r^2 c} \simeq (2.6 \times 10^{17}\,\mathrm{erg\,cm^{-3}})\, L_{\rm iso,43} r_7^{-2}. \tag{4.2}$$

We require that the total energy density of the source plasma to be a factor of $f_{\rm r}^{-1}$ ($f_{\rm r}$ being the radiation efficiency in the radio band) higher than $U_{\rm EM}$.

Moreover, for the external B-field to confine the plasma, the magnetic energy density $B^2/8\pi$ must exceed that of the plasma by at least a factor of $\zeta \gg 1$,

$$B(r)^2/8\pi \gtrsim \zeta U_{\rm EM}/f_{\rm r}. \tag{4.3}$$

Combining eqs. (4.1) and (4.3), we obtain

$$r \lesssim (3.5\times10^7\,{\rm cm})\, B_{*,14}^{1/2}\zeta_1^{-1/4}\left(\frac{L_{\rm iso,43}}{f_{\rm r}}\right)^{-1/4}, \tag{4.4}$$

and

$$B \gtrsim (2.4\times10^9\,{\rm G})\, B_{*,14}^{-1/2}\zeta_1^{3/4}\left(\frac{L_{\rm iso,43}}{f_{\rm r}}\right)^{3/4}, \tag{4.5}$$

where we have used $\zeta_1 = \zeta/10$. Therefore, the radiation process occurs much below the light cylinder $R_{\rm LC} = Pc/2\pi \simeq 4.8\times10^8 P_{-1}\,{\rm cm}$ and the emission region has a strong B-field $B \gtrsim 10^9\,{\rm G}$. The transverse momentum of an electron or positron is lost in a short time $\sim 10^{-9}\gamma(B/10^9\,{\rm G})^{-2}\,{\rm s}$ due to cyclotron/synchrotron cooling (γ being the Lorentz factor), so particles are forced to stay at the lowest Landau level and only move along the B-field lines (unless there is a mechanism that keeps exciting them to higher Landau levels). For later usage, we also note that the ratio between cyclotron frequency $\omega_{\rm B} \equiv eB/m_{\rm e}c$ and the frequency of the observed radio waves $\omega \equiv 2\pi\nu$ has a lower limit

$$\omega_{\rm B}/\omega \gtrsim 2.2\times10^6\,\nu_9^{-1}B_{*,14}^{-1/2}\zeta_1^{3/4}\left(\frac{L_{\rm iso,43}}{f_{\rm r}}\right)^{3/4}. \tag{4.6}$$

4.0.1 Explosive particle injection needed for masers

In this subsection, we show that, in the conventional picture, particles above the polar cap of a rotating NS [64, 65, 62, 66, 67] or in the twisted magne-

tosphere of a magnetar [68] do not have enough kinetic energy to power FRBs. Some explosive particle injection process is needed for any maser mechanism powered by particles' kinetic energy.

Throughout this thesis, particle number density is often expressed as a multiplication factor $\mathcal{M}$ times the Goldreich-Julian (G-J) density [64]

$$n_{\rm GJ} \simeq \frac{B}{ecP} \simeq (6.9 \times 10^{13}\,{\rm cm}^{-3})\, B_{14} P_{-1}^{-1}. \tag{4.7}$$

When the density of the pair plasma falls below either the G-J density or the minimum density required to support the induced current $J = (c/4\pi)|\nabla \times \boldsymbol{B}|$, the region becomes charge starved and the E-field parallel to the B-field cannot be screened. Thus, particles are accelerated by the unscreened E-field to high Lorentz factors and then produce γ-rays which may turn into pairs via B-assisted photon decay $\gamma + {\rm B} \rightarrow {\rm e}^+ + {\rm e}^-$ [69]. When the B-field strength is super-critical $B \gtrsim B_{\rm QED} = 4.4 \times 10^{13}\,{\rm G}$, some γ photons with polarization perpendicular to the osculating plane of the B-field may split into two photons (with polarization parallel to the osculating plane) before the B-assisted photon decay. The energies of the two daughter photons are only slightly smaller (by a factor of $\sim$2), so they may still turn into pairs. Two photon annihilation process $\gamma + \gamma \rightarrow e^+ + e^-$ may also occur but is subdominant [70]. The secondary ${\rm e}^\pm$ pairs will produce more γ-rays and then more pairs. Such pair cascade proceeds until the number density of pairs is high enough to screen the parallel E-field.

Above the polar cap of a rotating NS, the initial γ-rays are produced

by curvature radiation [62]. The maximum kinetic energy density of the plasma (before or after pair cascade) in the open field line region is given by $\gamma_{\rm th} n_{\rm GJ} m_{\rm e} c^2$, where $\gamma_{\rm th}$ is the threshold Lorentz factor for the initiation of pair cascade. This is because primary particles accelerated by the parallel E-field to $\gamma \gtrsim \gamma_{\rm th}$ will produce copious pairs, and then the parallel E-field is quickly shielded when the number density reaches $n \gtrsim n_{\rm GJ}$. Below, we provide a rough estimate of the threshold Lorentz factor $\gamma_{\rm th}$ above the polar cap, following Ref. [71].

Curvature radiation (CR) has characteristic energy

$$\frac{\epsilon_{\rm CR}}{m_{\rm e}c^2} \simeq \frac{\gamma^3 hc}{2\pi\rho m_{\rm e}c^2} = 3.9\times10^3\,\gamma_7^3\rho_7^{-1}, \tag{4.8}$$

where we have normalized the energy by the electron rest mass energy, γ is the Lorentz factor of the electron (or positron), h is the Planck constant, and ρ is the local curvature radius. The electron (or positron) is accelerated by the parallel E-field within the charge-deficit ($n \ll n_{\rm GJ}$) gap above the polar cap of the NS

$$\gamma m_{\rm e}c^2 = e\Phi_{\rm gap} \simeq 2\pi n_{\rm GJ} e^2 H^2, \tag{4.9}$$

where $\Phi_{\rm gap}$ is the voltage drop across the gap and H is the gap height. Note that, in eq. (4.9), we have assumed H to be much smaller than the size of the polar cap $\sim R_*^{3/2} R_{\rm LC}^{-1/2}$, this is because, as we will show later, $\Phi_{\rm gap}$ is much smaller than the total voltage drop across the polar cap [62]

$$\Phi_{\rm pc} \simeq 2\pi^2 R_*^3 B_*/(P^2c^2) \simeq (6.6\times10^{16}\,{\rm V})\,B_{*,14}P_{-1}^{-2}. \tag{4.10}$$

Then, γ-ray photons with energy $\epsilon_{\rm CR} \gg m_{\rm e}c^2$ will undergo B-assisted decay into pairs within a propagation length $\rho m_{\rm e}c^2/\epsilon_{\rm CR}$ (when the angle between the photon's momentum vector and the B-field becomes $\sim m_{\rm e}c^2/\epsilon_{\rm CR}$). Thus, the height of the charge-deficit gap is given by

$$H \simeq \rho m_{\rm e}c^2/\epsilon_{\rm CR} \simeq (2.6\times10^3\,{\rm cm})\,\rho_7^2\gamma_7^{-3}. \tag{4.11}$$

We combine eqs. (4.9) and (4.11) and obtain the threshold Lorentz factor

$$\gamma_{\rm th} \simeq 1.9\times10^7\,\rho_7^{4/7}(B_{*,14}/P_{-1})^{1/7}. \tag{4.12}$$

The voltage drop across the gap is $\Phi_{\rm gap} = \gamma_{\rm th}m_{\rm e}c^2/e \simeq (1\times10^{13}\,{\rm eV})\,\rho_7^{4/7}\,(B_{*,14}/P_{-1})^{1/7} \ll \Phi_{\rm pc}$. Therefore, the maximum (instantaneous) isotropic luminosity powered by particles accelerated above the polar cap can be estimated

$$\begin{aligned} L_{\rm iso,max}^{\rm (pc)} &\simeq 4\pi R_*^2\gamma_{\rm th}n_{\rm GJ}m_{\rm e}c^3 \\ &\simeq (4.1\times10^{38}\,{\rm erg\,s^{-1}})\,\rho_7^{4/7}(B_{*,14}/P_{-1})^{8/7}. \end{aligned} \tag{4.13}$$

We note that the giant pulses from e.g. the Crab pulsar can reach an instantaneous isotropic luminosity of $\sim 10^{37}\,{\rm erg\,s^{-1}}$ [72], which is consistent with the constraints from eq. (4.13), considering that the B-field curvature radius above the polar cap may be $\rho \gtrsim 10^7\,{\rm cm}$ for a dipolar geometry. However, we see that traditional pair creation processes above the polar cap of a rotating NS cannot produce FRB isotropic luminosities $\sim 10^{43}\,{\rm erg\,s^{-1}}$.

On the other hand, the magnetosphere of a magnetar is believed to be different from normal NSs in that the evolution of the ultrastrong ($\gtrsim 10^{14}\,{\rm G}$)

B-field anchored on the active stellar crust leads to a twisted external magnetosphere with strong persistent currents [68]. For a large twist angle ~ 1 radian, the current flowing along B-field lines at radius r can be estimated

$$J = \frac{c}{4\pi}|\nabla \times \boldsymbol{B}| \sim \frac{cB}{4\pi r}, \tag{4.14}$$

which corresponds to a *minimum* plasma density

$$n_{\rm min} = J/(ec) \sim (1.7 \times 10^{16}\,{\rm cm}^{-3}) B_{14} r_6^{-1}. \tag{4.15}$$

Pair cascade is initiated by γ-rays produced by resonant inverse-Compton scattering of electrons (or positrons) off ambient X-ray photons [73]. In this case, the threshold Lorentz factor is given by the resonance condition $\gamma_{\rm th} \simeq \gamma_{\rm res}$, when the energy of X-ray photons in the electron's comoving frame equals to the Landau energy increment

$$\gamma_{\rm res}\epsilon_{\rm x} \simeq (B/B_{\rm QED}) m_{\rm e}c^2, \tag{4.16}$$

where $\epsilon_{\rm x}$ is the X-ray photon's energy in the NS frame and $B_{\rm QED} = 4.4\times10^{13}\,{\rm G}$ is the critical B-field strength. The X-ray spectra of Galactic magnetars usually show a power-law component extending beyond 10 keV, which may be due to atmospheric heating or Comptonization of low-energy thermal X-rays from the surface [74]. The mean energy of the scattered photons is

$$\begin{aligned} \frac{\epsilon_{\rm IC}}{m_{\rm e}c^2} &\simeq \gamma_{\rm res} \min\left(1, \frac{B}{B_{\rm QED}}\right) \\ &\simeq 1.2 \times 10^2 \left(\frac{\epsilon_{\rm x}}{10\,{\rm keV}}\right)^{-1} B_{14} \min\left(1, \frac{B}{B_{\rm QED}}\right). \end{aligned} \tag{4.17}$$

If $B \gtrsim B_{\rm QED}$, the scattered photons, initially at an angle $\lesssim \gamma_{\rm res}^{-1}$ wrt the B-field, undergo B-assisted decay into pairs within a propagation length[1] $\rho m_{\rm e}c^2/\epsilon_{\rm IC} \ll \rho$. In this way, the voltage drop in the corona loops above a magnetar is maintained near the $e^{\pm}$ production threshold. The maximum (instantaneous) isotropic luminosity powered by particles in these current-threading corona loops near the surface of a magnetar is

$$\begin{aligned} L_{\rm iso,max}^{\rm (magnetar)} &\sim 4\pi R_*^2 \gamma_{\rm res} n_{\rm min} m_{\rm e} c^3 \\ &\sim (6.1\times 10^{35}\,{\rm erg\,s^{-1}})\left(\frac{\epsilon_{\rm x}}{10\,{\rm keV}}\right)^{-1} B_{*,14}^2. \end{aligned} \tag{4.18}$$

We see that FRBs with $L_{\rm iso} \sim 10^{43}\,{\rm erg}^{-1}$ cannot be produced by particles' kinetic energy stored in the magnetosphere of magnetars, unless the B-field strength is unrealistically high $B_* \gtrsim 4\times 10^{17}(\epsilon_{\rm x}/10\,{\rm keV})^{1/2}\,{\rm G}$ (which means the magnetic energy is comparable to the gravitational binding energy of the NS).

We conclude that some explosive particle injection process is needed for any maser mechanism powered by particles' kinetic energy (but not for antenna mechanism powered by E-fields, as shown later in §6). We note that pairs may be injected by magnetic reconnection processes near the surface of magnetars. A catastrophic example of explosive pair production is magnetar giant flares [75], although here the magnetic fields undergo large-scale reconfiguration and the resultant plasma is highly optically thick to photons from radio up to γ-ray wavelengths.

[1] If $B \gg B_{\rm QED}$, a fraction of the photons scattered at an angle $\gg \gamma_{\rm res}^{-1}$ wrt the B-field may turn into pairs right away [73].

In the following two subsections, we discuss plasma maser (§4.2) and then masers in vacuum (§4.3), under the assumption that a large number of pairs are suddenly injected by some other process. General constraints on the particle distribution function are derived in each case.

4.0.2 Plasma maser (collective plasma emission)

We consider the situation where a beam of particles runs into a target plasma and subluminal waves are excited and then amplified due to a certain beam instability. Two instabilities are considered: cyclotron-Cherenkov (or anomalous Doppler) instability and Cherenkov instability.

In §4.1, we have shown that some explosive particle injection process is needed for any maser mechanism powered by particles' kinetic energy. Thus, we assume both the beam and target plasma to be made of electrons and positrons with number densities $n_{\rm b} = n_{\rm b-} + n_{\rm b+} \gg n_{\rm GJ}$ and $n = n_- + n_+ \gg n_{\rm GJ}$, respectively. To maintain the charge balance in the magnetosphere, we require $|n_{\rm b-} - n_{\rm b+}| \sim n_{\rm GJ}$ and $|n_- - n_+| \sim n_{\rm GJ}$.

We take the B-field to be along the $\hat{\boldsymbol{z}}$ direction ($\boldsymbol{B} = B\hat{\boldsymbol{z}}$), which points towards the observer. The (1-dimensional) distribution functions of the beam and target plasma in the NS frame are denoted as $f_{\rm b}(u_{\rm b})$ and $f(u)$, where $u_{\rm b}$ and u are 4-velocities in the $\hat{\boldsymbol{z}}$ direction and we have normalized $\int f_{\rm b} {\rm d}u_{\rm b} = \int f {\rm d}u = 1$. We assume that beam particles are moving towards the observer at relativistic speeds, thus $u_{\rm b} \gg 1$. To make our discussion as general as possible, we allow particles in the target plasma to be moving

towards ($u > 0$) or away from ($u < 0$) the observer. Particle velocities divided by speed of light are denoted as $\beta_{\rm b}$ and β and their Lorentz factors are $\gamma_{\rm b}$ and γ. Our goal is to explore the general constraints on these two distribution functions in order for plasma maser mechanism to produce FRBs.

We introduce another inertial frame (hereafter the *plasma frame*) which is moving at velocity $\beta_{\rm p}c$ (Lorentz factor $\gamma_{\rm p}$) wrt the NS frame. Note that both $\beta_{\rm p} > 0$ and $\beta_{\rm p} \leq 0$ are possible. All quantities in the plasma frame are denoted with a prime ($'$) and unprimed quantities are measured in the NS frame. We also denote the mean value of a quantity K' as $\langle K' \rangle \equiv \int K' f' {\rm d}u'$. The relative Lorentz factor $\gamma_{\rm p}$ between the two frames is defined such that the mean 4-velocity is zero $\langle u' \rangle = \langle \gamma' \beta' \rangle = 0$ in the plasma frame. The mean Lorentz factor in the plasma frame can be considered as the temperature of the plasma, so we denote $T' \equiv \langle \gamma' \rangle$. In the NS frame, a large variation of particle Lorentz factors cannot be avoided during pair creation, so the plasma is at least mildly hot ($T' \gtrsim 2$) and most likely extremely hot ($T' \gg 1$). The discussion in this subsection is applicable for both cases.

The emission is powered by the free energy associated with the *relative* motion between the two plasmas. The EM waves strongly interact and exchange energy/momentum with the target plasma during wave excitation and amplification. In the plasma frame, the incoming beam is decelerated due to the pressure of the target plasma $\sim T' n' m_{\rm e} c^2$. We define $f_{\rm r} < 1$ as the fraction of the momentum loss from the beam that goes to the momentum flux of the FRB EM waves, so we obtain $T' n' m_{\rm e} c^2 f_{\rm r} \simeq U'_{\rm EM}$, where $U'_{\rm EM}$ is the

energy density of the EM waves of the FRB in the plasma frame. Another way of understanding is that the inertia of the target plasma $\sim T' n' m_{\rm e}$ needs to be large enough to extract momentum from the beam at the rate of $U'_{\rm EM} c$. When the target plasma is moving towards the observer ($\beta_{\rm p} > 0$), we have $U'_{\rm EM} = U_{\rm EM}/\gamma_{\rm p}^2$ (where $U_{\rm EM}$ is given by eq. 4.2), which means

$$\gamma_{\rm p}^2 T' n' \simeq (3.2 \times 10^{23}\ {\rm cm}^{-3})(L_{\rm iso,43}/f_{\rm r}) r_7^{-2}. \tag{4.19}$$

When the target plasma is at rest or moving away from the observer ($\beta_{\rm p} \leq 0$), the energy density in the plasma frame is $U'_{\rm EM} = \gamma_{\rm p}^2 U_{\rm EM}$. Since the following derivations only require $f_{\rm r} < 1$, we keep using eq. (4.19) for simplicity but one should keep in mind that $f_{\rm r}$ should be substituted by $f_{\rm r}/\gamma_{\rm p}^4$ in the case of counter-streaming beam and target plasma.

The number density can be expressed in unit of the G-J density (we assume a dipolar B-field $B = B_*(r/R_*)^{-3}$ for $r \gg R_*$)

$$\mathcal{M} = \frac{\gamma_{\rm p} n'}{n_{\rm GJ}} \simeq 4.6 \times 10^{10} \frac{L_{\rm iso,43}}{\gamma_{\rm p,2} T' f_{\rm r}} B_{*,14}^{-1} P_{-1} r_7. \tag{4.20}$$

We define the non-relativistic plasma frequency $\omega'_{\rm p}$ and cyclotron frequency $\omega'_{\rm B}$ (note that $\omega'_{\rm B} = \omega_{\rm B}$) as

$$\begin{aligned} \omega'_{\rm p} &= \sqrt{\frac{4\pi e^2 n'}{m_{\rm e}}} \simeq (3.2 \times 10^{14}\,{\rm s}^{-1}) \frac{(L_{\rm iso,43}/f_{\rm r})^{1/2}}{r_7 \gamma_{\rm p,2} T'^{1/2}}, \\ \omega'_{\rm B} &= \frac{eB}{m_{\rm e} c} = (1.8 \times 10^{18}\,{\rm s}^{-1})\, B_{11}. \end{aligned} \tag{4.21}$$

We assume that the dispersion relation of the interesting wave-mode with frequency ω' and wave-vector $\boldsymbol{k}'$ is purely determined by the target plasma,

which is reasonable if $n' \gg n'_{\rm b}$. Instabilities due to the existence of the beam plasma will be considered as a perturbation. Without loss of generality, we take the wave vector to be in the x'-z' plane at an angle θ' wrt the z'-axis, i.e. $\boldsymbol{k}' = k'(\sin\theta'\hat{\boldsymbol{x}}' + \cos\theta'\hat{\boldsymbol{z}}')$. The refractive index is defined as $\widetilde{n}' \equiv k'c/\omega'$ and the phase velocity along the $\hat{\boldsymbol{z}}'$ direction is $\beta'_\phi \equiv \omega'/(k'c\cos\theta') = (\widetilde{n}'\cos\theta')^{-1}$. Only subluminal waves ($|\beta'_\phi| < 1$) can be excited, so we can define a Lorentz factor corresponding to the phase velocity $\gamma'_\phi = (1-\beta'^2_\phi)^{-1/2}$. The unprimed version of these symbols have the same meanings but in the NS frame.

To avoid severe Landau damping, we only consider waves with $\gamma'_\phi \gg T'$ (and hence $\gamma'_\phi \gg 1$, $|\beta'_\phi| \approx 1$). In the absence of the beam particles (which will be included later), the wave-number k' and frequency ω' are both real positive numbers. Lorentz transformation of the 4-wavevector $(\omega, \boldsymbol{k})$ gives

$$\omega = \gamma_{\rm p}\omega'(1+\beta_{\rm p}/\beta'_\phi), k\cos\theta c = \gamma_{\rm p}\omega'(\beta_{\rm p}+1/\beta'_\phi). \tag{4.22}$$

We are interested in waves with frequency $\nu = \omega/(2\pi) = \nu_9\,{\rm GHz}$ in the NS frame. For convenience, we introduce three more variables

$$\begin{aligned}
\Delta_1 &\equiv T'\omega'^2_{\rm p}/\omega'^2_{\rm B} \lesssim \frac{1}{2\gamma_{\rm p}^2\zeta} \ll 1, \\
\Delta_2 &\equiv \frac{\omega'^2_{\rm p}}{\mathcal{M}\omega'_{\rm B}\omega'} \simeq 2.0\times10^{-8}\,\frac{\beta'_\phi+\beta_{\rm p}}{\beta'_\phi P_{-1}\nu_9} \ll 1, \\
\Delta_3 &\equiv T'\omega'^2_{\rm p}/\omega'^2 \simeq 2.6\times10^{13}\,(\beta'_\phi+\beta_{\rm p})^2\frac{L_{\rm iso,43}/f_{\rm r}}{r_7^2\nu_9^2},
\end{aligned} \tag{4.23}$$

where $\zeta \gg 1$ is the minimum ratio between the energy density of the B-field and that of the target plasma in the NS frame (according to eqs. 4.3 and 4.19). We also note that the B-field is invariant ($B = B'$) under Lorentz

transformation parallel to $\hat{\boldsymbol{z}}$. The fact that $\Delta_1 \ll 1$ and $\Delta_2 \ll 1$ greatly simplifies the dispersion relation. In order for the wave to be in resonance with the beam particles, its phase velocity must be in nearly the same direction ($+z'$ direction) as the beam at a relativistic speed. The phase velocity of the wave must also be pointing towards the observer ($+z$ direction) in the NS frame. Thus, we require

$$\beta'_\phi > 0,\ \gamma'_\phi \gg 1,\ \beta'_\phi + \beta_\mathrm{p} > 0. \tag{4.24}$$

An upper limit of the beam (and plasma) Lorentz factor is given by the requirement that particles do not lose more than half of their energy due to curvature cooling over a propagation length ρ (curvature radius), so we have

$$\gamma_\mathrm{b,max} = \left(\frac{3m_\mathrm{e}c^2\rho}{4e^2}\right)^{1/3} \simeq 3.0\times10^6\rho_7^{1/3}. \tag{4.25}$$

We also note that two drift velocities associated with the inhomogeneities of the B-field — curvature drift and grad-B drift — are both extremely small near the NS surface. The curvature drift velocity in the NS frame is given by

$$v_\mathrm{d}/c = \frac{\gamma_\mathrm{b}m_\mathrm{e}\beta_\mathrm{b}^2c^3}{eB\rho} \simeq (1.7\times10^{-9})\,\gamma_{\mathrm{b},6}\rho_7^{-1}B_{11}^{-1}. \tag{4.26}$$

The grad-B drift is even smaller because it is proportional to the particle's transverse velocity squared $\beta_{\mathrm{b},\perp}^2$, which is suppressed by cyclotron/synchrotron cooling. Therefore, the Cherenkov-drift resonance (at $\omega-\beta_\mathrm{b}kc\cos\theta-kv_\mathrm{d}\sin\theta = 0$ in the NS frame), whose growth rate is proportional to the drift velocity [76], can be ignored. Then the dispersion relation can be calculated in the uniform B-field approximation.

We denote the normalized 1-dimensional distribution function along the B-field to be $f'_s(u')$ (and $\int f'_s \mathrm{d}u' = 1$), where $s = -$ (or $+$) means electrons (or positrons). Since $|n'_- - n'_+|/n' \simeq \mathcal{M}^{-1} \ll 1$ (see eq. 4.20), the distribution functions of electrons and positrons are nearly identical and are simply denoted as $f'(u')$ without subscript. The non-relativistic plasma frequencies of these two species are nearly the same $\omega'_{\mathrm{p},-} \approx \omega'_{\mathrm{p},+}$, so we have (following eq. 4.23)

$$\Delta_{1,-} \approx \Delta_{1,+} \approx T'\omega'^2_{\mathrm{p},\pm}/\omega'^2_{\mathrm{B},\pm} \approx \Delta_1/2. \tag{4.27}$$

Since the cyclotron frequency is an odd function of charge sign, we have

$$\sum_s \frac{\omega'^2_{\mathrm{p,s}}}{\omega'_{\mathrm{B,s}}\omega'} \approx \frac{1}{\mathcal{M}}\frac{\omega'^2_{\mathrm{p},\pm}}{\omega'_{\mathrm{B}}\omega'} \approx \Delta_{2,-} \approx \Delta_{2,+} \approx \Delta_2/2. \tag{4.28}$$

Consider a plane-wave ($\propto \mathrm{e}^{i\boldsymbol{k}'\cdot\boldsymbol{r}'-i\omega' t'}$) perturbation with wave-vector $\boldsymbol{k}' = k'(\sin\theta'\hat{\boldsymbol{x}}' + \cos\theta'\hat{\boldsymbol{z}}')$. We take the Fourier-Laplace transform of the Maxwell equations

$$\begin{aligned} &c\nabla' \times \boldsymbol{B}' = 4\pi\boldsymbol{J}' + \partial\boldsymbol{E}'/\partial t', \boldsymbol{J}' = \overleftrightarrow{\sigma}\boldsymbol{E}', \\ &c\nabla' \times \boldsymbol{E}' = -\partial\boldsymbol{B}'/\partial t', \end{aligned} \tag{4.29}$$

and then obtain

$$\boldsymbol{k}' \times [\boldsymbol{k}' \times \boldsymbol{E}'] + \omega'^2\boldsymbol{E}'/c^2 + 4\pi i\omega'\overleftrightarrow{\sigma} \cdot \boldsymbol{E}'/c^2 = 0, \tag{4.30}$$

where $\boldsymbol{E}'(\omega', \boldsymbol{k}')$ is the amplitude of the transformed E-field perturbation and the conductivity tensor $\overleftrightarrow{\sigma}(f', \omega', \boldsymbol{k}')$ depends on the distribution function f'. Making use of the refractive index $\widetilde{n}' \equiv \omega'/\boldsymbol{k}'c$ and dielectric tensor

$\overleftrightarrow{\mathcal{E}}(f', \omega', \boldsymbol{k}') \equiv \overleftrightarrow{I} + 4\pi i \overleftrightarrow{\sigma}/\omega'$, we obtain the dispersion relation in the plasma frame

$$\det\left[\widetilde{n}'^2\left(\frac{\boldsymbol{k}'\boldsymbol{k}'}{k'^2} - \overleftrightarrow{I}\right) + \overleftrightarrow{\mathcal{E}}\right] = 0, \tag{4.31}$$

where $\overleftrightarrow{I}$ is a unit tensor and we have

$$\frac{\boldsymbol{k}'\boldsymbol{k}'}{k'^2} - \overleftrightarrow{I} = \begin{bmatrix} -\cos^2\theta' & 0 & \sin\theta'\cos\theta' \\ 0 & -1 & 0 \\ \sin\theta'\cos\theta' & 0 & -\sin^2\theta' \end{bmatrix}. \tag{4.32}$$

For wave modes far away from the cyclotron resonance for *target plasma particles* ($\omega_{\rm B}/\gamma'\omega' \gg |1 - \beta'\widetilde{n}'\cos\theta'|$), the dielectric tensor is (e.g. [77, 78, 79])

$$\overleftrightarrow{\mathcal{E}} = \begin{bmatrix} 1+\chi_1 & -i\chi_2 & -\chi_4 \\ i\chi_2 & 1+\chi_1 & -i\chi_5 \\ -\chi_4 & i\chi_5 & 1-\chi_3 \end{bmatrix}, \tag{4.33}$$

where

$$\begin{aligned} &\chi_1 = \Delta_1\langle\gamma'\mu'^2\rangle/T',\ \chi_2 = -\frac{\Delta_2}{2}\langle\mu'\rangle, \\ &\chi_3 = \Delta_3\left\langle\frac{1}{\gamma'^3\mu'^2}\right\rangle/T' - \Delta_1\widetilde{n}'^2\sin^2\theta'\left\langle\gamma'\beta'^2\mu'\right\rangle/T', \\ &\chi_4 = -\Delta_1\widetilde{n}'\sin\theta'\left\langle\gamma'\beta'\mu'\right\rangle/T',\ \chi_5 = \frac{\Delta_2}{2}\widetilde{n}'\sin\theta'\left\langle\beta'\right\rangle, \\ &\mu' \equiv 1 - \beta'\widetilde{n}'\cos\theta',\ \gamma' = \sqrt{u'^2+1}, \\ &\beta' = u'/\sqrt{u'^2+1},\ \langle\ldots\rangle \equiv \int(\ldots)f'(u')\mathrm{d}u'. \end{aligned} \tag{4.34}$$

We are interested in waves with $\beta'_\phi \approx 1$ and $\gamma'_\phi \gg \langle\gamma'\rangle = T'$ (to avoid Landau damping) and hence $\mu' = 1 - \beta'/\beta'_\phi \approx 1 - \beta'$. We ignore the terms χ_2 and χ_5 associated with $\Delta_2 \sim 10^{-8}$ (eq. 4.23). Making use of $\langle\gamma'\beta'\rangle = \langle u'\rangle = 0$, $\langle\gamma'\rangle = T'$, we obtain $\langle\gamma'\mu'^2\rangle \simeq 2T'$ and $\langle\gamma'\beta'\mu'\rangle \simeq -T'$, and hence

$$\chi_1 \simeq 2\Delta_1 = (\gamma_{\rm p}^2\zeta)^{-1} \ll 1,\ \chi_4 \simeq \Delta_1\widetilde{n}'\sin\theta' \ll 1. \tag{4.35}$$

For waves with phase velocities corresponding to Lorentz factors much higher than the plasma temperature $\gamma'_\phi \gg T'$, we have $\langle \gamma'^{-3}\mu'^{-2}\rangle \simeq T'$ and hence $\chi_3 \simeq \Delta_3$. Therefore, the dispersion relation (eq. 4.31) gives two branches of solutions for the X-mode ($\boldsymbol{E}$ perpendicular to the $\boldsymbol{k}$-$\boldsymbol{B}$ plane) and Alfvén-mode ($\boldsymbol{E}$ in the $\boldsymbol{k}$-$\boldsymbol{B}$ plane)

$$\widetilde{n}'^2_{\rm X} = 1 + \chi_1 = 1 + 2\Delta_1, \text{ for X-mode,} \tag{4.36}$$

and

$$\widetilde{n}'^2_{\rm A}\cos^2\theta' \approx 1 + 2\Delta_1 + \frac{\sin^2\theta'}{\Delta_3\cos^2\theta' - 1}, \text{ for Alvén-mode.} \tag{4.37}$$

where higher order terms $\mathcal{O}(\Delta_1^2)$ have been ignored and we have made use of $\gamma'_\phi \gg 1$ and hence $\chi_1(\widetilde{n}'_{\rm A}\cos\theta' - 1) \approx \Delta_1/\gamma'^2_\phi \ll 1$.

We are interested in wave growth at either cyclotron-Cherenkov instability or Cherenkov instability when a beam runs through the target plasma. There are two possible cases:

(1) The target plasma is moving in the same direction as the beam towards the observer ($\beta_{\rm p} > 0$). This is a natural consequence of injection of a high-Lorentz factor beam (along open or closed B-field lines) which is capable of initiating pair cascades (as described in §4.1).

(2) The target plasma is moving away from the observer ($\beta_{\rm p} < 0$) in the opposite direction of the beam. This is possible if there are two independent particle injection (e.g. magnetic reconnection) regions near the NS surface where the feet of the closed B-field lines are anchored. Since Alfvén-mode

waves propagate along the B-field line and hence cannot escape [80], we only consider the excitation and growth of X-mode waves.

First, we consider the cyclotron-Cherenkov resonance at

$$\omega' - \beta'_{\rm b} k' \cos\theta' + \frac{\omega'_{\rm B}}{\gamma'_{\rm b}} = 0 \iff 1 - \beta'_{\rm b}/\beta'_{\phi} + \frac{\omega'_{\rm B}}{\gamma'_{\rm b}\omega'} = 0. \tag{4.38}$$

Such resonance can only occur when $\beta'_{\rm b} > \beta'_{\phi}$. In the limit $\gamma'_{\rm b} \gg \gamma'_{\phi} \gg 1$, we obtain

$$\omega' = 2\gamma'^2_{\phi}\omega'_{\rm B}/\gamma'_{\rm b}. \tag{4.39}$$

Making use of eq. (4.22) and $\gamma'_{\rm b} = \gamma_{\rm b}\gamma_{\rm p}(1-\beta_{\rm p})$, we obtain the beam Lorentz factor in the lab frame

$$\begin{aligned} \gamma_{\rm b} &= \frac{2(\beta'_{\phi}+\beta_{\rm p})}{1-\beta_{\rm p}}\gamma'^2_{\phi}\frac{\omega_{\rm B}}{\omega} \\ &\gtrsim 2.2\times10^6 \frac{2(\beta'_{\phi}+\beta_{\rm p})}{1-\beta_{\rm p}}\gamma'^2_{\phi}\nu_9^{-1}B_{*,14}^{-1/2}\zeta_1^{3/4}\left(\frac{L_{\rm iso,43}}{f_{\rm r}}\right)^{3/4}, \end{aligned} \tag{4.40}$$

where we have used the minimum ratio between the cyclotron frequency $\omega_{\rm B}$ and the frequency of the observed radio waves $\omega \equiv 2\pi\nu$ given by eq. (4.6). For this beam Lorentz factor to be compatible with the constraint from curvature cooling (eq. 4.25), we require

$$0 < \frac{2(\beta'_{\phi}+\beta_{\rm p})}{1-\beta_{\rm p}}\gamma'^2_{\phi} \lesssim 1. \tag{4.41}$$

This is not possible for the case (1) where both the beam and target plasma are moving towards the observer ($\beta_{\rm p} > 0, \beta'_{\phi} \approx 1$, and $\gamma'_{\phi} \gg 1$). For case (2)

where the target plasma is moving away from the observer ($\beta_{\rm p} \approx -1$), this condition gives

$$0 < \beta'_\phi + \beta_{\rm p} \lesssim \gamma'^{-2}_\phi \iff \gamma'_\phi/\sqrt{3} \lesssim \gamma_{\rm p} < \gamma'_\phi. \tag{4.42}$$

This is not possible with the X-mode, which only allows $\beta'_\phi \simeq (1-\Delta_1)/\cos\theta' \geq 1-\Delta_1$, i.e. $\gamma'_\phi \gtrsim \gamma_{\rm p}\sqrt{\zeta} \gg \gamma_{\rm p}$. Note that here $\zeta \gg 1$ is the minimum ratio of the magnetic energy density to the kinetic energy density of the plasma. Therefore, we conclude cyclotron-Cherenkov resonance condition cannot be satisfied given that the B-field needs to be strong enough to confine the beam and the target plasma.

Next, we consider the Cherenkov instability, which occurs when the velocity of the beam particles equals to the phase velocity of a certain wave. In the presence of the beam, the dielectric tensor (eq. 4.33) needs to be modified to include both the beam and the target plasma. Since the cyclotron-Cherenkov resonance of the beam particles can be ignored (it requires $\gamma_{\rm b}$ to be much greater than the upper limit given by from curvature cooling), the modification of the dielectric tensor is done by re-defining the averaged quantities as $\langle \ldots \rangle \equiv \int (\ldots)[f'(u'){\rm d}u' + f_{\rm b}(u'_{\rm b}){\rm d}u'_{\rm b}]$ and using different densities $n'_{\rm b}$ and n' in the definitions of the plasma frequencies of the beam $\omega'_{\rm pb}$ and target plasma $\omega'_{\rm p}$. Under this new definition, all the terms in the dielectric tensor involving χ_1, χ_2, χ_4, and χ_5 are real, except $\mathcal{E}_{zz}$. This is because $\chi_3 = \Delta_3 \langle \gamma'^{-3}\mu'^{-2} \rangle$ has significant imaginary part close to the Cherenkov resonance

$$\mu'_{\rm b} = 1 - \beta'_{\rm b}\widetilde{n}'_{\rm A}\cos\theta' = 0, \text{ i.e. } \beta'_{\rm b} = \beta'_\phi. \tag{4.43}$$

The beam particles only couple to the z-component of the electric field of the wave, so X-mode waves with $\boldsymbol{E} \perp \boldsymbol{B}$ cannot be excited by the beam particles due to this instability. Therefore, we are only interested in the excitation and growth of Alfvén-mode waves in case (1) where both the beam and target plasma are moving towards the observer. In this case, we have

$$\Delta_3 \simeq 1.0 \times 10^{14} \, (L_{\rm iso,43}/f_{\rm r}) r_7^{-2} \nu_9^{-1} \ggg 1, \tag{4.44}$$

and the dispersion relation of the Alfvén-mode is

$$\widetilde{n}'_{\rm A} \cos\theta' \approx 1 + \frac{\chi_1}{2} + \frac{\tan^2\theta'}{2\chi_3}. \tag{4.45}$$

The growth rate of Alfvén-mode waves excited at the Cherenkov resonance is given by the imaginary part of the complex frequency $\mathrm{Im}(\omega')$, which will be calculated below.

We only consider the beam particles near the resonance with fractional Lorentz factor spread $\Delta\gamma'_{\rm b}/\gamma'_{\rm b} \lesssim 1$. Thus, the Lorentz factor of the beam particles $\gamma'_{\rm b} \simeq \gamma'_\phi$ must be much greater than the temperature of the target plasma T'. Therefore, χ_1 and χ_4 are dominated by the target plasma and the contribution by the beam particles can be ignored ($|\mu'_{\rm b}| \lesssim \gamma'^{-2}_{\rm b}$ is very small). Since $\widetilde{n}'_{\rm A} \cos\theta' \approx 1 + \chi_1/2$ (to the first order), the resonant beam Lorentz factor is

$$\gamma'_{\rm b} \approx \chi_1^{-1/2} \gtrsim \sqrt{2\zeta}\, \gamma_{\rm p} \tag{4.46}$$

and the Lorentz factor $\gamma_{\rm b}$ in the NS frame is a factor of $2\gamma_{\rm p}$ larger. At a sufficiently large distance from the NS surface (e.g. $r \sim 10^7\,{\rm cm}$), this beam

Lorentz factor $2\sqrt{2\zeta}\gamma_{\rm p}^2$ may not violate the constraint from curvature cooling in eq. (4.25), so the growth of Cherenkov instability is possible. From eq. (4.45), the growth rate of the Cherenkov instability is

$$\mathrm{Im}(\omega') \approx \frac{k'c\cos\theta'\sin^2\theta'}{2}\frac{\mathrm{Im}(\chi_3)}{|\chi_3|^2} \lesssim \frac{k'c\cos\theta'\sin^2\theta'}{2|\chi_3|}, \tag{4.47}$$

where χ_3 has two components given by the beam and target plasma and we have $|\chi_3| \gtrsim \Delta_3 \ggg 1$. Therefore, the growth rate is negligibly small at radio wavelengths. We note that the growth of Cherenkov instability is faster at higher frequencies (up to $\omega' \sim \omega'_{\rm p}T'^{1/2}$, as pointed out by e.g. [78]). Therefore, even if the beam-plasma resonance condition is met, most of the radiation will be at much higher frequencies than ∼GHz.

To summarize the main results of this subsection, we find that it is unlikely that the plasma maser mechanism is responsible for FRBs, because of the following inconsistencies: (i) in the case where both the beam and target plasma are moving towards the observer, the cyclotron-Cherenkov resonance condition requires unrealistically high beam Lorentz factors that are inconsistent with curvature cooling; (ii) in the case where the beam and target plasma are counter-streaming, the cyclotron-Cherenkov resonance condition requires the ratio of magnetic energy density and particles' kinetic energy density to be less than unity; (iii) curvature drift velocity is negligibly small and hence Cherenkov-drift instability cannot be important for FRBs; (iv) Cherenkov instability associated with Alfvén mode has too small a growth rate to be important for FRBs. These inconsistencies basically come from the fact that

plasma maser is powered by particles' kinetic energy and the high luminosities of FRBs $L_{\rm iso} \sim 10^{43}\,{\rm erg\,s^{-1}}$ require very large particle number densities and hence plasma frequencies much higher than ∼GHz. Note that plasma maser may still be responsible for normal pulsar radio emission, which is persistent on timescales much longer than the rotation period and has much lower luminosities (by a factor of $\sim 10^{10}$).

4.0.3 Masers in vacuum

In this subsection, we consider the possibility of negative absorption in vacuum (refractive index $\tilde{n} = 1$) when particles' distribution function has population inversion. The source may be powered by either particles' kinetic energy or field energy which maintains the population inversion. Ref. [81] showed that negative curvature absorption is possible when the B-field lines have torsion. Ref. [82] proposed that vacuum synchrotron maser may be responsible for FRBs. For synchrotron maser to be in the radio band, the B-field strength should be smaller than $\sim 10^3\,{\rm G}$, which means that the source should operate far away from the NS's surface perhaps close to or beyond the light-cylinder. Nevertheless, we treat synchrotron and curvature emission in a unified way, because particles have (locally) helical trajectories and radiate similarly.

We consider a particle in gyro-motion around a uniform B-field with a helical trajectory of pitch angle α, as shown in Fig. (4.1). We use Cartesian coordinates with $\hat{\boldsymbol{x}}$ in the direction of the B-field ($\boldsymbol{B} = B\hat{\boldsymbol{x}}$) and the component

of the particle's momentum parallel to the B-field is $\boldsymbol{p}_{\parallel} = p_{\mathrm{z}}\hat{\boldsymbol{x}} = \gamma\beta_{\mathrm{x}}mc\hat{\boldsymbol{x}}$. Here, γ is the Lorentz factor, $\beta_{\mathrm{x}} = v_{\mathrm{x}}/c$, and m is the particle mass. The perpendicular momentum component is in the direction of the z-axis, i.e. $\boldsymbol{p}_{\perp} = p_{\mathrm{z}}\hat{\boldsymbol{z}} = \gamma\beta_{\mathrm{z}}mc\hat{\boldsymbol{z}}$ ($\beta_{\mathrm{z}} = v_{\mathrm{z}}/c$). The y-axis is in the direction of $\boldsymbol{p} \times \boldsymbol{B}$. Thus, the 4-momentum of the particle can be written in Cartesian (t, x, y, z) components

$$\vec{p} = \gamma mc(1,\ \beta_{\mathrm{x}},\ 0,\ \beta_{\mathrm{z}}). \tag{4.48}$$

The ratio of the transverse momentum and parallel momentum is given by the pitch angle

$$\tan\alpha = \frac{p_{\mathrm{x}}}{p_{\mathrm{z}}} = \frac{\beta_{\mathrm{x}}}{\beta_{\mathrm{z}}}, \tag{4.49}$$

so we have $\beta_{\mathrm{x}} = \beta\cos\alpha$ and $\beta_{\mathrm{z}} = \beta\sin\alpha$ (where $\beta = v/c$ is the total velocity).

We introduce another inertial frame which is moving in the $\hat{\boldsymbol{x}}$ direction at velocity $\beta_{\mathrm{x}}c$ or Lorentz factor $\gamma_{\mathrm{x}} = (1-\beta_{\mathrm{x}}^2)^{-1/2}$. The new frame is called O'-frame and all quantities measured in this frame are denoted with a prime ($'$), while the old frame is called the O-frame where all quantities are unprimed. The x′y′z′-axes in the O'-frame are parallel to the xyz-axes in the O-frame. It is easy to show that the 4-momentum of the particle in the O'-frame is $\vec{p'} = (\gamma/\gamma_{\mathrm{x}})mc(1,\ 0,\ 0,\ \gamma_{\mathrm{x}}\beta_{\mathrm{z}})$. Thus, in the O'-frame, the particle has effective mass $\gamma' m = (\gamma/\gamma_{\mathrm{x}})m$ and is in a circular orbit with velocity $\beta'_{\mathrm{z}} = \gamma_{\mathrm{x}}\beta_{\mathrm{z}}$. The radius of the circular orbit in the O'-frame is the same as the Larmor radius in the O-frame, i.e.

$$r_{\mathrm{L}} = \frac{\gamma\beta_{\mathrm{z}}mc^2}{eB} = \frac{\gamma\beta mc^2\sin\alpha}{eB}. \tag{4.50}$$

The B-field is invariant under Lorentz transformation in the $\hat{\boldsymbol{x}}$ direction.

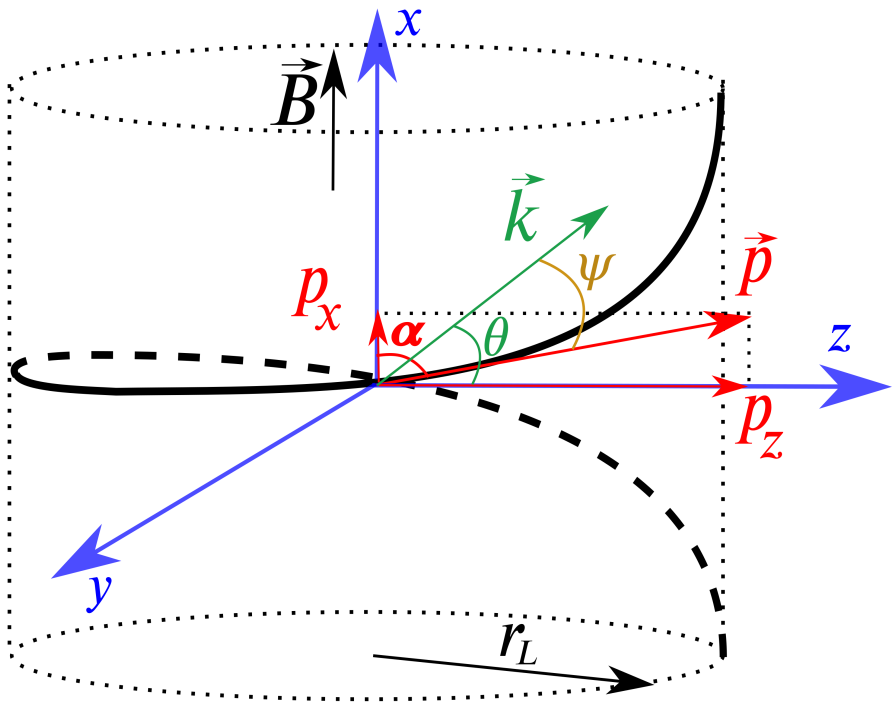

Figure 4.1: A particle in a synchrotron orbit with pitch angle α given by $\tan\alpha = p_z/p_x$. The magnetic field is uniform $\boldsymbol{B} = B\hat{\boldsymbol{x}}$ and the Larmor radius r_L is given by eq. (4.50). We are interested in the emissivity in the direction of the wave vector $\boldsymbol{k}$, which is in the x-z plane at an angle θ wrt the z-axis. The angle between the wave vector $\boldsymbol{k}$ and the particle's momentum vector $\boldsymbol{p}$ is denoted as ψ.

In the limit $\gamma' = \gamma/\gamma_{\rm x} \gg 1$, the particle's gyrophase-averaged emissivity in the O'-frame at an angle $\theta' \ll 1$ wrt the particle's momentum vector is given by (e.g. [83, 84])

$$\begin{aligned} j'_{\nu'}(\gamma', \theta') = \frac{4e^2 r_{\rm L}}{3c^2}\frac{\nu'^2}{\gamma'^4}(1+\gamma'^2\theta'^2)\times \\ \left[\gamma'^2\theta'^2 K^2_{\frac{1}{3}}(y') + (1+\gamma'^2\theta'^2)K^2_{\frac{2}{3}}(y')\right], \\ y' = \frac{\nu'}{2\nu'_{\rm c}}(1+\gamma'^2\theta'^2),\ \nu'_{\rm c} = \frac{3c}{4\pi r_{\rm L}}\gamma'^3, \end{aligned} \tag{4.51}$$

where K_a is the modified Bessel function of order a. Since $\beta \approx 1$, we have $\gamma_{\rm x} = (1-\beta^2\cos^2\alpha)^{-1/2} \approx (\sin\alpha)^{-1}$ and $\gamma' \approx \gamma\sin\alpha$. We are interested in the emissivity in the O-frame at frequency ν in the $\boldsymbol{k}$ (wavevector) direction at an angle θ wrt the z-axis in the x-z plane, and it can be obtained by Lorentz transformations

$$\begin{aligned} j_\nu(\gamma,\theta) = j'_{\nu'}(\gamma',\theta')(\nu/\nu')^2, \\ \nu = \frac{\nu'}{\gamma_{\rm x}(1-\beta_{\rm x}\sin\theta)},\ \sin\theta' = \frac{\sin\theta - \beta_{\rm x}}{1-\beta_{\rm x}\sin\theta}. \end{aligned} \tag{4.52}$$

We define the angle between the wavevector $\boldsymbol{k}$ and the particle's momentum $\boldsymbol{p}$ to be ψ, i.e.

$$\cos\psi = \boldsymbol{k}\cdot\boldsymbol{p}/kp, \tag{4.53}$$

so we have $\psi = \theta - (\pi - \alpha)$ and $\sin\theta = \sin\psi\sin\alpha + \cos\psi\cos\alpha$. We are interested in the regime $\theta' \ll 1$, $\gamma' \gg 1$ and $\psi \ll 1$, and it is straightforward to show that

$$\gamma'\theta' \approx \gamma\psi\left(1 + \frac{\cot\alpha}{2\gamma^2\psi}\right),\ \text{and}\ 1+\gamma'^2\theta'^2 \approx 1+\gamma^2\psi^2, \tag{4.54}$$

where higher order terms smaller by a factor of $\sim\gamma^{-2}$ or $\sim\psi^2$ have been ignored. We have also assumed that the pitch angle α is not much smaller than 1 (otherwise the particle is moving almost in a straight line with very little emission) but α can be arbitrarily close to 90°. Then, we make use of $\nu' \approx \nu \sin\alpha$ and calculate the emissivity in the O-frame in the $\boldsymbol{k}$ direction (at an angle $\psi \ll 1$ wrt the particle's momentum vector)

$$
\begin{aligned}
j_\nu(\gamma,\psi) &= \frac{4e^2 r_{\rm L}}{3c^2}\frac{\nu^2}{\gamma^4\sin^4\alpha}(1+\gamma^2\psi^2)\times \\
&\left[\gamma^2\psi^2\left(1+\frac{\cot\alpha}{2\gamma^2\psi}\right)^2 K^2_{\frac{1}{3}}(y) + (1+\gamma^2\psi^2)K^2_{\frac{2}{3}}(y)\right], \qquad (4.55)\\
y &= \frac{\nu}{2\nu_{\rm c}\sin^2\alpha}(1+\gamma^2\psi^2)^{3/2},\ \nu_{\rm c} = \frac{3c}{4\pi r_{\rm L}}\gamma^3.
\end{aligned}
$$

The first term [$\propto K^2_{1/3}(y)$] is polarized in the $(\hat{\boldsymbol{B}}\times\hat{\boldsymbol{k}})\times\hat{\boldsymbol{k}}$ direction and is hence called O-mode. The second term [$\propto K^2_{2/3}(y)$] is polarized in the $\hat{\boldsymbol{B}}\times\hat{\boldsymbol{k}}$ direction and is hence called X-mode. We note that the X-mode emissivity is symmetric about ψ but the O-mode is asymmetric due to the $\cot\alpha/(2\gamma^2\psi)$ term. This asymmetry vanishes at pitch angle $\alpha = 90°$ when the trajectory is confined in a plane.

We also note that the emissivity in eq. (4.55) is also valid for curvature radiation as the particle follows the infinitely strong B-field lines with or without torsion (corresponding to $\alpha \neq 90°$ and $\alpha = 90°$ respectively), as long as the Larmor radius is replaced by the curvature radius ρ. In the curvature radiation scenario (assuming infinitely strong B-field), we have $\hat{\boldsymbol{p}} \parallel \hat{\boldsymbol{B}}$, and then the polarization of the first term [$\propto K^2_{1/3}(y)$] in eq. (4.55) is still in the

$(\hat{\boldsymbol{B}} \times \hat{\boldsymbol{k}}) \times \hat{\boldsymbol{k}}$ direction and the second term in the $\hat{\boldsymbol{B}} \times \hat{\boldsymbol{k}}$ direction, as long as $\psi \neq 0$. The X-mode/O-mode characteristics are the same as in synchrotron radiation scenario.

In the limit $\gamma \gg 1$, the net absorption cross-section per particle in the $\hat{\boldsymbol{k}}$ direction at frequency ν is directly related to the emissivity and is given by ([61] and references therein)

$$\sigma_{\rm abs}(\nu, \gamma, \psi) \approx \frac{1}{2m\nu^2} \frac{1}{\gamma^2} \frac{\partial}{\partial \gamma} [\gamma^2 j_\nu(\gamma, \psi)], \tag{4.56}$$

which is valid for any classical radiating particle (as long as the correct emissivity is used). If the particles encountered by a certain light ray in the $\boldsymbol{k}$ direction have Lorentz factor distribution $N_\gamma = {\rm d}N/{\rm d}\gamma$ (in unit ${\rm cm}^{-3}$), the absorption coefficient in this direction is

$$\begin{aligned} \mu_{\rm abs} &= \frac{1}{2m\nu^2} \int_1^\infty {\rm d}\gamma \frac{N_\gamma}{\gamma^2} \frac{\partial}{\partial \gamma} [\gamma^2 j_\nu(\gamma, \psi)] \\ &= -\frac{1}{2m\nu^2} \int_1^\infty {\rm d}\gamma \frac{\partial}{\partial \gamma} \left(\frac{N_\gamma}{\gamma^2} \right) \gamma^2 j_\nu(\gamma, \psi), \end{aligned} \tag{4.57}$$

and the absorption optical depth is $\tau_{\rm abs} \sim \mu_{\rm abs} \times \ell$, where ℓ is the propagation length. Therefore, two necessary conditions for negative absorption are: (i) $\partial[\gamma^2 j_\nu(\gamma, \psi)]/\partial\gamma < 0$ at least for some γ and ψ; (ii) $\partial(\gamma^{-2} N_\gamma)/\partial\gamma > 0$ for the same γ as in condition (i). The second condition means population inversion.

In order for a particle to radiate significantly at $\sim$ GHz frequencies, we require $\nu_{\rm c} \simeq \gamma^3 c/(2\pi r_{\rm L}) \sim 1\,{\rm GHz}$, i.e. $\gamma \sim 10^2 r_{\rm L,7}^{1/3}$. For synchrotron radiation $r_{\rm L} \sim \gamma mc^2/(eB) \sim 2 \times 10^{-4}\,{\rm cm}\,\gamma_2 (m/m_{\rm e})\,(B/10^9\,{\rm G})^{-1}$. The characteristic synchrotron frequency is much higher than GHz in the NS magnetosphere

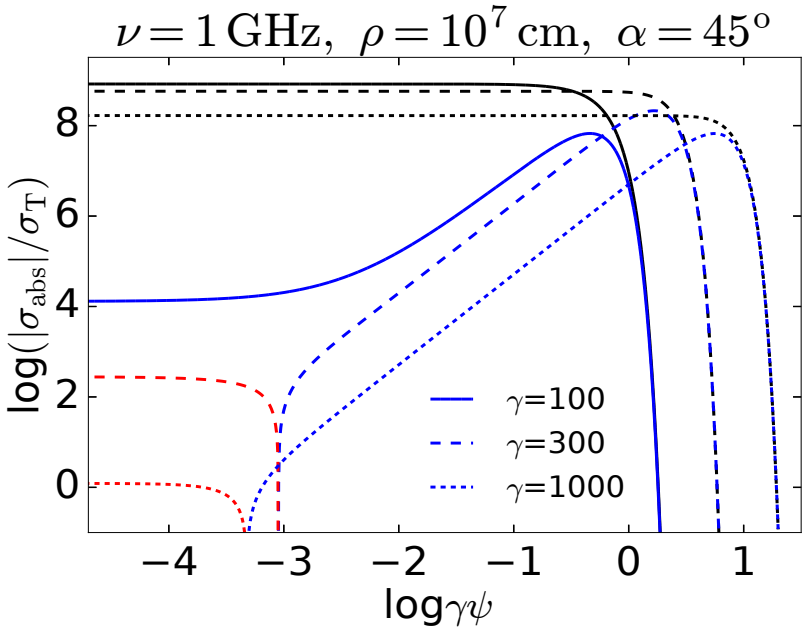

Figure 4.2: Net curvature absorption cross-section (absorption minus stimulated emission) at $\nu = 1\,\mathrm{GHz}$ for curvature radius $\rho = 10^7\,\mathrm{cm}$ and B-field torsion angle $\alpha = 45^\circ$. The blue and red curves are for the O-mode, and the black curves are for the X-mode. We can see that negative absorption (red curves) only occurs in the O-mode at very small angles ψ wrt the cone occupied by the particle's gyrating momentum vector.

near the surface, so synchrotron maser can be rule out for this case (later in §5, we will consider synchrotron maser due to dissipation of free energy in an outflow at large distances where the B-field is much weaker). In the following, we only consider curvature radiation by particles with Lorentz factors not too far from $\gamma \sim 10^2$. The detailed particle injection physics is likely complicated, so we simply *assume* that population inversion $\partial(\gamma^{-2}N_\gamma)/\partial\gamma > 0$ is *achieved and maintained* by some unknown mechanism near Lorentz factor $\gamma \sim 10^2$.

It is widely known that the net absorption cross-section for curvature

radiation is positive for any frequency or angle if the particle's trajectory is confined in a plane (corresponding to $\alpha = 90^{\rm o}$ in our notation, [85]). From eq. (4.26), we know that curvature drift velocity is very small in that the pitch angle of the helical orbit is extremely close to $90^{\rm o}$: $\cos\alpha \approx v_{\rm d}/c \lesssim 10^{-11}(B/10^9\,{\rm G})^{-1}$ (for $\gamma \sim 10^2$). The plasma is nearly charge-neutral when its density is much higher than the G-J density ($\mathcal{M} \gg 1$). Note that electrons and positrons drift in the opposite directions, so the negative absorption coefficient is further suppressed by a factor of $\mathcal{M}^{-1}$. Thus, the drift-induced curvature maser scenario [86] can be ignored. The B-field configuration in the NS magnetosphere may have torsion due to the existence of high-order multipoles, and the field line may be locally helical. As shown by Ref. [81] and in Fig. (4.2) in this thesis, a *necessary* condition for the absorption cross-section to be negative is $\psi \lesssim \cot\alpha/2\gamma^2$ for the O-mode (and the absorption is always positive for the X-mode).

To produce the observed high brightness temperatures by curvature maser, an absorption optical depth of $\tau_{\rm abs} \lesssim -30$ is needed, which means

$$\gamma N_\gamma |\sigma_{\rm abs}| \frac{\rho}{\gamma} \gtrsim 30, \text{ or } \gamma N_\gamma \gtrsim 5\times 10^{17}\,{\rm cm}^{-3}\,\frac{\gamma_2}{\rho_7}\frac{10^3\sigma_{\rm T}}{|\sigma_{\rm abs}|}. \tag{4.58}$$

Such a high density may be achieved near the NS surface ($r \sim 10^6$ cm) with particle number density a factor of $\mathcal{M} \sim 10^4$ above the G-J density (eq. 4.7).

However, it can be seen in Fig. (4.2) that, even if the absorption cross-section is negative at $\psi \lesssim (2\gamma^2)^{-1}$, it becomes positive with absolute value a factor of $\gtrsim 10^5$ greater at larger angles $\psi \sim \gamma^{-1}$. Due to the B-field curvature,

photon trajectories will unavoidably intersect with other B-field lines at larger angles before escaping, and hence torsion-induced curvature maser requires extreme fine-tuned conditions where particle number density drops by a factor of $\gtrsim 10^5$ immediately outside the maser region.

The above argument applies regardless of whether the maser is powered by particles' kinetic energy or field energy. For a kinetic-energy powered maser, an additional issue is that the minimum number density (given by eq. 4.20) must be a factor of $\mathcal{M} \gtrsim 10^{10}$ greater than G-J density. It is unclear how these particles are injected[2]. Also, we can see from Fig. (4.2) that such a high density will lead to strong positive curvature self-absorption and the radiation cannot escape.

Under the assumption that the source plasma is in the corotating magnetosphere of a NS, we conclude that neither plasma maser nor masers in vacuum are consistent with the basic properties of FRBs. In the next section, we discuss the possibility that the source plasma is inside a relativistic outflow

[2] Many theoretical studies of pair production along open field lines above the polar cap of pulsars show that $\mathcal{M}$ ranges between 10^2 and 10^5 [87, 70, 71, 88], although detailed dynamical processes of pair production under different (non-dipolar) B-field geometries still have large uncertainties. Observational studies of non-thermal emission from pulsar wind nebulae (PWN) arrive at similar conclusion [89, 90, 91]. We note that these PWN studies only focus on optical to γ-ray frequencies and that accounting for the radio emitting electrons/positrons in the Crab Nebula require $\mathcal{M} \sim 10^6$. These radio emitting particles (with Lorentz factors a few$\times 10^2$) only contributes to $\sim 1\%$ of the total energy of the nebula and their origin has been an unsolved puzzle for decades [92, 93]. These low energy particles, with their large number and long synchrotron cooling time, could be relics from the wind injection in the past (the pulsar spin-down luminosity could be much higher in the past, [94]), or acceleration of electrons from the Rayleigh-Taylor filaments penetrating the shocked wind region [95, 96].

launched from a NS or BH.

Chapter 5

Masers in an outflow with internal/external dissipation

In §4, we have discussed various maser mechanisms under the assumption that the source plasma is confined by the B-field in the corotating magnetosphere of a NS. In this section, we consider that FRBs are produced by maser mechanisms in an outflow launched from either a BH or NS. The emission is powered by the dissipation of free energy in the outflow at large distances from the central object.

For a BH progenitor, we assume that, due to sudden accretion, an outflow is launched from the inner disk near the event horizon. For a NS progenitor, we assume such an outflow is originally launched from near the stellar surface, based on the fact that most of the magnetic energy in the magnetosphere is concentrated near the surface. In both cases, dissipation of free energy in the outflow may occur due to external shocks when it runs into some dense clouds or accumulates enough circum-stellar medium in the forward shock region, or internal dissipation processes such as magnetic reconnection and collisions between shells of different speeds.

We consider that the outflow is moving towards the observer with

Lorentz factor Γ. At a distance r from the central object, the maser formation length is limited by the dynamical time and speed of light to be $\lesssim r/(2\Gamma^2)$, which constrains the FRB duration to be

$$t_{\rm FRB} \lesssim \frac{r}{2\Gamma^2 c} \simeq (3\,{\rm ms})\, r_{12}\Gamma_2^{-2}, \tag{5.1}$$

The variations of Γ and r may cause different FRB durations. Note that eq. (5.1) also takes into account (through the "$<$" sign) the possibility that the FRB source plasma is only a small local patch[1] in the causally-connected region that meets the maser condition, although the radiation efficiency and the maser amplification length are reduced when $t_{\rm FRB} \ll r/(2\Gamma^2 c)$.

In the external shock scenario, the emission radius r is roughly given by the deceleration radius $r_{\rm dec}$ (defined as where the Lorentz factor of the outflow drops by a factor of ~ 2, see eq. B.1 in Appendix B), and the duration is roughly given by $t_{\rm FRB} \sim r_{\rm dec}/(2\Gamma^2 c)$. In Appendix B, we consider the dynamics of two consecutive outflows and show that the second outflow should have a much longer deceleration time than the first one (because it propagates

[1]Ref. [40] proposed that FRBs may be produced by modulational instability induced cavitons under strong plasma turbulence during the interaction of a relativistic lepton beam and a target plasma. In the astrophysical context, they consider electrons and positrons in a relativistic leptonic jet *passing through* a cloud of size $R_{\rm c} \simeq \Gamma^2 c t_{\rm FRB} \simeq (3\times10^{13}\,{\rm cm})\,\Gamma_3^2 t_{\rm FRB,-3}$, which could be much smaller than the causally-connected region of the jet at large distances from the central engine. The frequency of the escaping radiation is near (but above) the plasma frequency of the cloud. However, the dynamics of the jet-cloud interaction is different from the laboratory beam-plasma interaction they referred to (e.g. [97]), because astrophysical plasmas are magnetized and particles' Larmor radii are many orders magnitude smaller than the cloud size. Therefore, collisionless shocks form and a contact discontinuity at the two-fluid interface prevents particles in the jet (or "beam") from penetrating through the cloud (or "plasma").

inside the cavity opened by the first one). This is in contradiction with the observation that two consecutive FRBs separated by $\sim 40\,\mathrm{ms}$ have very similar durations ($\sim 2\,\mathrm{ms}$, [98]).

Still, FRBs could be powered by internal dissipations in the outflow due to e.g. magnetic reconnection or collisions between different ejected shells. In the following two subsections, we discuss the physical conditions required to produce FRBs by synchrotron maser mechanism in vacuum [82] in §5.1 and in plasma [57] in §5.2. In our general discussion, we assume that, after the onset of internal dissipation (e.g. propagation of a shock front or magnetic reconnection trigger), particles have random gyration phases.

We also note that bunching in the gyration phase can occur in the case of quasi-perpendicular shocks at high magnetization, as a result of coherent reflection of (cold) upstream particles by the shock-compressed B-field [99, 100, 101]. In this situation, coherent gyration of incoming particles generates an X-mode EM wave precursor ahead of the main shock near the gyrofrequency. We discuss this possibility in §5.3.

5.0.1 Synchrotron maser in vacuum

Based on eqs. (4.55) and (4.56), we calculate the single-particle synchrotron absorption cross-section for a given frequency ν at an arbitrary angle ψ away from the particle's momentum vector. In Fig. (5.1) we show one case where an electron is in a helical synchrotron orbit with pitch angle $\alpha = 45^{\rm o}$ in a uniform B-field $B = 0.03\,\mathrm{G}$. We see that vacuum synchrotron maser is possible

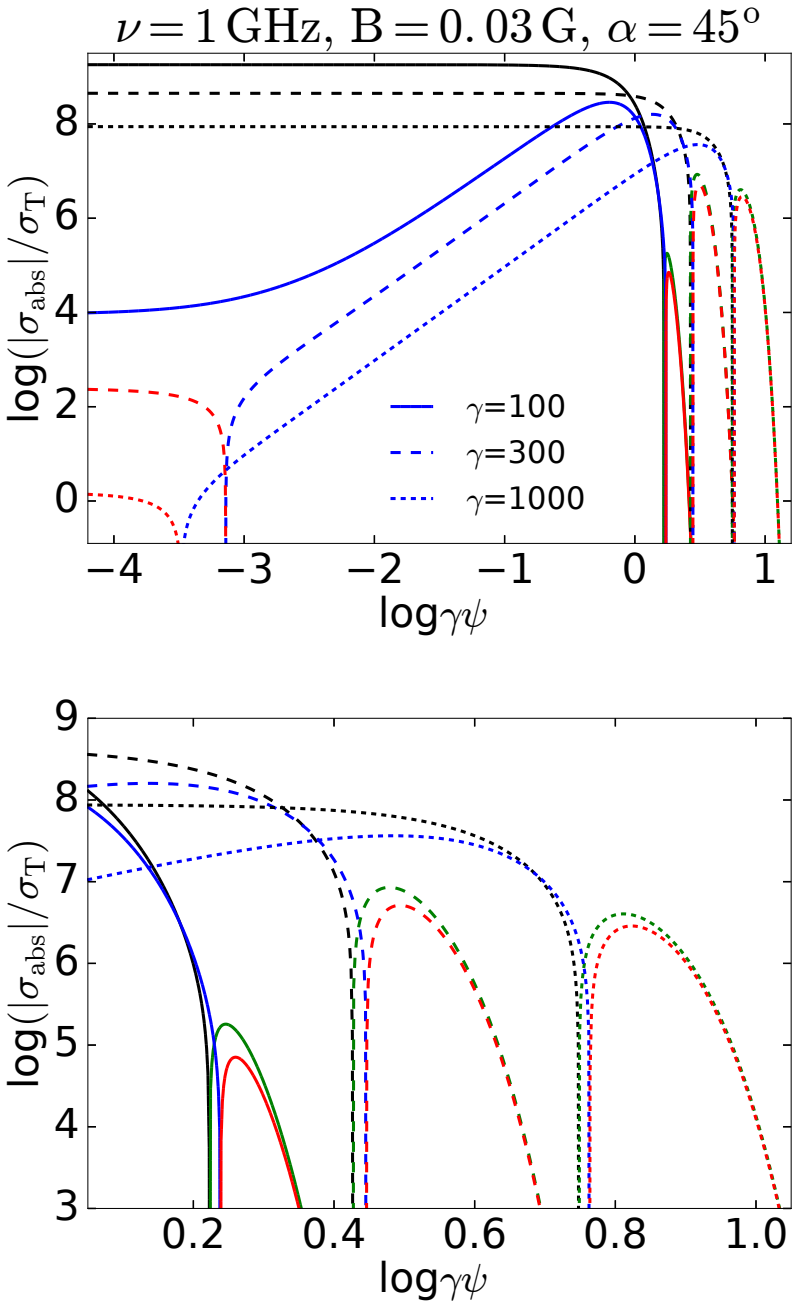

Figure 5.1: *Upper Panel:* Net synchrotron absorption cross-section (absorption minus stimulated emission) at frequency $\nu = 1\,\mathrm{GHz}$ for an electron moving in a uniform B-field $B = 0.03\,\mathrm{G}$ with pitch angle $\alpha = 45^{\mathrm{o}}$. The blue and red curves are for the O-mode, and the black and green curves are for the X-mode. The cross-sections are negative for the red and green curves. The angle between the line of sight and the electron's momentum vector is denoted as ψ. *Lower Panel:* Zoom-in of the negative cross-section regions immediately outside the γ^{-1} beaming cone.

because the absorption cross-section is negative at angles $\psi \gtrsim$a few$\times\gamma^{-1}$ for both O-mode and X-mode. However, the absorption cross-section at smaller angles on the order of γ^{-1} is positive with a much larger absolute value. There is also a very narrow negative absorption region at $\psi \lesssim \gamma^{-2}$ for the O-mode if the pitch angle $\alpha \neq 90^{\rm o}$, but the cross-section is very small.

We can see that, other than population inversion $\partial(N_\gamma/\gamma^2)/\partial\gamma > 0$, vacuum synchrotron maser requires the following two extra conditions: (i) the B-field is nearly uniform to within an angle of $\lesssim \gamma^{-1}$; (ii) particles' pitch angle distribution is narrowly peaked with spread $\Delta\alpha \lesssim \gamma^{-1}$, where γ is the typical Lorentz factor of the radiating particles in the comoving frame of the source plasma. The maximum efficiency of vacuum synchrotron maser is $\sim \gamma^{-1}$ because particles' pitch angles are not allowed to change by more than $\sim \gamma^{-1}$ as they cool.

Keeping these points in mind, we consider the emitting plasma to be in a relativistic outflow moving towards the observer with arbitrary Lorentz factor Γ. For electrons with Lorentz factor γ' in the comoving frame, the synchrotron frequency in the observer's frame is

$$\nu \simeq \Gamma\gamma'^2\nu'_{\rm B}\sin\alpha', \tag{5.2}$$

where $\nu'_{\rm B} = eB'/(2\pi m_{\rm e}c)$ is the cyclotron frequency, α' is the pitch angle, and B' is the B-field strength in the plasma comoving frame. The outflow kinetic power must exceed the FRB luminosity $L_{\rm iso}$, so we have

$$4\pi r^2(B'^2/8\pi)\Gamma^2 c\epsilon_{\rm B}^{-1} \gtrsim L_{\rm iso}, \tag{5.3}$$

where $\epsilon_{\rm B} < 1$ is the fraction of outflow power in magnetic energy. Combining eqs. (5.2) and (5.3) above, we obtain a lower limit on the radius of emission

$$r \gtrsim (7.2 \times 10^{13}\,{\rm cm})\,\epsilon_{\rm B}^{1/2}\gamma'^{2}\sin\alpha' L_{\rm iso,43}^{1/2}\nu_9^{-1}. \tag{5.4}$$

When the outflow undergoes dissipation (shocks or magnetic reconnection) at such a large distance from the central object, the extremely fine-tuned requirements on the B-field and pitch-angle distribution are unlikely to be realized. Moreover, even if population inversion $\partial(N_\gamma/\gamma^2)/\partial\gamma > 0$ is initially achieved, since high-energy electrons radiate faster than lower-energy ones, the population inversion may be quickly destroyed.

5.0.2 Synchrotron maser in plasma

The synchrotron emissivity (eq. 4.55) is strongly modified at frequencies below the Razin frequency (the plasma frequency multiplied by the Lorentz factor of the particle). This is because the Liénard-Wiechert potential of a particle undergoing acceleration is significantly modified by wave dispersion at these frequencies. In this subsection, we consider synchrotron maser in a plasma which is moving towards the observer with bulk Lorentz factor Γ. Quantities in the comoving frame of the radiating plasma are denoted with a prime ($'$) and unprimed quantities are in the rest frame of the central object.

For a weakly magnetized plasma with randomly oriented B-field, under the *assumption* that the population-inversion condition $\partial(N'_{\gamma'}/\gamma'^2)/\partial\gamma' > 0$ is satisfied, synchrotron maser may operate below the effective Razin frequency

$\nu'_{\rm R*} = \nu'_{\rm p}\min(\gamma'_{\rm e}, \sqrt{\nu'_{\rm p}/\nu'_{\rm B}})$ [102], where $\gamma'_{\rm e}$ is the Lorentz factor of the radiating electrons and the plasma frequency and gyrofrequency are defined as

$$\nu'_{\rm p} = \frac{1}{2\pi}\left(\frac{4\pi n' e^2}{\bar{\gamma}' m_{\rm e}}\right)^{1/2}, \ \nu'_{\rm B} = \frac{eB'}{2\pi\bar{\gamma}' m_{\rm e} c}, \tag{5.5}$$

and $\bar{\gamma}'$ is the mean Lorentz factor of electrons in the comoving frame of the emitting plasma. We allow $\bar{\gamma}'$ to be a free parameter and take $\bar{\gamma}' = 10^2\bar{\gamma}'_2$ as our fiducial value (constraints on $\bar{\gamma}'$ will be shown later). The ratio of these two frequencies can be expressed as $\nu'_{\rm p}/\nu'_{\rm B} \simeq (\epsilon_{\rm e}/2\epsilon_{\rm B})^{1/2}$, where $\epsilon_{\rm e}$ and $\epsilon_{\rm B}$ are the fractions of the energy density in electrons and B-field in the emitting region. Note that, since EM waves below the plasma frequency cannot propagate, synchrotron maser near the effective Razin frequency can only operate when $\epsilon_{\rm e}/\epsilon_{\rm B} \gg 1$, which means the radiating plasma is not dominated by magnetic energy.

In the following, we discuss the propagation of the coherent radiation through the source plasma. To make our discussion as general as possible, we parameterize the frequency of the emitted radiation in the comoving frame of the plasma as $\nu' = \xi\nu'_{\rm p}$. For instance, in the model of Ref. [57], we have $\xi = \sqrt{\nu'_{\rm p}/\nu'_{\rm B}} = (\epsilon_{\rm e}/2\epsilon_{\rm B})^{1/4}$. For other maser-type collective plasma emission in a weakly magnetized plasma, the radiating frequency may be near the plasma frequency $\nu' \sim \nu'_{\rm p}$ and $\xi \sim 1$.

The frequency in the observer's frame is $\nu = \nu_9$ GHz $\simeq \Gamma\xi\nu'_{\rm p}$, so we obtain

$$\Gamma^2 n' \simeq (1.1\times10^{13}\,{\rm cm}^{-3})\,\bar{\gamma}'_2\,(\nu_9/\xi)^2\,, \tag{5.6}$$

If the emission occurs at a distance r from the central engine, the isotropic equivalent kinetic luminosity of electrons is

$$L_{\rm ke,iso} \simeq 4\pi r^2 \Gamma^2 n' \bar{\gamma}' m_{\rm e} c^3. \tag{5.7}$$

Since $\epsilon_{\rm e}/\epsilon_{\rm B} \gg 1$, the total luminosity of the outflow is a factor $\epsilon_{\rm e}^{-1}$ higher (a large fraction of the energy may be in protons). The radiative efficiency in the radio band is denoted as $f_{\rm r} < 1$, so the isotropic FRB luminosity is $L_{\rm iso} = L_{\rm ke,iso}\epsilon_{\rm e}^{-1} f_{\rm r}$. We eliminate $\Gamma^2 n'$ with eqs. (5.6) and (5.7) and then obtain the emission radius

$$r \simeq (1.7\times10^{11}\,{\rm cm})\,\bar{\gamma}_2' \left(\frac{L_{\rm iso,43}\epsilon_{\rm e}}{f_{\rm r}}\right)^{1/2} \left(\frac{\nu_9}{\xi}\right)^{-1}, \tag{5.8}$$

which has no direct dependence on the bulk Lorentz factor. The emission radius is related to the FRB duration through $t_{\rm FRB} \lesssim r/(2\Gamma^2 c)$ (eq. 5.1), so we can constrain the bulk Lorentz factor

$$\Gamma \lesssim 53\,\bar{\gamma}_2'^{-1/2} t_{\rm FRB,-3}^{-1/2} \left(\frac{L_{\rm iso,43}\epsilon_{\rm e}}{f_{\rm r}}\right)^{1/4} \left(\frac{\nu_9}{\xi}\right)^{-1/2}. \tag{5.9}$$

The isotropic equivalent number of electrons in the causally-connected region is

$$\begin{aligned} N &\simeq 4\pi r^3 n'/\Gamma \\ &\gtrsim 4.6\times10^{42}\,\bar{\gamma}_2'^{-1/2} t_{\rm FRB,-3}^{3/2} \left(\frac{L_{\rm iso,43}\epsilon_{\rm e}}{f_{\rm r}}\right)^{3/4} \left(\frac{\nu_9}{\xi}\right)^{1/2}, \end{aligned} \tag{5.10}$$

where the upper bound of Γ in eq. (5.9) has been used. For a NS progenitor, the total number of electrons and positrons in the magnetosphere is roughly given by

$$\frac{4\pi R_*^3 \mathcal{M} n_{\rm GJ}}{3} \simeq (2.9\times10^{38})\,\mathcal{M}_6 B_{*,14} P_{-1}^{-1}. \tag{5.11}$$

Thus, any model based on outflows from a NS must explain how this extremely large amount of particles $\mathcal{M} \gg 10^6$ are created and ejected (for instance, the outflow has to break the magnetic confinement if it is launched in the closed field line region).

The entire outflow has Thomson optical depth

$$\begin{aligned}\tau_{\rm T} &= n'\sigma_{\rm T} r/\Gamma = \frac{L_{\rm iso} f_{\rm r}^{-1}\epsilon_{\rm e}\sigma_{\rm T}}{4\pi r\Gamma^3\bar{\gamma}' m_{\rm e}c^3} \\ &\gtrsim 8.4\times 10^{-6}\,\bar{\gamma}_2'^{3/2} t_{\rm FRB,-3}^{3/2}\left(\frac{L_{\rm iso,43}\epsilon_{\rm e}}{f_{\rm r}}\right)^{-1/4}\left(\frac{\nu_9}{\xi}\right)^{5/2}.\end{aligned} \tag{5.12}$$

We note that induced (or stimulated) Compton scattering may be important even when the Thomson optical depth is small[2]. If the source radiates isotropically in the comoving frame and the spectrum is moderately broad with $\Delta\nu/\nu \gtrsim 1$, the brightness temperature $T'_{\rm B}$ in the plasma comoving frame is limited by (see Appendix C)

$$\frac{kT'_{\rm B}}{\bar{\gamma}'^5 m_{\rm e}c^2}\tau_{\rm T} \lesssim 1. \tag{5.13}$$

An intuitive understanding of the $\bar{\gamma}'^{-5}$ factor is as follows. For the conservative case with spectrum width $\Delta\nu \sim \nu$, induced-Compton scattering is only important when the fractional frequency change before and after the scattering is of order unity. Thus, the incident photon only interacts with a fraction $\sim\bar{\gamma}'^{-2}$ of electrons whose momentum vectors are nearly parallel to the wavevector

[2]The wavelength of the FRB EM wave is much shorter than the Debye length in the source region, the strong E-fields associated to the EM wave cannot be screened, so an electron can interact with many photons at the same time. Even for wavelength much longer than the Debye length, induced Raman scattering creating Langmuir waves may become an important obstacle hindering the propagation of coherent waves.

(to within an angle $\sim\bar{\gamma}'^{-1}$). Therefore, the effective Thomson optical depth is $\sim\bar{\gamma}'^{-2}n'\sigma_{\rm T}r/(\bar{\gamma}'^{2}\Gamma) = \tau_{\rm T}/\bar{\gamma}'^{4}$. Another factor of $\bar{\gamma}'^{-1}$ comes from Lorentz transformation that the brightness temperature in the electron' comoving frame is $T'_{\rm B}/\bar{\gamma}'$. When the source is relativistic, the relationship between $T'_{\rm B}$ (the true brightness temperature in the comoving frame) and the *apparent* brightness temperature $T_{\rm B}$ given by eq. (1.2) is $T'_{\rm B} \simeq T_{\rm B}/\Gamma^3$. Thus, eq. (5.13) constrains the *apparent* brightness temperature

$$T_{\rm B} \lesssim (1.1\times10^{30}\,{\rm K})\,\bar{\gamma}_2'^{2}t_{\rm FRB,-3}^{-3}\frac{L_{\rm iso,43}\epsilon_{\rm e}}{f_{\rm r}}\left(\frac{\nu_9}{\xi}\right)^{-4}. \tag{5.14}$$

Note that the constraint on $T_{\rm B}$ in eq. (5.14) will be stronger if the FRB spectrum is broader than $\Delta\nu/\nu \sim 1$ or if the Lorentz factor distribution below $\bar{\gamma}'$ is flatter than $N'_{\gamma'} \propto \gamma'^{4}$ (see Appendix C).

Violation of eq. (5.13) or (5.14) causes exponential loss of photon energy with time and the energy goes back to the plasma. Note that this constraint is only correct in the linear regime (when the non-linearity parameter $a_0 < 1$), which is valid for a source powered by particle kinetic energy. It can be shown by inserting the effective particle mass $\bar{\gamma}'m_{\rm e}$ into eq. (3.2) that the non-linearity parameter becomes $a_0 \simeq (f_{\rm r}/\epsilon_{\rm e})^{1/2}\xi^{-1}$. Since $f_{\rm r}/\epsilon_{\rm e} < 1$ (only a fraction of the electrons' energy is radiated in the radio band) and $\xi \gtrsim 1$ (for waves to escape), we obtain $a_0 \lesssim 1$.

We compare eq. (5.14) with the apparent brightness temperature in eq. (1.2) and obtain a constraint on the radiative efficiency

$$f_{\rm r} \lesssim 2.3\times10^{-6}\xi^{4}\epsilon_{\rm e}\bar{\gamma}_2'^{2}t_{\rm FRB,-3}^{-1}\nu_9^{-2}\Delta\nu_9, \tag{5.15}$$

where $\Delta\nu_9$ is the width of the FRB spectrum. The maximum mean Lorentz factor $\bar{\gamma}'_{\rm max}$ corresponds to the condition when the synchrotron/inverse-Compton cooling time $t'_{\rm cool}$ equals to the dynamical time $t'_{\rm dy} = r/\Gamma c$ (smaller $\bar{\gamma}'$ corresponds to $t'_{\rm cool} > t'_{\rm dy}$), and we obtain

$$\frac{r}{\Gamma c} = \frac{3\bar{\gamma}'_{\rm max} m_{\rm e} c^2}{4\sigma_{\rm T} c \bar{\gamma}'^2_{\rm max} \max(U'_{\rm B}, U'_{\rm rad})}, \tag{5.16}$$

where the magnetic and radiation energy densities are

$$\max(U'_{\rm B}, U'_{\rm rad}) = \frac{L_{\rm iso}/f_{\rm r}}{4\pi r^2 \Gamma^2 c} \max(\epsilon_{\rm B}, \epsilon_{\rm e}). \tag{5.17}$$

Then making use of the expressions for r and Γ in eqs. (5.8) and (5.9) and $\epsilon_{\rm B} \ll \epsilon_{\rm e}$, we obtain

$$\bar{\gamma}'^2_{\rm max,2} \simeq 3.5 \left(\frac{L_{\rm iso,43}\epsilon_{\rm e}}{f_{\rm r}}\right)^{1/7} \left(\frac{\nu_9}{\xi}\right)^{-10/7} t_{\rm FRB,-3}^{-6/7}. \tag{5.18}$$

Thus, we combine eqs. (5.15) and (5.18) and obtain

$$f_{\rm r} \lesssim 3.5 \times 10^{-5} \xi^{19/4} \epsilon_{\rm e} L_{\rm iso,43}^{1/8} t_{\rm FRB,-3}^{-13/8} \nu_9^{-3} \Delta\nu_9^{7/8}. \tag{5.19}$$

Note that $f_{\rm r}$ is defined as the radiative efficiency in the radio band. When $\bar{\gamma}' \simeq \bar{\gamma}'_{\rm max}$, the source plasma is radiatively efficient and electrons radiate almost all their kinetic energy at frequencies $\gg$GHz through multiple scattering, since the Compton-Y parameter $Y \sim \bar{\gamma}'^2 \tau_{\rm T}$ is of order unity. For synchrotron maser in a relativistic plasma, we have $\xi \simeq (\epsilon_{\rm e}/2\epsilon_{\rm B})^{1/4}$, and then the constraint in eq. (5.19) becomes

$$f_{\rm r} \epsilon_{\rm B}^{19/16} \lesssim 1.5 \times 10^{-5} \epsilon_{\rm e}^{35/16} L_{\rm iso,43}^{1/8} t_{\rm FRB,-3}^{-13/8} \nu_9^{-3} \Delta\nu_9^{7/8}. \tag{5.20}$$

Hereafter, we consider the recent detections of bursts from FRB 121102 at ∼6 GHz by [103] and take $\Delta\nu_9 \simeq 1$ and $t_{\rm FRB,-3} \simeq 1$. The electron energy fraction has been shown to be near equipartition value $\epsilon_{\rm e} \sim 0.3$ observationally (from the afterglows of gamma-ray bursts, [104]) and theoretically (from particle-in-cell simulations, [105]). Thus, the radiative efficiency in the radio band must be very low $f_{\rm r} \lesssim 5\times10^{-9}\epsilon_{\rm B}^{-19/16}$, as long as $\epsilon_{\rm B}$ is not much smaller than $\sim 10^{-5}$. On the other hand, for possible plasma masers in weakly magnetized plasma $\xi \sim 1$, the apparent brightness temperature implies extremely low radiative efficiency in the radio band $f_{\rm r} \lesssim 5 \times 10^{-8}$.

5.0.3 Bunching in the gyration phase

It has been proposed that FRBs may be produced by a maser mechanism due to bunching in gyration phase at quasi-perpendicular shocks with high magnetization when the upstream particles are coherently reflected by the shock-compressed B-field [56, 58]. These authors considered the external shock scenario where a magnetar outflow drives a shock into the magnetized circumstellar medium (the wind nebula). Although this scenario is inconsistent with the durations of closely-separated burst pairs (as shown in Appendix B), the same maser mechanism may operate in internal shocks between colliding shells as well, which is discussed in this subsection.

Bunching in gyration phase due to coherent reflection of incoming particles at quasi-perpendicular shocks has been well studied in 1D simulations with magnetization $\sigma \in (10^{-2}, 5)$ [106, 100, 101], where a fraction of $\lesssim 10^{-1}$ of

the incoming particles' kinetic energy is converted to a coherent EM precursor. Note that the magnetization parameter σ is defined as the ratio between the upstream Poynting flux and particles' kinetic flux. Later 2D simulations with $\sigma = 0.1$ by Ref. [107] show that the precursor gets increasingly weaker with time as the coherence of particle reflections between different locations along the shock surface is lost, and the authors speculated that the maser emission may disappear in sufficiently long simulations or in 3D. More recent 2D simulations with higher resolutions by Ref. [108] show that the precursor persists until the end of the simulations (at time $\sim 10^3 \nu_{\rm p}'^{-1}$) and that the efficiency appears to converge to $\sim 10^{-2}$ when $\sigma \in (0.1, 1)$. In this thesis, we take the results from the above 1D simulations as upper limits but note that longer simulations at higher magnetization in 2D and 3D are needed to draw a firm conclusion on the efficiency of the coherent precursor.

Consider two consecutive shells ejected from the central engine colliding at certain radius r and then the coherent EM waves propagates through the upstream plasma of the first (slower) shell whose bulk Lorentz factor is Γ. The emission frequency in the comoving frame of the first shell is $\sim \mathcal{R}^{1/4} \nu_{\rm B}'$, where $\mathcal{R}$ is the ratio between the luminosities of the second and first shells and $\mathcal{R}^{1/4} > 1$ is the relative Lorentz factor between the upstream and downstream. The magnetization parameter of the first shell is $\sigma = \nu_{\rm B}'^2 / \nu_{\rm p}'^2$, so the emission frequency can be rewritten as $\nu \sim \mathcal{R}^{1/4} \sigma^{1/2} \nu_{\rm p}'$. We also note that coherent reflection of incoming particles is only possible when the upstream plasma in the first shell is initially cold, i.e. electrons' thermal Lorentz factor $\bar{\gamma}' \ll \mathcal{R}^{1/4}$.

We put $\xi \sim \mathcal{R}\sigma^{1/2}$ and $\bar{\gamma}' < \mathcal{R}^{1/4}/2$ into eq. (5.15), which comes from the constraint on the brightness temperature imposed by induced-Compton scattering, and hence the radiative efficiency (in the radio band) has an upper limit

$$f_{\rm r} \lesssim 6 \times 10^{-11}\, \mathcal{R}^{3/2}\sigma^2\epsilon_{\rm e}t_{\rm FRB,-3}^{-1}\nu_9^{-2}\Delta\nu_9. \tag{5.21}$$

When the first shell is highly magnetized with $\sigma \gg 1$, we have $\epsilon_{\rm e} \lesssim \sigma^{-1}$. We further put in $\nu \sim 6\,{\rm GHz}$, $\Delta\nu_9 \simeq 1$ and $t_{\rm FRB,-3} \simeq 1$ [103] and obtain a stringent constraint on the radiative efficiency $f_{\rm r} \lesssim 1.6\times10^{-12}\mathcal{R}^{3/2}\sigma$. Another constraint comes from the above mentioned particle-in-cell simulations, which showed that only a small fraction $\lesssim 10^{-1}$ of the incoming *particles' kinetic energy* can be converted into coherent EM wave ahead of the main shock, so we also have $f_{\rm r} \lesssim 10^{-1}\sigma^{-1}$ when $\sigma \gg 1$. Combining the constraint from induced-Compton scattering with that from numerical simulations, we obtain $f_{\rm r} \lesssim 4 \times 10^{-7}\mathcal{R}^{3/4}$ (the maximum is reached when $\sigma \simeq 2.5 \times 10^5\mathcal{R}^{-3/4}$). Therefore, as long as the luminosity ratio $\mathcal{R}$ between two consecutive shells ejected from the central engine is not much greater than $\sim 10^{4.5}$, the maser due to bunching in gyration phase at quasi-perpendicular shocks must have a very low radiative efficiency.

To summarize the main results of this section, we find that FRB models based on masers powered by internal/external dissipation of the free energy of an outflow suffer from the following potential inconsistencies: (i) external shock model cannot reproduce the durations of some closely-separated FRB pairs; (ii) synchrotron maser in vacuum requires fine-tuned plasma conditions

where the B-field is nearly uniform (to within an angle $\sim\gamma'^{-1}$) and particles' pitch-angle distribution is narrowly peaked with spread $\lesssim \gamma'^{-1}$; (iii) synchrotron maser in plasma requires a low radiation efficiency $f_{\rm r} \lesssim 5\times10^{-9}\epsilon_{\rm B}^{-19/16}$ for FRBs detected at high frequencies $\sim$6 GHz; (iv) it is unclear how the population inversion condition $\partial(N'_{\gamma'}/\gamma'^2)/\partial\gamma' > 0$ is achieved[3]; (v) during the maser amplification process, high-energy electrons radiate faster than low-energy ones, so the population inversion condition may be quickly destroyed; (vi) the maser due to bunching in gyration phase at quasi-perpendicular shocks requires a low radiative efficiency $f_{\rm r} \lesssim 4\times10^{-7}\mathcal{R}^{3/4}$, where $\mathcal{R}$ is the luminosity ratio of the two colliding shells.

[3]Note that our constraint on the radiation efficiency $f_{\rm r}$ is conservative, because the limit on the brightness temperature given by induced Compton scattering via eq. (5.13) will be stronger for mild population inversion with $\partial(N'_{\gamma'}/\gamma'^4)/\partial\gamma' < 0$.

Chapter 6

The antenna mechanism

In §4 and §5, we have explored many possible maser mechanisms operating either inside the magnetosphere of a NS or when a relativistic outflow undergoes internal/external dissipation. We find that various maser mechanisms (in either vacuum or plasma) proposed in the literature require unrealistic or extremely fine-tuned plasma conditions. Thus, we are left with the antenna mechanism, which will be described in this section. This mechanism requires coherently moving charge bunches with sizes smaller than the wavelength of emission $\lambda \sim 30\,\mathrm{cm}$. This is only possible when there is large-scale ordered B-field lines, so we only consider the plasma to be inside the magnetosphere of a NS. In the situation where the dissipation of outflow energy occurs at large distances from the central object, the B-field in the emitting plasma is weak, and particles typically gyrate around B-field lines at random gyration phases instead of forming coherent bunches. In §6.1, we first go through the basic properties of bunches needed to produce FRB luminosities, following Ref. [55]. Then in §6.2, we discuss possible bunch formation channels and show, for the first time, bunches can form via two-stream instability in the twisted magnetosphere of a magnetar.

6.0.1 Properties of bunches

Traditionally, coherent curvature radiation by bunches has long been considered as a possible mechanism to explain pulsar radio emission [62], but it suffers from a number of critiques (e.g. [109]). First, the growth time for bunches due to two-stream instability is too long under the classical two-beam condition[1] (a primary beam with $\gamma_{\rm b} \sim 10^6$-10^7 interacting with a secondary pair plasma with $\gamma_{\pm} \sim 10^2$-10^3, e.g. [113, 114]). Second, the number of particles per bunch required by the observed high brightness temperature leads to too strong Coulomb repulsion and hence bunch dispersion (e.g. [110]). Third, none of the treatment in the literature has included the formation of bunches and their coherent radiation processes simultaneously. On the other hand, it has also been proposed that charge bunches (solitons) could be produced by modulational instability in a turbulent plasma provided that species of different charge signs have different effective mass (electrons and positrons with different streaming Lorentz factors do have different mass, and there could also be some mixing of ions, e.g. [115, 116, 117, 118]). In this thesis, we do not attempt to unify pulsar radio emission with FRB radiation mechanism, because the properties of the source plasma for FRBs is drastically different from pulsars (as shown in §4.1).

Ref. [55] considered coherent curvature emission by the antenna mechanism in detail. If the local curvature radius of the B-field line is ρ and an

[1] However, it has also been proposed that using different particle distribution functions, the instability may grow on much shorter time-scales [110, 111, 112].

electron is moving very close to c, the acceleration perpendicular to the velocity is c^2/ρ. To produce curvature radiation at frequency $\nu = \nu_9$ GHz, we require

$$\gamma \simeq 60\,\nu_9^{1/3}\rho_6^{1/3}. \tag{6.1}$$

At such low Lorentz factors, the single-particle curvature power is very small

$$P_{\rm curv} \simeq \frac{\gamma^4 e^2 c}{\rho^2} \simeq (8.5\times10^{-14})\,{\rm erg\,s^{-1}}\,\nu_9^{4/3}\rho_6^{-2/3}. \tag{6.2}$$

When the particle is moving towards the observer, the isotropic equivalent luminosity is

$$\delta L_{\rm iso} \simeq \gamma^4 P_{\rm curv} \simeq (1.1\times10^{-6}\,{\rm erg\,s^{-1}})\,\nu_9^{8/3}\rho_6^{2/3}. \tag{6.3}$$

We see that single-particle curvature radiation is extremely inefficient. To produce the observed FRB luminosity $L_{\rm iso}\sim10^{43}\,{\rm erg\,s^{-1}}$, electrons must form bunches and radiate coherently.

The size of a bunch in the direction parallel to the line of sight (hereafter *longitudinal* direction) must not significantly exceed $\lambda\!\!\!^{-} = \lambda/2\pi = 4.8\,\nu_9^{-1}\,{\rm cm}$. The radiation formation length is ρ/γ, which corresponds to a time $\rho/(\gamma^2 c)$ in the electrons' comoving frame. Thus, the maximum size allowed by coherence in the *transverse* direction is $\rho/\gamma^2 \simeq \gamma\lambda\!\!\!^{-} \simeq (2.9\times10^2\,{\rm cm})\,\nu_9^{-2/3}\rho_6^{1/3}$. Therefore, the maximum number of particles in one coherent bunch is given by

$$N_{\rm coh} \simeq \pi n \gamma^2 \lambda\!\!\!^{-3} \simeq 1.3\times10^{24}\,n_{18}\nu_9^{-7/3}\rho_6^{2/3}, \tag{6.4}$$

where $n = 10^{18} n_{18}\,\mathrm{cm}^{-3}$ is the fiducial number density in the NS frame. The isotropic equivalent luminosity from one such bunch is

$$L_{\rm iso}^{\rm bunch} \simeq N_{\rm coh}^2 \delta L_{\rm iso}. \tag{6.5}$$

In reality, the transverse size of one local patch of particles may be a factor[2] of $\eta > 1$ greater than $\gamma\lambda$ but coherence cannot be maintained due to causality, and then the total luminosity is the incoherent sum of the emission from η^2 bunches

$$L_{\rm iso} = \eta^2 L_{\rm iso}^{\rm bunch} \simeq (1.8 \times 10^{42}\,\mathrm{erg\,s^{-1}})\,\eta^2 n_{18}^2 \nu_9^{-2} \rho_6^2. \tag{6.6}$$

Therefore, the observed FRB luminosity $L_{\rm iso} \sim 10^{43}\,\mathrm{erg\,s^{-1}}$ can be easily achieved by tuning the parameters n_{18}, ρ_6 and η. Variations in these parameters can also lead to a large range of FRB luminosities as observed. In the observer's frame, the emission from each bunch lasts for $\nu^{-1} \sim 1\,\mathrm{ns}$ and it requires 10^6 such bunches to produce an FRB with intrinsic duration $\sim 1\,\mathrm{ms}$. The beaming factor of one bunch is $f_{\rm b} \sim \gamma^{-2}$, so the minimum energy budget per FRB is $\sim \gamma^{-2} L_{\rm iso} t_{\rm FRB} \sim 3 \times 10^{36}\,\mathrm{erg}\, L_{\rm iso,43} t_{\rm FRB,-3}$, for the Lorentz factor in eq. (6.1) and $\nu_9^{1/3} \rho_6^{1/3} \sim 1$.

In a man-made antenna, the kinetic energy of particles is minuscule and the radiating power is supplied by the *ac* electromotive force. Similarly, in the astrophysical antenna model of FRBs, the power comes from a parallel E-field $E_\parallel$ which sustains the Lorentz factor of electrons as required by eq.

[2] This factor was denoted as $\eta^{1/2}$ in Ref. [55].

(6.1). Since each electron is losing energy at a rate $N_{\rm coh}P_{\rm curv}$, we obtain from energy conservation[3] $E_\parallel ec \simeq N_{\rm coh}P_{\rm curv}$, i.e.

$$E_\parallel \simeq \frac{\gamma^4 e N_{\rm coh}}{\rho^2} \simeq (7.5\times10^9\,{\rm esu})\, n_{18}\nu_9^{-1}. \tag{6.7}$$

Such a strong, large-scale (length $\gtrsim \rho/\gamma$) E-field may come from magnetic reconnection at small inclination angles in the magnetosphere [55]. We also note that the isotropic luminosity (eq. 6.6) can be expressed in terms of the parallel E-field $E_\parallel = 10^{10}E_{\parallel,10}\,{\rm esu}$

$$L_{\rm iso} \simeq \eta^2 E_\parallel^2 \rho^2 c \simeq (3.0\times10^{42}\,{\rm erg\,s^{-1}})\,\eta^2 E_{\parallel,10}^2\rho_6^2. \tag{6.8}$$

The flow of the radiating particles (and counter-streaming particles of the opposite charge sign) along the primary B-field leads to a current $j = 2nce$ within a cylinder of radius $\eta\gamma\lambda$ (transverse length of the coherent bunch), which induces a strong B-field in the transverse direction

$$B_{\rm ind} \simeq \frac{4\pi j}{c}\frac{\eta\gamma\lambda}{2} \simeq (4.0\times10^{12}\,{\rm G})\, L_{\rm iso,43}^{1/2}\nu_9^{1/3}\rho_6^{-2/3}. \tag{6.9}$$

This induced B-field leads to a torsion on the primary B-field. Considering the fact that particles are locked in the lowest Landau level and only move along local B-field lines, it is crucial that the combined primary plus induced B-field still point towards the observer within an angle of $\sim\gamma^{-1}$. This sets a

[3] Another way of thinking is that the radiation backreaction force operates on all particles within the coherent bunch, because the EM fields are nearly uniform within the coherent region. Each particle experiences a backreaction force due to all other radiating particles and this force must be balanced by the force from an external E-field $E_\parallel$.

lower limit on the strength of the primary B-field

$$B \gtrsim \gamma B_{\rm ind} \simeq (2.4 \times 10^{14}\,{\rm G})\, L_{\rm iso,43}^{1/2} \nu_9^{2/3} \rho_6^{-1/3}. \tag{6.10}$$

This lower limit is stronger than the one from the energy requirement in eq. (2.4), meaning the latter can be easily satisfied.

6.0.2 Formation of bunches and high-frequency FRB analogs

In the model of Ref. [55], it was shown that bunches may form due to two-stream instability in the situation of counter-streaming electrons and positrons with Lorentz factor given by eq. (6.1) and density $n \gtrsim 10^{17}\,{\rm cm}^{-3}$. However, since the formation of bunches must occur simultaneously with the coherent curvature radiation in their model, proper treatment of radiation backreaction is needed. Moreover, the bunch formation length $\sim \gamma^2 \lambda$ is on the same order as the radiation formation length $\sim \rho/\gamma$. It remains unclear whether bunches can form spontaneously (and survive the radiation formation process) during magnetic reconnection in a plasma of quasi-uniform density.

Another possible way of bunching is a radiative instability proposed by Ref. [119], where an initial uniform distribution of particles moving along a thin circular ring spontaneously develops bunches due to the backreaction of curvature radiation. However, since the two non-linear processes — the formation of bunches and coherent emission by bunches — were not treated together in a self-consistent way, it is currently unclear whether radiation backreaction acts to increase or decrease bunching [120].

In this thesis, we propose a new mechanism for bunch formation. In Appendix A, we show that, the plasma in the twisted magnetosphere of a magnetar[4] is turbulent and clumpy due to two-stream instability. When magnetic reconnection occurs, the pre-existing density clumps may provide charge bunches for the antenna mechanism to operate.

Guided by §6.1, we use a fiducial number density $n = 10^{18} n_{18}\,\mathrm{cm}^{-3}$ and a fiducial B-field $B = 10^{14} B_{14}\,\mathrm{G}$ in the following. This number density exceeds the G-J density [$n_{\rm GJ} = B/(ecP)$] by a factor of $\mathcal{M} \simeq 10^4 n_{18} B_{14}^{-1} P_{-1}$. The twist-induced currents are supported by counter-streaming particles of opposite charges from pair creation avalanches. In the traditional model of pair creation above the polar cap of a rotating NS [65, 62], γ-rays are produced by curvature radiation of primary particles with Lorentz factor exceeding $\sim 10^7$. In the magnetar model, the creation of γ-rays is mainly due to resonant scattering of ambient X-ray photons by initial electrons pulled from the NS surface (e.g. [73]). The resonant scattering condition is $\gamma_{\rm res}\epsilon_{\rm x} \simeq (B/B_{\rm QED}) m_{\rm e}c^2$ (eq. 4.16), i.e.

$$\gamma_{\rm res} \simeq 1.2 \times 10^2\, B_{14} (\epsilon_{\rm x}/10\,\mathrm{keV})^{-1}. \tag{6.11}$$

The scattered photons have energy $\epsilon_{\rm IC}/m_{\rm e}c^2 \simeq 1.2 \times 10^2 B_{14} (\epsilon_{\rm x}/10\,\mathrm{keV})^{-1}$ (eq. 4.17) in the NS frame. When $B \gtrsim B_{\rm QED}$, these γ-rays convert into pairs within a propagation length $\rho m_{\rm e}c^2/\epsilon_{\rm IC} \simeq (10^4\,\mathrm{cm})\,\rho_6 B_{14}^{-1} (\epsilon_{\rm x}/10\,\mathrm{keV})$ when the pitch

[4] Strong surface B-field is required by two independent arguments from (i) the energetics of the repeater FRB 121102 (eq. 2.4), (ii) emission coherence (eq. 6.10). These arguments imply that the progenitor is a magnetar rather than a normal radio pulsar.

angle becomes $\lesssim m_{\rm e}c^2/\epsilon_{\rm IC}$.

In the counter-streaming electron-positron plasma[5], two-stream instability naturally leads to density fluctuations with a broad spatial power spectrum at wavenumbers smaller than a critical value $k < k_{\rm max} \equiv \omega_{\rm p,eff}/c$, and the effective plasma frequency $\omega_{\rm p,eff}$ depends on the distribution function. In Appendix A, we show that, for a homogeneous counter-streaming electron-positron plasma, the effective plasma frequency is

$$\begin{aligned} \omega_{\rm p,eff} &= \left(\frac{4\pi e^2 n}{\gamma_{\rm c} m_{\rm e}}\right)^{1/2} \simeq (1.8\times10^{12}\,{\rm s}^{-1})\left(\frac{n_{18}}{\gamma_{\rm c,3}}\right)^{1/2}, \\ \gamma_{\rm c}^{-1} &\equiv \langle\gamma^{-3}\rangle = \int_{-\infty}^{+\infty}\gamma^{-3} f(u){\rm d}u, \end{aligned} \tag{6.12}$$

where $f(u)$ is the normalized one-dimensional distribution function of particles' 4-velocities u. Thus, large density fluctuations with $\Delta n/n \sim 1$ can develop on length-scales longer than the effective skin depth

$$\ell_{\rm skin} = c/\omega_{\rm p,eff} \simeq (1.7\times10^{-2}\,{\rm cm})\,\gamma_{c,3}^{1/2} n_{18}^{-1/2}. \tag{6.13}$$

The distribution function of the counter-streaming pair plasma in the twisted magnetosphere is highly uncertain (depending on $\boldsymbol{B}$, ρ, $\epsilon_{\rm x}$, etc.), and hence $\gamma_{\rm c}$ could range from $\sim \langle\gamma\rangle$ (near Maxwellian distribution) to $\sim \langle\gamma^3\rangle$ (near

[5] Note that the curvature antenna model may not require a large amount of particle injection from an explosive pair production process, so the pre-existing plasma could be made of electrons and protons (instead of electrons and positrons). Charge-to-mass ratio does not make a difference in the curvature radiation process, but the two-stream instability behaves differently. It can be shown that our discussion is qualitatively correct for an electron-proton plasma, as long as the parameter $\gamma_{\rm c}$ in eq. (6.12) is redefined to include the proton-to-electron mass ratio.

mono-energetic distribution). Since typical Lorentz factors $\gamma < \gamma_{\rm res} \sim 10^2$ (eq. 6.11), hereafter we take take $\gamma_{\rm c} = 10^3\gamma_{\rm c,3}$ as our fiducial parameter. More work is needed to determine this quantity from the distribution function and composition of the plasma in the pre-existing twisted magnetosphere. As long as $\ell_{\rm skin} < \lambda\!\!\!^{-} = 4.8\nu_9^{-1}\,{\rm cm}$, fractional density fluctuations of $\Delta n/n \sim 1$ over lengthscales $\sim \lambda\!\!\!^{-}$ can be produced and our discussion is not affected.

According to Appendix A, the growth rate of two-stream instability scales linearly with wave number k up to $k \sim k_{\rm max} = \ell_{\rm skin}^{-1}$, but growth is impossible at $k > k_{\rm max}$. Therefore, FRB analogs should exist at frequencies up to $\omega_{\rm eff}/2\pi \simeq (2.8\times10^{11}\,{\rm Hz})\,n_{18}^{1/2}\gamma_{\rm c,3}^{-1/2}$ (or wavelength $\lambda \sim 1\,{\rm mm}$). We also note that both n and $\gamma_{\rm c} \equiv \langle\gamma^{-3}\rangle^{-1}$ have large uncertainties due to the unknown particle distribution function in the magnetosphere of a magnetar. Since the pair annihilation mean free path must be longer than the curvature radius, i.e. $\gamma_{\rm c}/(\sigma_{\rm T}n) \sim (10^9\,{\rm cm})\,\gamma_{\rm c,3}n_{18}^{-1} \gtrsim (10^6\,{\rm cm})\,\rho_6$, i.e. $n_{18}^{1/2}\gamma_{\rm c,3}^{-1/2} \lesssim 10^{1.5}\rho_6^{-1/2}$, some very special conditions may in principle allow FRB analogs at frequencies up to $\sim10^{13}\,{\rm Hz}$ (wavelength $\sim30\,\mu{\rm m}$). We encourage searching for millisecond transients in the mm up to far infrared wavelengths.

In the following, we discuss the rate and luminosities of FRB analogs at different frequencies in the curvature antenna framework. We consider a charge bunch with longitudinal length $\ell_\parallel \gtrsim \ell_{\rm skin}$ (eq. 6.13) and transverse length $\ell_\perp$, which is moving with Lorentz factor γ. To maintain coherence within the radiation formation time, the longitudinal length is limited by the emission wavelength $\ell_\parallel \lesssim \lambda\!\!\!^{-}$. Note that, if particles in the bunch have Lorentz factor

spread $\Delta\gamma/\gamma \sim 1$, the bunch will disperse after traveling a distance $\sim \gamma^2 \ell_\parallel$. In this case, to avoid bunch dispersion within the curvature radiation formation length ρ/γ, we have $\ell_\parallel \gtrsim \lambda\!\!\!^{-} \simeq \rho/\gamma^3$. However, smaller $\ell_\parallel < \lambda\!\!\!^{-}$ is allowed if $\Delta\gamma/\gamma < 1$. In the following, we keep $\ell_\parallel$ as a free parameter within the range $(0,\ \sim\lambda\!\!\!^{-})$. Similar to the situation in man-made antennas, the inertia of the charge carriers is minuscule and particles' motion is controlled by the balance between power input (from a parallel E-field) and output (due to radiation), i.e.

$$\begin{aligned} E_\parallel e &\simeq \pi n \ell_\parallel \min[(\gamma\lambda\!\!\!^{-})^2, \ell_\perp^2]\, P_{\rm curv}/c \\ &\simeq \pi n \ell_\parallel e^2 \min[1, (\ell_\perp/\gamma\lambda\!\!\!^{-})^2] \end{aligned} \tag{6.14}$$

If the reconnecting B-field lines have inflow speed $\beta_{\rm in} c$ and inclination angle $\theta_{\rm B}$, then the parallel E-field is roughly given by $E_\parallel \simeq B \sin\theta_{\rm B} \beta_{\rm in}$. Thus, we obtain

$$B \sin\theta_{\rm B} \simeq \pi n \ell_\parallel e \beta_{\rm in}^{-1} \min[1, (\ell_\perp/\gamma\lambda\!\!\!^{-})^2]. \tag{6.15}$$

The transverse size of the bunch $\ell_\perp$ is unknown. A natural length-scale of the system is the thickness of the current sheet $\ell_{\rm cs}$ given by $\nabla \times B \simeq B \sin\theta_{\rm B}/\ell_{\rm cs} \simeq 4\pi n e$, i.e.

$$\ell_{\rm cs} \simeq B \sin\theta_{\rm B}/(4\pi n e) \simeq (1.7\times 10^2\,{\rm cm})\, B_{14} \theta_{\rm B,-2} n_{18}^{-1}. \tag{6.16}$$

Note that we have ignored the displacement current term, because $c|\nabla \times \boldsymbol{B}|(\partial E_\parallel/\partial t)^{-1} \sim B\sin\theta_{\rm B}/(\beta_{\rm in} E_\parallel) \sim \beta_{\rm in}^{-2} \gg 1$. In the following, we take $\ell_\perp \sim \ell_{\rm cs}$ as given by the magnetic reconnection physics (according to eq. 6.16). When $\ell_{\rm cs} \gtrsim \gamma\lambda\!\!\!^{-}$, which applies to bursts at frequency $\nu \gtrsim (0.8\,{\rm GHz})\, \rho_6^{1/2} \ell_{\rm cs,2.5}^{-3/2}$,

we make use of eqs. (6.15) and (6.16) to eliminate $B \sin\theta_{\rm B}$ and obtain $\beta_{\rm in} \simeq \ell_\parallel/4\ell_{\rm cs} \lesssim \ell_\parallel/(4\gamma\lambda\!\!\!^{-})$. The FRB luminosity should be dominated by bunches with maximum longitudinal length allowed by coherence $\ell_\parallel \sim \lambda\!\!\!^{-}$, so we find that the inflow speed of magnetic reconnection is small

$$\beta_{\rm in} \lesssim (4\gamma)^{-1} \simeq 4 \times 10^{-3} \nu_9^{-1/3} \rho_6^{-1/3}. \tag{6.17}$$

The isotropic equivalent luminosity from the entire clump is given by the incoherent sum of $(\ell_{\rm cs}/\gamma\lambda\!\!\!^{-})^2$ coherently radiating bunches of transverse area $\pi(\gamma\lambda\!\!\!^{-})^2$, i.e.

$$\begin{aligned} L_{\rm iso}^{(1)} &\simeq (\pi n \gamma^2 \lambda\!\!\!^{-3})^2 P_{\rm curv} \gamma^4 \left(\frac{\ell_{\rm cs}}{\gamma\lambda\!\!\!^{-}}\right)^2 \simeq \frac{\pi^2 n^2 \rho^2 \ell_{\rm cs}^2 e^2 c}{\gamma^2} \\ &\simeq (1.9 \times 10^{42}\,{\rm erg/s})\, n_{18}^2 \rho_6^{4/3} \ell_{\rm cs,2.5}^2 \nu_9^{-2/3}, \text{ for } \ell_{\rm cs} \gtrsim \gamma\lambda\!\!\!^{-}. \end{aligned} \tag{6.18}$$

On the other hand, when $\ell_{\rm cs} \lesssim \gamma\lambda\!\!\!^{-}$ (for bursts at frequency $\nu \lesssim (0.8\,{\rm GHz})\, \rho_6^{1/2} \ell_{\rm cs,2.5}^{-3/2}$), we again make use of eqs. (6.15) and (6.16) and obtain $\beta_{\rm in} \simeq \ell_\parallel \ell_{\rm cs}/(4\gamma^2\lambda\!\!\!^{-2}) \lesssim \ell_\parallel/(4\gamma\lambda\!\!\!^{-})$. Note that the constraint on the inflow speed is the same as in eq. (6.17) for the case $\ell_{\rm cs} \gtrsim \gamma\lambda\!\!\!^{-}$. The isotropic luminosity is given by the coherent radiation by all particles in the clump, i.e.

$$\begin{aligned} L_{\rm iso}^{(2)} &\simeq (\pi n \lambda\!\!\!^{-} \ell_{\rm cs}^2)^2 P_{\rm curv} \gamma^4 \simeq \pi^2 n^2 \gamma^2 \ell_{\rm cs}^4 e^2 c \\ &\simeq (2.5 \times 10^{42}\,{\rm erg/s})\, n_{18}^2 \rho_6^{2/3} \ell_{\rm cs,2.5}^4 \nu_9^{2/3}, \text{ for } \ell_{\rm cs} \lesssim \gamma\lambda\!\!\!^{-}. \end{aligned} \tag{6.19}$$

Due to differences among reconnection events — variations of particle density n, curvature radius ρ, and current sheet thicknesses $\ell_{\rm cs}$ — we expect a wide range of FRB luminosities. It is currently not possible to predict FRB luminosities at a given frequency, due to the unknown plasma conditions and

magnetic reconnection physics in the magnetosphere of the NS. However, FRB analogs at higher frequencies are expected to have lower burst rate due to narrower beaming angle (γ^{-2}), i.e. the burst rate should decline with frequency as $f_{\rm b} \sim \gamma^{-2} \propto \nu^{-2/3}$. Moreover, we can see from eq. (6.18) that FRB analogs at frequencies much higher than ∼GHz are most likely dimmer, because the coherent volume decreases faster than the luminosity gain from stronger beaming.

According to the antenna curvature model described here, the durations of FRBs are controlled by the physics of magnetic reconnection. For quasi-uniform density distribution, the radiative resistivity is negligible (incoherent curvature emission is inefficient), and magnetic reconnection cannot proceed unless there is another mechanism that can provide a much higher resistivity. Charge bunches may flow into the current sheet in the longitudinal and transverse directions. The former case has characteristic timescale $\pi\rho/c \sim 100\rho_6\,\mu$s. The characteristic timescale in the transverse direction is $\ell_{\rm cs}/\beta_{\rm in}c \sim (10\,\mu{\rm s})\,\ell_{\rm cs,2.5}\beta_{\rm in,-3}^{-1}$. Both of these timescales are much shorter than the typical duration of FRBs $t_{\rm FRB} \sim 1\,$ms. Therefore, the reconnection process may be unsteady and hence FRBs may be made of multiple sub-bursts (each lasting for ∼10-100 μs).

The total FRB duration corresponds to the time over which the accumulated stress in the reconnection region is released. From eq. (6.17), we see that the reconnection inflow speed is much smaller than the Alvén speed ($\approx c$) in the magnetosphere. This is because the energy inflow rate is

limited by the energy outflow rate in the form of coherent radiation. Thus, individual FRBs do not require global reconnection on lengthscales of the NS radius. The *maximum* size of the reconnection region in the transverse direction is $t_{\rm FRB}\beta_{\rm in}c \sim (3\times10^4\,{\rm cm})\,t_{\rm FRB,-3}\beta_{\rm in,-3}$. Without a detailed model for the magnetic configuration and activity[6] near the surface of the magnetar, it is currently not possible to predict FRB durations from first principles.

The typical time resolution of current FRB observations is $\sim$1 ms, which is limited by the signal-to-noise ratio and intra-band dispersion (the latter can be eliminated by coherent de-dispersion). Future observations of brighter bursts or by more sensitive telescopes may be able to resolve the sub-burst structures and provide valuable information on the reconnection physics.

To summarize the main results of this section, we find that the curvature antenna model can reproduce the basic properties of FRBs provided that the B-field strength of the NS is stronger than $\sim10^{14}$ G and that bunches with longitudinal size $\ell_\parallel \lesssim \lambda$ can form. We propose that two-stream instability in the twisted magnetosphere of magnetars (with persistent currents) provides a broad spectrum of density fluctuations at length-scales larger than the plasma skin depth (eq. 6.13). Then, the coherent emission by charge clumps is sustained by a strong E-field, which is produced by magnetic reconnection. A

[6] One possibility mentioned by Ref. [55] is that the buried magnetic flux emerges out of the NS surface and reconnects with the pre-existing magnetospheric B-fields. This process occurs on a time-scale $\Delta R/v_{\rm A} \sim (1\,{\rm ms})\,\Delta R_4 B_{14}^{-1}\rho_{0,13}^{1/2}$, where $\Delta R = 10^4\Delta R_4$ cm is the depth from which the flux emerges, $\rho_0 = 10^{13}\rho_{0,13}\,{\rm g\,cm^{-3}}$ is the mass density of the surface layer, and $v_{\rm A} = B/(4\pi\rho_0)^{1/2}$ is the Alfvén speed.

prediction of this model is that, since the initial two-stream instability leads to density fluctuations on all length-scales $\gtrsim c/\omega_{\rm p,eff}$, FRB analogs should exist at frequencies much higher than $\sim$GHz, up to mm (or even far-infrared) wavelengths. We have also shown that FRB analogs at frequencies $\gg$ GHz are most likely dimmer (due to smaller coherent volume) and that their rate may be lower (due to smaller beaming angle).

Chapter 7

Comparison between FRBs and pulsar radio emission

In this section, we briefly discuss some of the differences between the mechanisms of FRBs and pulsar radio emission.

After many decades of debate, there is still no compelling answer to the mechanism of pulsar radio emission. The basic reason behind the debate is that only a tiny fraction ($\lesssim 10^{-6}$ for the Crab) of the pulsar's energy loss (via electromagnetic spin-down) goes to radio photons, and therefore many maser or collective plasma emission mechanisms are viable [59, 29].

However, constraining the radiation mechanism for FRBs may be much easier than for pulsar radio emission. This is because, as explained in the following, the total energy release in a FRB event may not be much larger than the energy coming out in the radio band. In other words, the radiation in the radio band is likely the dominant channel of energy release in these transients. We have shown in previous sections that the much higher isotropic luminosities of FRB compared to radio pulsars (by more than 10 orders of magnitude) severely constrains the radiation mechanism for FRBs. We have shown in §4.1 and §5 that FRBs cannot be powered by the rotational energy of NSs

or internal/external dissipation of the free energy of relativistic outflows from BHs or NSs. This leads us to conclude that FRBs are most likely produced by the dissipation of magnetic energy near the surface of NSs. If the progenitor of FRB 121102 stays active for $\gtrsim 30\,\mathrm{yr}$, then the cumulative energy output in the radio band is $E_{\rm tot} \gtrsim 10^{44}(f_{\rm b,tot}/f_{\rm r})\,\mathrm{erg}$ (eq. 2.3), where $f_{\rm b,tot}$ is the combined solid angle of the radiation cones[1] of all bursts divided by 4π and $f_{\rm r}$ is the radio emission efficiency for each burst. Although these two factors are not well constrained by observations, they tend to cancel each other, and hence $E_{\rm tot}$ may be a significant fraction of the total magnetic energy in the magnetosphere of a magnetar, $\sim 10^{45} B_{*,14}^2\,\mathrm{erg}$.

When we consider collective plasma emission (or plasma maser) within the magnetosphere of NSs, the requirement that the magnetic energy density is much greater than particles' kinetic energy density and the energy density of the FRB EM waves provides a stringent lower limit on the B-field strength in the emitting region (eq. 4.5), and hence the emission is generated close to the NS surface (eq. 4.4). The plasma frequency must be much lower than the cyclotron frequency so that the B-field is strong enough to confine the emitting plasma. Based on these constraints, it can be shown that various beam

[1] If the radiation cones are not concentrated near the spin axis, we have $f_{\rm b,tot} \sim \Delta\theta$, where $\Delta\theta$ is the range of polar angles (with respect to the spin axis) occupied by the radiation cones of all bursts. The magnetic axis may be tilted with respect to the spin axis of the progenitor at a large angle. If the emission is from the polar cap regions at the magnetic poles (as in pulsars), we have $f_{\rm b,tot} \sim \Delta\theta \sim (R_*/R_{\rm LC})^{1/2} \simeq 4.6\times10^{-2} P_{-1}^{-1/2}$. On the other hand, if the emission region is not concentrated near the magnetic poles (as implied by the non-detection of periodicity from FRB 121102), then $\Delta\theta$ is a fairly large angle, which means $f_{\rm b,tot}$ may be of order unity.

instabilities proposed in the pulsar literature either do not grow or have too small growth rates at ∼GHz frequencies, which are many orders of magnitude lower than the plasma frequency and cyclotron frequency. By the process of elimination, we arrive at a unique solution for the FRB radiation mechanism — the coherent curvature emission. For pulsar radio emission, on the other hand, whose isotropic equivalent luminosity is lower than typical FRB luminosity a factor $\sim 10^{10}$, these constraints on the plasma frequency and cyclotron frequency become so weak that almost any emission radius within the light cylinder is viable and many beam instabilities may grow efficiently at ∼GHz frequencies.

We also note that the antenna mechanism for FRBs described in this thesis is significantly different from the antenna mechanism considered in the radio pulsar literature. In the latter case, people have invoked a fast primary beam colliding with a slower secondary plasma [62]. It is suggested that particle bunches form due to two-stream instability and then produce coherent curvature radiation. One of the major drawbacks with this proposal is that the density contrast between bunches and inter-bunch medium is small due to Coulomb repulsion within the bunch, which severely limits the ability of this process to explain radio pulsar emission [109].

The bunch formation process for FRBs we have proposed is a two-step process. Step one is formation of roughly charge-neutral clumps in the counter-streaming plasmas associated with strong current in the twisted magnetosphere of a magnetar. And the second step is charge separation of neu-

tral clumps by the strong E-field inside the current sheet associated with the magnetic reconnection process. This two-step process avoids the well-known problem that Coulomb repulsion prevents charge clumping. We also note that this two-step bunch formation process may only work for transients like FRBs but not for regular pulsars.

Chapter 8

Summary

In this thesis, we have described the constraints on possible radiation mechanisms for FRBs.

The extremely high brightness temperatures ($\gtrsim 10^{35}\,\mathrm{K}$) of FRBs require that the EM fields radiated by individual particles add up coherently. There are generally two classes of such processes: maser and the antenna mechanism. We consider collective plasma emission as a special type of maser (named plasma maser). We use the observational properties of the repeater FRB 121102 and general physical considerations to constrain the plasma conditions needed for each of the coherent processes. We find that various maser mechanisms require extremely fine-tuned plasma conditions or unphysical parameters as summarized below; only the antenna curvature mechanism operating near the surface of a magnetar is consistent with the high isotropic luminosity of the repeater FRB 121102.

Plasma masers in the magnetosphere of NSs can in principle operate when a beam of particles runs into a target plasma and subluminal waves are excited and amplified due to beam instabilities. However, we find that the cyclotron-Cherenkov (or anomalous Doppler) resonance condition cannot be

satisfied, because the B-field must be strong enough to confine the motion of plasma whose kinetic energy density must be at least as high as the FRB EM waves. The Cherenkov resonance condition can be satisfied, but the growth rate of the instability is too slow to be important for FRBs.

Vacuum curvature maser is possible only if the curved B-field is not confined in a plane. This can be achieved when the B-field lines have significant torsion, which could be caused by crustal motions at the NS surface. However, the absorption cross-section is negative only for O-mode waves propagating at an angle $\psi \lesssim \gamma^{-2}$ wrt the momentum vector of the emitting particle. The absorption cross-section becomes positive at larger angles, and for $\psi \sim \gamma^{-1}$ the cross-section is larger by at least a factor 10^5 compared with the peak cross-section for wave amplification at $\psi \sim \gamma^{-2}$. Due to the B-field curvature, photon trajectories will unavoidably intersect with other nearby B-field lines at larger angles, and then strong positive curvature self-absorption will prevent the radiation from escaping.

Vacuum synchrotron maser is possible only when the B-field is nearly uniform to within an angle $\lesssim \gamma^{-1}$ and particles' pitch-angle distribution is narrowly peaked with spread $\Delta\alpha \lesssim \gamma^{-1}$, where γ is the typical Lorentz factor of radiating particles in the comoving frame of the source plasma. In order for the electron cyclotron frequency to be in the radio band, the radiating plasma must be at a large distance $\gtrsim 10^{14}\,\mathrm{cm}$ from the central object. It is highly unlikely that the fine-tuned plasma conditions above can be realized during internal/external dissipations of an outflow at such large distances (much be-

yond the light cylinder of a NS).

For synchrotron maser near the effective Razin frequency of a relativistic plasma (due to internal/external dissipations of a relativistic outflow), the brightness temperature is limited by induced Compton scattering. To produce the observed brightness temperature $\gtrsim 10^{35}\,\mathrm{K}$, the radiation efficiency must be extremely low $f_{\rm r} \lesssim 5\times10^{-9}\epsilon_{\rm B}^{-19/16}$, where $\epsilon_{\rm B}$ is the fraction of energy density in B-fields in the emitting region. Moreover, it is unclear how the population inversion condition $\partial(N_\gamma/\gamma^2)/\partial\gamma > 0$ can be achieved *and maintained* when electrons lose energy to radiation (high-energy electrons radiate energy at a higher rate than low-energy ones and the population inversion is quickly destroyed unless it is actively maintained by some unknown process). Bunching in gyration phase may occur due to coherent reflection of incoming particles at quasi-perpendicular shocks with high magnetization, and hence maser emission may be produced when two consecutive shells ejected from the central engine collide. However, we show that the brightness temperature for such a maser mechanism is also limited by induced-Compton scattering. The observed FRB brightness temperature requires an extremely low radiation efficiency $f_{\rm r} \lesssim 4\times10^{-7}\mathcal{R}^{3/4}$, where $\mathcal{R}$ is the luminosity ratio of the two colliding shells.

We find that the basic properties of FRBs are consistent with the antenna mechanism, where charge bunches with longitudinal sizes $\lesssim \lambda$ move along the curved B-field lines with $B \gtrsim 10^{14}\,\mathrm{G}$ and produce coherent curvature emission. Similar to the situation in man-made antennas, the kinetic

energy of the radiating particles is minuscule and the radiative power is supplied by an E-field, which is produced by magnetic reconnection. We find that bunches can form via two-stream instability in the twisted magnetosphere of magnetars *before* the magnetic reconnection is triggered. Electric currents flow along the strong B-field lines of a magnetar whenever the field lines are twisted by crustal motions. These currents are carried by counter-streaming electrons and positrons. We have shown that two-stream instability leads to density fluctuations on length-scales longer than the effective plasma skin depth. A prediction of this curvature antenna model is that FRB analogs should exist at frequencies much higher than ∼GHz, up to mm or even far-infrared wavelengths (depending on the plasma distribution function). FRB analogs at higher frequencies are expected to be dimmer (due to smaller coherent volume) and have a lower occurring rate (due to smaller beaming angle).

The analysis presented in this thesis, and the identification of the most likely radiation mechanism for FRB 121102 (the curvature antenna mechanism) should apply to all those FRBs that have multiple outbursts like FRB 121102.

Based on the calculations presented in this thesis, the antenna mechanism seems to be the most promising candidate for the radiation process in FRBs. However, there are a number of technical issues that require closer scrutiny and further study: (1) pair creation and plasma distribution function in the twisted magnetosphere of magnetars; (2) the physics of radiative magnetic reconnection in the magnetosphere of magnetars; (3) propagation of

large amplitude radio waves (with non-linearity parameter $a_0 \gg 1$) through the magnetosphere of magnetars.

With forthcoming telescopes such as UTMOST [121], Apertif [122], CHIME [123] and SKA [124], the FRB sample is expected to grow by 2-3 orders of magnitude. Some of these wide field-of-view telescopes will be able to monitor 10-10^2 FRBs simultaneously and hence will be better at finding repeaters (which can then be localized). Observational search for analogs of FRBs at much higher frequencies (mm to far-infrared) would provide very useful test of the antenna mechanism and other radiation processes.

Appendices

Appendix A

Two-stream instability

We consider counter-streaming electrons and positrons with 1-D distribution function $f(u)$, where $u = \gamma\beta$ is the four velocity ($u > 0$ for electrons and $u < 0$ for positrons). We assume $f(u)$ to be symmetric $f(u) = f(-u)$ and normalized $\int_{-\infty}^{+\infty} f(u)\mathrm{d}u = 1$. The two streams have identical number densities $n_- = n_+ = n/2$, where n is the total number density in the lab frame. We take $c = 1$ and define the non-relativistic plasma frequency as

$$\omega_\mathrm{p} = (4\pi e^2 n/m_\mathrm{e})^{1/2}. \tag{A.1}$$

The following derivation is valid from non-relativistic to ultra-relativistic distribution functions.

The dispersion relation for longitudinal Langmuir waves of real wavenumber k and complex frequency ω is given by

$$1 = \int_{-\infty}^{+\infty} \frac{\omega_\mathrm{p}^2}{\gamma^3} \frac{f(u)}{(\omega - \beta k)^2} \mathrm{d}u = \int_{-1}^{+1} \omega_\mathrm{p}^2 \frac{f(\beta)}{(\omega - \beta k)^2} \mathrm{d}\beta, \tag{A.2}$$

which can be solved for any given distribution function $f(u)$. We plug the complex phase velocity $\omega/k = z + iy$ into eq. (A.2) and obtain two separate equations for two real unknowns z and y (from the real and imaginary parts

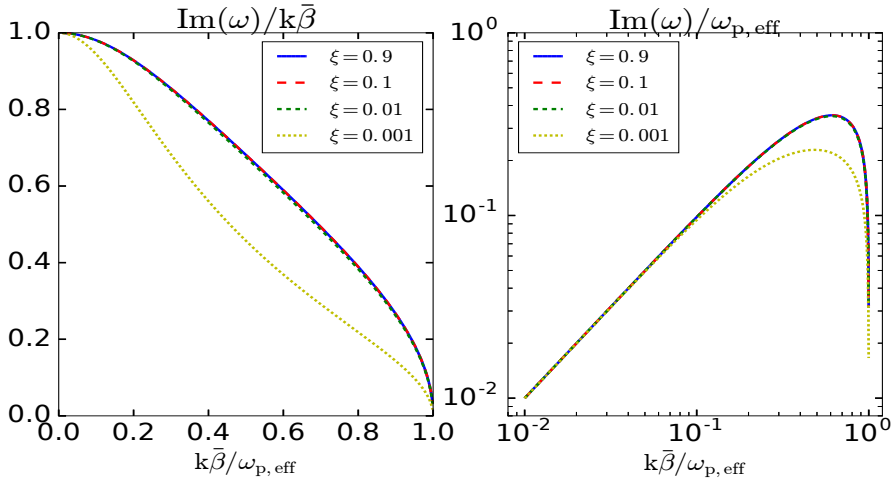

Figure A.1: The growth rate of two-stream instability for counter-streaming $e^{\pm}$ with "waterbag" (flat) distribution function between ξu_0 and u_0. Here we use $u_0 = 100\,(\approx \gamma_0)$. The geometric mean speed is defined as $\bar{\beta} = \sqrt{\beta_{\rm min}\beta_{\rm max}}$. The three cases with $\xi = 0.9, 0.1, 0.01$ are relativistic in that $\bar{\beta} \approx 1$ and the case with $\xi = 0.001$ has a fraction ($\sim u_0^{-1}$) of non-relativistic particles and $\bar{\beta} \sim 10^{-1/2}$. According to eq. (A.8), the maximum unstable wave-numbers for the four cases are $k_{\rm max}/(\omega_{\rm p}\gamma_0^{-3/2}) = 1.08$ ($\xi = 0.9$), 7.4 ($\xi = 0.1$), 65 ($\xi = 0.01$), 3.0×10^2 ($\xi = 0.001$). The fact that the curves overlap for the three relativistic cases ($\xi = 0.9$, 0.1, 0.01) do not mean the growth rates are the same, because $k_{\rm max}$ (or $\omega_{\rm p,eff}$) are different in these cases. The $\xi = 0.9$ case is close to mono-energetic distribution and the $\xi = 0.001$ case is close to Maxwell-Jüttner distribution with a low u cut-off.

of eq. A.2 respectively)

$$\begin{aligned} \frac{k^2}{\omega_{\rm p}^2} &= \int_{-1}^{+1} \frac{(z-\beta)^2 - y^2}{[(z+\beta)^2+y^2]^2} f(\beta) \mathrm{d}\beta, \\ 0 &= \int_{-1}^{+1} \frac{(z-\beta) y}{[(z+\beta)^2+y^2]^2} f(\beta) \mathrm{d}\beta. \end{aligned} \tag{A.3}$$

We are interested in $y > 0$ solutions which correspond to wave growth. If we make use of the symmetry $f(\beta) = f(-\beta)$, it can be shown that the second expression above can only be satisfied when $z = 0$. This means that only (purely imaginary or electrostatic) standing waves can grow via two-stream instability. Then the first expression in eq. (A.3) becomes

$$\frac{k^2}{\omega_{\rm p}^2} = 2 \int_0^1 \frac{\beta^2 - y^2}{[\beta^2+y^2]^2} f(\beta) \mathrm{d}\beta. \tag{A.4}$$

Our goal is to solve this equation for the growth rate $\mathrm{Im}(\omega) = yk$ under different distribution functions $f(\beta)$.

A simple but interesting case is the "waterbag" (or step-function) distribution given by two parameters $u_0 > 0$ and $0 \leq \xi < 1$

$$f(u) = \begin{cases} \frac{1}{2(1-\xi)u_0}, & \text{if } \xi u_0 < |u| < u_0, \\ 0, & \text{otherwise.} \end{cases} \tag{A.5}$$

This distribution has the property that, when $\xi \to 0$, it resembles the relativistic Maxwell-Jüttner distribution of temperature $T \sim u_0$ (in unit of $mc^2/k_{\rm B}$)

$$f_{\rm MJ} = \frac{1}{2K_1(T^{-1})} \mathrm{e}^{-\gamma/T}, \tag{A.6}$$

where $K_1(z)$ is the modified Bessel function of order one. On the other hand, when $\xi \to 1$, the distribution in eq. (A.5) describes two mono-energetic beams

running against each other. The particle injection in the twisted magnetosphere of magnetars may be somewhere in the middle of these two extreme cases ($0 < \xi < 1$).

We define the maximum and minimum Lorentz factors as $\gamma_{\rm max} \equiv \sqrt{1+u_0^2}$ and $\gamma_{\rm min} \equiv \sqrt{1+\xi^2 u_0^2}$ and the corresponding speeds as $\beta_{\rm max} \equiv u_0/\gamma_{\rm max}$ and $\beta_{\rm min} \equiv \xi u_0/\gamma_{\rm min}$. The analytical solution to eqs. (A.4) and (A.5) is

$$\left(\frac{{\rm Im}(\omega)}{k\beta_{\rm max}}\right)^2 = \frac{\sqrt{(1+r^2+a)^2+4r(a-r)}-(1+r^2+a)}{2}, \tag{A.7}$$

where

$$\begin{aligned}
&\omega_{\rm p,eff} \equiv \omega_{\rm p}\left[\frac{\beta_{\rm max}-\beta_{\rm min}}{(1-\xi)u_0}\right]^{1/2} = \omega_{\rm p}\langle\gamma^{-3}\rangle^{1/2},\\
&\langle\ldots\rangle = \int_{-\infty}^{+\infty}(\ldots)f(u){\rm d}u,\ r \equiv \frac{\beta_{\rm min}}{\beta_{\rm max}},\ a \equiv \frac{\omega_{\rm p,eff}^2}{k^2\beta_{\rm max}^2},\\
&k < k_{\rm max} \equiv \frac{\omega_{\rm p,eff}}{\bar{\beta}},\ \bar{\beta} = (\beta_{\rm min}\beta_{\rm max})^{1/2}.
\end{aligned} \tag{A.8}$$

Unstable Langmuir waves are possible only when $a > r$, which is equivalent to $k < k_{\rm max}$. As can be seen in Fig. A.1, the growth rate ${\rm Im}(\omega)$ at very small wave-number $k \ll k_{\rm max}$ equals to $k\bar{\beta}$; the growth rate near the maximum wave-number $k \sim k_{\rm max}$ roughly equals to $\omega_{\rm p,eff}/\bar{\beta}$. In the limiting case of $\xi \to 0$ (or Maxwell-Jüttner distribution), we have $\bar{\beta} = 0$ ($k_{\rm max} \to 0$), so the growth rate at any wave-number k is zero, which is expected because the system is already in equilibrium.

The effective plasma frequency is $\omega_{\rm p,eff} = \omega_{\rm p}\langle\gamma^{-3}\rangle^{1/2}$ and the effective skin depth is $\ell_{\rm skin,eff} \equiv k_{\rm max}^{-1} = \bar{\beta}/\omega_{\rm p,eff}$. For mono-energetic ultra-relativistic

case ($\xi \approx 1$ and $\gamma_0 \approx u_0 \gg 1$), we have $\omega_{\rm p,eff} \approx \omega_{\rm p}\gamma_0^{-3/2}$. For a broad but ultra-relativistic distribution ($\xi \ll 1$ and $\gamma_{\rm min} \approx \xi u_0 \gg 1$), we have $\omega_{\rm p,eff} \approx \omega_{\rm p}(2\gamma_{\rm min}^2\gamma_0)^{-1/2} = \omega_{\rm p}\gamma_0^{-3/2}/(\sqrt{2}\,\xi)$, which is significantly greater (by a factor of $\sim \xi^{-1}$) than that in the mono-energetic case.

Appendix B

Dynamics of external shocks

When a relativistic outflow of isotropic equivalent energy $E_{\rm iso}$ and Lorentz factor Γ ploughs its way through the cold circumstellar medium (CSM), two shocks form in this process, the forward shock going into the CSM and the reverse shock going into the ejecta. The bolometric emission from the outflow peaks roughly when the ejecta reaches the deceleration radius $r_{\rm dec}$, which is given by

$$E_{\rm iso} \sim \Gamma^2 m_p c^2 \int^{r_{\rm dec}} 4\pi r^2 n_{\rm CSM}(r) {\rm d}r. \tag{B.1}$$

In the observer's frame, the typical emission timescale is the deceleration time $t_{\rm dec} \simeq r_{\rm dec}/(2\Gamma^2 c)$.

In the following, we assume a power-law density profile $n_{\rm CSM} \propto r^{-k}$ (our discussion can be generalized to an arbitrary density profile). After the deceleration time, the Lorentz factor of the forward shock decreases with radius as a power-law $\Gamma(r/r_{\rm dec})^{(k-3)/2}$ [127] before it decelerates to Newtonian speeds. The emission from the forward-shocked region decreases with time as a power-law. For some FRBs without significant scattering broadening, we usually see a sharp cuf-off instead of a power-law at the end of the burst. On the other hand, the emission from the reverse shock may have a sharp cut-off due to

adiabatic sideway expansion after the reverse shock crosses the ejecta.

Now we consider a second outflow with a similar initial Lorentz factor $\sim \Gamma$ but launched with a delay of $t_{\rm dec} \ll t_{\rm delay} \ll r_{\rm dec}/c$ wrt the first outflow. We note that the time intervals between some burst pairs from FRB 121102 can be as short at $\sim 30\,{\rm ms}$ to $40\,{\rm ms}$ [98, 130], so the CSM does not have time to recover to its original undisturbed state after the first outflow passed by. When the second outflow catches up with the first one, if the first one is still ultra-relativistic, then the catch-up radius $r_{\rm c}$ is can be estimated by

$$2ct_{\rm delay}\Gamma^2(r_{\rm c}/r_{\rm dec})^{k-3} \simeq r_{\rm c} - ct_{\rm delay} \simeq r_{\rm c}, \tag{B.2}$$

i.e.

$$r_{\rm c} \simeq r_{\rm dec}(t_{\rm delay}/t_{\rm dec})^{1/(4-k)}, \tag{B.3}$$

This means that the second FRB will have a longer duration than the first one by a factor of $(t_{\rm delay}/t_{\rm dec})^{1/(4-k)}$, where $t_{\rm dec}$ is the duration of the first FRB. If the first outflow has decelerated to a Newtonian speed when it is caught up by the second one, the duration of the second FRB is determined by the radius where the first outflow becomes Newtonian $r_{\rm N}$ ($\gg r_{\rm dec}$) divided by $2\Gamma^2 c$. Still, the duration of the second FRB should be much longer than the first one. This is inconsistent with observations. For instance, the two bursts detected by Ref. [98], "GBT-1" and "GBT-2", were separated by $\sim 40\,{\rm ms}$ and they have very similar durations of $\sim 2\,{\rm ms}$.

Appendix C

Induced Compton scattering

We consider a spatially uniform electron-radiation mixture. The electron distribution function is isotropic and mono-energetic with Lorentz factor γ and number density $n_{\rm e}$ (a distribution of Lorentz factors will be considered later). The radiation field is also isotropic with intensity I_ν only a function of frequency ν. In terms of the distribution function of the radiation field $f(\boldsymbol{r}, \boldsymbol{p}, t)$, the photon occupation number $\widetilde{f}$ is defined as the number of photons in a phase-space volume h^3 (h being the Planck constant) and we have

$$\widetilde{f} \equiv h^3 f(\boldsymbol{r}, \boldsymbol{p}, t) = \frac{I_\nu c^2}{2h\nu^3}. \tag{C.1}$$

We are interested in the time evolution of the photon occupation number $\widetilde{f}_0 \equiv \widetilde{f}(\nu_0, \boldsymbol{\Omega}_0)$ at a given frequency ν_0 along a given direction $\boldsymbol{\Omega}_0$ due to induced (or stimulated) Compton scattering in the regime $\widetilde{f} \gg 1$.

We consider a subgroup of electrons moving in the $\hat{\boldsymbol{z}}$ direction within an infinitesimal solid angle $\mathrm{d}\Omega_{\rm e}$. The angle between $\boldsymbol{\Omega}_0$ and $\hat{\boldsymbol{z}}$ is denoted as $\theta_{\rm e}$. The number density of these electrons in their comoving frame is $\mathrm{d}n'_{\rm e} = n_{\rm e}\mathrm{d}\Omega_{\rm e}/(4\pi\gamma)$. Hereafter, all quantities in the electrons' comoving frame are denoted with a prime ($'$) and the unprimed quantities are measured in the lab frame.

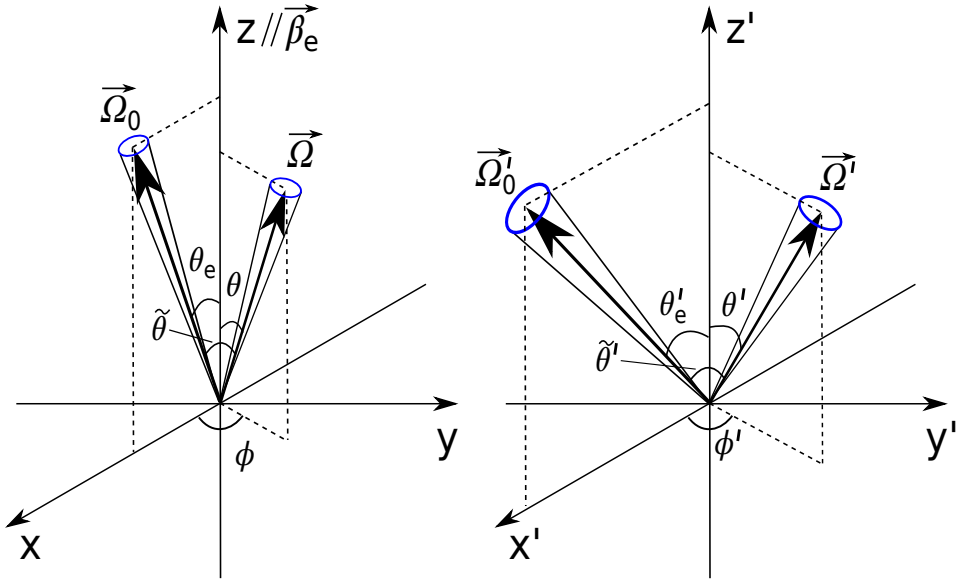

Figure C.1: Geometry for induced Compton scattering. In the lab frame (left panel), we consider the time evolution of the intensity in the given direction $\mathbf{\Omega}_0$ due to induced Compton scattering from and into other directions $\mathbf{\Omega}(\theta, \phi)$. The polar coordinate system has polar axis aligned with electrons' velocity vector $\boldsymbol{\beta}_e$. We put $\mathbf{\Omega}_0$ in the x-z plane. The angle between $\mathbf{\Omega}_0$ and $\boldsymbol{\beta}_e$ is denoted as θ_e and the angle between $\mathbf{\Omega}_0$ and $\mathbf{\Omega}$ is $\widetilde{\theta}$. The calculation is done in the comoving frame of electrons (right panel), where all quantities are denoted with a prime ($'$).

As shown in the right panel (comoving frame) of Fig. C.1, photons originally moving near the $\boldsymbol{\Omega}_0'$ direction can be scattered to an arbitrary direction $\boldsymbol{\Omega}'$ and there will also be photons scattered from $\boldsymbol{\Omega}'$ back to $\boldsymbol{\Omega}_0'$. The direction $\boldsymbol{\Omega}'$ is given by two angles (θ', ϕ') in a polar coordinate system with polar axis $\boldsymbol{z}$ aligned with electrons' velocity vector $\boldsymbol{\beta}_{\rm e}$ in the lab frame. In this coordinate system, the direction $\boldsymbol{\Omega}_0'$ is taken to be in the x'-z' plane, given by $(\theta' = \theta_{\rm e}', \phi' = 0)$. The angle between $\boldsymbol{\Omega}'$ and $\boldsymbol{\Omega}_0'$ is denoted as $\widetilde{\theta}'$ (and $\widetilde{\mu}' \equiv \cos\widetilde{\theta}'$).

For convenience, we define two Doppler factors

$$\begin{aligned} &\mathcal{D} = \gamma(1+\beta\mu'),\ \mathcal{D}_{\rm e} = \gamma(1+\beta\mu_{\rm e}'), \\ &\mu' \equiv \cos\theta',\ \mu_{\rm e}' \equiv \cos\theta_{\rm e}', \end{aligned} \tag{C.2}$$

and then the Lorentz transformation of frequencies and angles are given by

$$\begin{aligned} &\nu' = \nu/\mathcal{D},\ \nu_0' = \nu_0/\mathcal{D}_{\rm e},\ \phi' = \phi, \\ &\mu' = \frac{\mu-\beta}{1-\beta\mu},\ \mu_{\rm e}' = \frac{\mu_{\rm e}-\beta}{1-\beta\mu_{\rm e}},\ {\rm d}\mu_{\rm e}' = \mathcal{D}_{\rm e}^2 {\rm d}\mu_{\rm e}. \end{aligned} \tag{C.3}$$

The photon occupation number $\widetilde{f}$ is Lorentz invariant. The rate of change in $\widetilde{f}_0 \equiv \widetilde{f}(\nu_0', \boldsymbol{\Omega}_0') = \widetilde{f}(\nu_0, \boldsymbol{\Omega}_0)$ in the comoving frame is given by [135]

$$\frac{{\rm d}(\ln\widetilde{f}_0)}{{\rm d}t'} = \frac{3hc\sigma_{\rm T}}{8\pi m_{\rm e}c^2} {\rm d}n_{\rm e}' \int {\rm d}\Omega' (1+\widetilde{\mu}'^2)(1-\widetilde{\mu}') \left.\frac{\partial(\nu'^2\widetilde{f})}{\partial\nu'}\right|_{\nu_0'}, \tag{C.4}$$

where $\sigma_{\rm T}$ is the Thomson cross-section.

From ${\rm d}\nu' = {\rm d}\nu/\mathcal{D}(\mu')$ (for a given direction $\boldsymbol{\Omega}'$), we obtain

$$\begin{aligned} \left.\frac{\partial[\nu'^2\widetilde{f}(\nu',\boldsymbol{\Omega}')]}{\partial\nu'}\right|_{\nu_0'} &= \frac{1}{\mathcal{D}} \left.\frac{\partial[\nu^2\widetilde{f}(\nu)]}{\partial\nu}\right|_{\nu=\nu_0'\mathcal{D}=\nu_0\mathcal{D}/\mathcal{D}_{\rm e}} \\ &= \frac{c^2}{2h\mathcal{D}} \left.\frac{\partial(I_\nu/\nu)}{\partial\nu}\right|_{\nu=\nu_0\mathcal{D}/\mathcal{D}_{\rm e}}. \end{aligned} \tag{C.5}$$

To compute the time evolution of $\widetilde{f}_0$ due to the scattering of all electrons, we need to integrate eq. (C.4) over the electrons' angle distribution

$$\int \mathrm{d}n'_{\mathrm{e}}(\ldots) = \frac{n_{\mathrm{e}}}{4\pi\gamma}\int \mathrm{d}\Omega_{\mathrm{e}}(\ldots) = \frac{n_{\mathrm{e}}}{2\gamma}\int_{-1}^{1}\mathrm{d}\mu'_{\mathrm{e}}\mathcal{D}_{\mathrm{e}}^{-2}(\ldots), \tag{C.6}$$

where we have made use of the fact that $(\ldots)$ has no ϕ_{e} dependence (due to the symmetry of the system) and $\mathrm{d}\mu_{\mathrm{e}} = \mathrm{d}\mu'_{\mathrm{e}}/\mathcal{D}_{\mathrm{e}}^2$. Then, we use $\mathrm{d}t' = \mathrm{d}t/\gamma$ and write out the full integral explicitly

$$\begin{aligned}\frac{\mathrm{d}(\ln\widetilde{f}_0)}{\mathrm{d}t} = \frac{c^2}{2m_{\mathrm{e}}c^2}\frac{3cn_{\mathrm{e}}\sigma_{\mathrm{T}}}{16\pi\gamma^2}\int_{-1}^{1}\mathrm{d}\mu'_{\mathrm{e}}\mathcal{D}_{\mathrm{e}}^{-2}\int_{-1}^{1}\mathrm{d}\mu'\mathcal{D}^{-1}\\ \cdot\int_0^{2\pi}\mathrm{d}\phi'(1+\widetilde{\mu}'^2)(1-\widetilde{\mu}')\left.\frac{\partial(I_\nu/\nu)}{\partial\nu}\right|_{\nu=\nu_0\mathcal{D}/\mathcal{D}_{\mathrm{e}}},\end{aligned} \tag{C.7}$$

where

$$\widetilde{\mu}' = \sin\theta'_{\mathrm{e}}\sin\theta'\cos\phi' + \mu'_{\mathrm{e}}\mu'. \tag{C.8}$$

In the limit where electrons are at rest ($\beta = 0, \gamma = 1, \mathcal{D} = \mathcal{D}_{\mathrm{e}} = 1$), we have $\int\mathrm{d}\mu'\int\mathrm{d}\phi'(1+\widetilde{\mu}'^2)(1-\widetilde{\mu}') = 16\pi/3$ and the classical result is recovered

$$\frac{\mathrm{d}(\ln\widetilde{f}_0)}{\mathrm{d}t} = \frac{c^2}{2m_{\mathrm{e}}c^2}cn_{\mathrm{e}}\sigma_{\mathrm{T}}\left.\frac{\partial(I_\nu/\nu)}{\partial\nu}\right|_{\nu_0}. \tag{C.9}$$

In the ultra-relativistic regime $\gamma \gg 1$, the factor $\int\mathrm{d}\phi'(1+\widetilde{\mu}'^2)$ roughly gives $8\pi/3$ (with error of order unity) and is hence not important in our order-of-magnitude estimate. In the following, we also drop the term $\sin\theta'_{\mathrm{e}}\sin\theta'\cos\phi'$ in $\widetilde{\mu}'$ because it is an odd function of $\cos\phi'$ and $\int\mathrm{d}\phi'\cos\phi' = 0$.

If the system has length-scale ℓ, the Thomson optical depth is $\tau_{\mathrm{T}} = \ell\sigma_{\mathrm{T}}n_{\mathrm{e}}$. After a light-crossing time ℓ/c, the photon occupation number changes

by a factor of $e^{\tau_{\rm eff}}$, where the effective optical depth is roughly given by

$$\tau_{\rm eff} \sim \frac{c^2\tau_{\rm T}}{4\gamma^2 m_{\rm e}c^2}\int_{-1}^{1}\frac{{\rm d}\mu'_{\rm e}}{\mathcal{D}_{\rm e}^2}\int_{-1}^{1}\frac{{\rm d}\mu'(1-\mu'_{\rm e}\mu')}{\mathcal{D}}\left.\frac{\partial(I_\nu/\nu)}{\partial\nu}\right|_{\frac{\mathcal{D}\nu_0}{\mathcal{D}_{\rm e}}}, \tag{C.10}$$

We note that, due to induced Compton scattering, the radiation field $I_\nu(\nu_0, \mathbf{\Omega}_0)$ is in principle coupled with the derivative of I_ν/ν in all other directions and at a wide range of frequencies $\mathcal{D}\nu_0/\mathcal{D}_{\rm e} \in (\gamma^{-1}\nu_0, \gamma\nu_0)$. Thus, the effective optical depth is sensitive not only to γ but also to the spectral broadness.

In the following, we discuss two extreme cases: (i) a narrow step-function or Gaussian spectrum with $\Delta\nu/\nu_0 \sim 1$ and (ii) a broad power-law spectrum in the range $\nu/\nu_0 \in (\gamma^{-1}, \gamma)$.

In case (i), the integral in eq. (C.10) is non-zero only when $\mathcal{D} \sim \mathcal{D}_{\rm e}$. In the range $\mu'_{\rm e} \in (-1, -1+\gamma^{-2})$, we can estimate $\mathcal{D} \sim \mathcal{D}_{\rm e} \sim \gamma^{-1}$, $\Delta\mu' \sim \gamma^{-2}$, $1-\mu'_{\rm e}\mu' \sim \gamma^{-2}$, and hence the contribution to the integral is roughly $\sim \gamma^{-3} I_{\nu_0}/\nu_0^2$. In the range where $\mu'_{\rm e}$ is far from -1 ($\Delta\mu'_{\rm e} \sim 1$), we can estimate $\mathcal{D} \sim \mathcal{D}_{\rm e} \sim \gamma$, $\Delta\mu' \sim 1$, $1-\mu'_{\rm e}\mu' \sim 1$, and hence the contribution to the integral is $\sim \gamma^{-3} I_{\nu_0}/\nu_0^2$. We define the brightness temperature $T_{\rm B}$ at ν_0 as

$$I_{\nu_0} = \frac{2\nu_0^2 k_{\rm B} T_{\rm B}}{c^2} \quad\Longrightarrow\quad k_{\rm B}T_{\rm B} = \frac{c^2 I_{\nu_0}}{2\nu_0^2}. \tag{C.11}$$

Then the effective optical depth is roughly

$$\tau_{\rm eff} \sim \frac{k_{\rm B}T_{\rm B}}{m_{\rm e}c^2}\frac{\tau_{\rm T}}{\gamma^5}. \tag{C.12}$$

In case (ii), we assume that the spectrum is a single power-law $I_\nu \propto \nu^p$ ($p \neq 1$) with normalization given by the brightness temperature at ν_0 as in eq.

(C.11). Then we have

$$\left.\frac{\partial(I_\nu/\nu)}{\partial\nu}\right|_{\mathcal{D}\nu_0/\mathcal{D}_\mathrm{e}} = (p-1)\frac{2k_\mathrm{B}T_\mathrm{b}(\nu_0)}{c^2}\left(\frac{\mathcal{D}}{\mathcal{D}_\mathrm{e}}\right)^{p-2}, \tag{C.13}$$

and the effective optical depth becomes

$$\begin{aligned}\tau_\mathrm{eff} &\sim \frac{(p-1)}{2}\frac{k_\mathrm{B}T_\mathrm{b}(\nu_0)}{m_\mathrm{e}c^2}\frac{\tau_\mathrm{T}}{\gamma^2}\cdot Q,\\ Q &\equiv \int_{-1}^{1}\mathrm{d}\mu'_\mathrm{e}[\mathcal{D}_\mathrm{e}(\mu'_\mathrm{e})]^{-p}\int_{-1}^{1}\mathrm{d}\mu'(1-\mu'_\mathrm{e}\mu')[\mathcal{D}(\mu')]^{p-3}.\end{aligned} \tag{C.14}$$

When $p<1$, we have $\tau_\mathrm{eff}<0$ and $\widetilde{f}_0$ decreases with time exponentially; when $p>1$, we have $\tau_\mathrm{eff}>0$ and $\widetilde{f}_0$ increases with time exponentially. We integrate eq. (C.14) analytically and obtain

$$Q\sim\begin{cases}\gamma^{1-2p}, & \text{if } p<1.5,\\ \gamma^{2p-5}, & \text{if } p>1.5.\end{cases} \tag{C.15}$$

For $p=1.5$ (a rising spectrum), the integral reaches the minimum $Q_\mathrm{min}\sim\gamma^{-2}$, which means $|\tau_\mathrm{eff}|\sim\gamma^{-4}\tau_\mathrm{T}(k_\mathrm{B}T_\mathrm{b}/m_\mathrm{e}c^2)$. For a flat spectrum $I_\nu\propto\nu^0$ (or $p=0$), we have $Q\sim\gamma$ and hence $|\tau_\mathrm{eff}|\sim\gamma^{-1}\tau_\mathrm{T}(k_\mathrm{B}T_\mathrm{b}/m_\mathrm{e}c^2)$. Above the peak of the spectral energy distribution $p<-1$, we have $Q\gtrsim\gamma^3$ and $|\tau_\mathrm{eff}|\gtrsim\gamma\tau_\mathrm{T}(k_\mathrm{B}T_\mathrm{b}/m_\mathrm{e}c^2)$, which means the photon occupation number (and hence flux) $\widetilde{f}_0$ drops even more quickly than in the flat-spectrum case. The net effect is that the peak of the spectrum moves towards lower and lower frequencies and the radiation energy is transferred to the kinetic energy of electrons.

Observationally, the spectrum of FRBs may or may not be broad. We note that co-detections at multiple telescopes operating at different frequencies

(e.g. 1.4 and 3 GHz) have been reported by Ref. [17] and [98]. In this paper (eq. 5.13), we take the most conservative limit $Q \sim \gamma^{-3}$ (for a narrow spectrum with $\Delta\nu/\nu_0 \sim 1$) and hence $|\tau_{\rm eff}| \gtrsim \gamma^{-5}\tau_{\rm T}(k_{\rm B}T_{\rm b}/m_{\rm e}c^2)$. For any spectra broader than $\Delta\nu/\nu_0 \sim 1$, the effective optical depth $|\tau_{\rm eff}|$ will be larger and hence induced Compton scattering will be more efficient.

Finally, we integrate eq. (C.14) over the (normalized) Lorentz factor distribution of electrons $\widetilde{N}_\gamma \equiv {\rm d}\widetilde{N}/{\rm d}\gamma$ ($\int_1^\infty \widetilde{N}_\gamma {\rm d}\gamma = 1$) and obtain the total effective optical depth

$$\tau_{\rm eff,tot} \gtrsim \frac{k_{\rm B}T_{\rm b}(\nu_0)}{m_{\rm e}c^2}\tau_{\rm T}\int_1^\infty \gamma^{-5}\widetilde{N}_\gamma {\rm d}\gamma. \tag{C.16}$$

We see that the contribution from high-energy electrons are strongly suppressed by the γ^{-5} factor. In realistic dissipations caused by shocks or magnetic reconnection, the distribution function is usually a power-law $\widetilde{N}_\gamma \propto \gamma^{-q}$ ($q > 1$) above the peak Lorentz factor, which is also roughly the mean Lorentz factor $\bar{\gamma}$, but the part below the peak Lorentz factor may be uncertain. In the case of a Maxwell-Jüttner distribution, we have $\widetilde{N}_\gamma \propto \gamma^2$ and hence most of the contribution comes from electrons near the lowest Lorentz factors ~ 1 and $\int \gamma^{-5}\widetilde{N}_\gamma {\rm d}\gamma \sim \bar{\gamma}^{-3}$. On the other hand, in the case of an infinitely sharp cut-off below the peak Lorentz factor, we have $\int \gamma^{-5}\widetilde{N}_\gamma {\rm d}\gamma \sim \bar{\gamma}^{-5}$. In this paper, we use the result in the latter (most conservative) case.

Bibliography

[1] D. R. Lorimer, M. Bailes, M. A. McLaughlin, D. J. Narkevic, and F. Crawford. A Bright Millisecond Radio Burst of Extragalactic Origin. *Science*, 318:777, November 2007.

[2] S. R. Kulkarni, E. O. Ofek, J. D. Neill, Z. Zheng, and M. Juric. Giant Sparks at Cosmological Distances? *ApJ*, 797:70, December 2014.

[3] D. Thornton, B. Stappers, M. Bailes, B. Barsdell, S. Bates, N. D. R. Bhat, M. Burgay, S. Burke-Spolaor, D. J. Champion, P. Coster, N. D'Amico, A. Jameson, S. Johnston, M. Keith, M. Kramer, L. Levin, S. Milia, C. Ng, A. Possenti, and W. van Straten. A Population of Fast Radio Bursts at Cosmological Distances. *Science*, 341:53–56, July 2013.

[4] E. Petroff, M. Bailes, E. D. Barr, B. R. Barsdell, N. D. R. Bhat, F. Bian, S. Burke-Spolaor, M. Caleb, D. Champion, P. Chandra, G. Da Costa, C. Delvaux, C. Flynn, N. Gehrels, J. Greiner, A. Jameson, S. Johnston, M. M. Kasliwal, E. F. Keane, S. Keller, J. Kocz, M. Kramer, G. Leloudas, D. Malesani, J. S. Mulchaey, C. Ng, E. O. Ofek, D. A. Perley, A. Possenti, B. P. Schmidt, Y. Shen, B. Stappers, P. Tisserand, W. van Straten, and C. Wolf. A real-time fast radio burst: polarization detection and multiwavelength follow-up. *MNRAS*, 447:246–255, February 2015.

[5] A. Rane, D. R. Lorimer, S. D. Bates, N. McMann, M. A. McLaughlin, and K. Rajwade. A search for rotating radio transients and fast radio bursts in the Parkes high-latitude pulsar survey. *MNRAS*, 455:2207–2215, January 2016.

[6] D. J. Champion, E. Petroff, M. Kramer, M. J. Keith, M. Bailes, E. D. Barr, S. D. Bates, N. D. R. Bhat, M. Burgay, S. Burke-Spolaor, C. M. L. Flynn, A. Jameson, S. Johnston, C. Ng, L. Levin, A. Possenti, B. W. Stappers, W. van Straten, D. Thornton, C. Tiburzi, and A. G. Lyne. Five new fast radio bursts from the HTRU high-latitude survey at Parkes: first evidence for two-component bursts. *MNRAS*, 460:L30–L34, July 2016.

[7] L. G. Spitler, J. M. Cordes, J. W. T. Hessels, D. R. Lorimer, M. A. McLaughlin, S. Chatterjee, F. Crawford, J. S. Deneva, V. M. Kaspi, R. S. Wharton, B. Allen, S. Bogdanov, A. Brazier, F. Camilo, P. C. C. Freire, F. A. Jenet, C. Karako-Argaman, B. Knispel, P. Lazarus, K. J. Lee, J. van Leeuwen, R. Lynch, S. M. Ransom, P. Scholz, X. Siemens, I. H. Stairs, K. Stovall, J. K. Swiggum, A. Venkataraman, W. W. Zhu, C. Aulbert, and H. Fehrmann. Fast Radio Burst Discovered in the Arecibo Pulsar ALFA Survey. *ApJ*, 790:101, August 2014.

[8] L. G. Spitler, P. Scholz, J. W. T. Hessels, S. Bogdanov, A. Brazier, F. Camilo, S. Chatterjee, J. M. Cordes, F. Crawford, J. Deneva, R. D. Ferdman, P. C. C. Freire, V. M. Kaspi, P. Lazarus, R. Lynch, E. C.

Madsen, M. A. McLaughlin, C. Patel, S. M. Ransom, A. Seymour, I. H. Stairs, B. W. Stappers, J. van Leeuwen, and W. W. Zhu. A repeating fast radio burst. *Nature*, 531:202–205, March 2016.

[9] S. Chatterjee, C. J. Law, R. S. Wharton, S. Burke-Spolaor, J. W. T. Hessels, G. C. Bower, J. M. Cordes, S. P. Tendulkar, C. G. Bassa, P. Demorest, B. J. Butler, A. Seymour, P. Scholz, M. W. Abruzzo, S. Bogdanov, V. M. Kaspi, A. Keimpema, T. J. W. Lazio, B. Marcote, M. A. McLaughlin, Z. Paragi, S. M. Ransom, M. Rupen, L. G. Spitler, and H. J. van Langevelde. A direct localization of a fast radio burst and its host. *Nature*, 541:58–61, January 2017.

[10] B. Marcote, Z. Paragi, J. W. T. Hessels, A. Keimpema, H. J. van Langevelde, Y. Huang, C. G. Bassa, S. Bogdanov, G. C. Bower, S. Burke-Spolaor, B. J. Butler, R. M. Campbell, S. Chatterjee, J. M. Cordes, P. Demorest, M. A. Garrett, T. Ghosh, V. M. Kaspi, C. J. Law, T. J. W. Lazio, M. A. McLaughlin, S. M. Ransom, C. J. Salter, P. Scholz, A. Seymour, A. Siemion, L. G. Spitler, S. P. Tendulkar, and R. S. Wharton. The Repeating Fast Radio Burst FRB 121102 as Seen on Milliarcsecond Angular Scales. *ApJL*, 834:L8, January 2017.

[11] Planck Collaboration, P. A. R. Ade, N. Aghanim, M. Arnaud, M. Ashdown, J. Aumont, C. Baccigalupi, A. J. Banday, R. B. Barreiro, J. G. Bartlett, and et al. Planck 2015 results. XIII. Cosmological parameters. *A&A*, 594:A13, September 2016.

[12] S. P. Tendulkar, C. G. Bassa, J. M. Cordes, G. C. Bower, C. J. Law, S. Chatterjee, E. A. K. Adams, S. Bogdanov, S. Burke-Spolaor, B. J. Butler, P. Demorest, J. W. T. Hessels, V. M. Kaspi, T. J. W. Lazio, N. Maddox, B. Marcote, M. A. McLaughlin, Z. Paragi, S. M. Ransom, P. Scholz, A. Seymour, L. G. Spitler, H. J. van Langevelde, and R. S. Wharton. The Host Galaxy and Redshift of the Repeating Fast Radio Burst FRB 121102. *ApJL*, 834:L7, January 2017.

[13] C. G. Bassa, S. P. Tendulkar, E. A. K. Adams, N. Maddox, S. Bogdanov, G. C. Bower, S. Burke-Spolaor, B. J. Butler, S. Chatterjee, J. M. Cordes, J. W. T. Hessels, V. M. Kaspi, C. J. Law, B. Marcote, Z. Paragi, S. M. Ransom, P. Scholz, L. G. Spitler, and H. J. van Langevelde. FRB 121102 Is Coincident with a Star-forming Region in Its Host Galaxy. *ApJL*, 843:L8, July 2017.

[14] B. D. Metzger, E. Berger, and B. Margalit. Millisecond Magnetar Birth Connects FRB 121102 to Superluminous Supernovae and Long-duration Gamma-Ray Bursts. *ApJ*, 841:14, May 2017.

[15] J. I. Katz. Coherent emission in fast radio bursts. *Phys. Rev. D*, 89(10):103009, May 2014.

[16] P. Scholz, L. G. Spitler, J. W. T. Hessels, S. Chatterjee, J. M. Cordes, V. M. Kaspi, R. S. Wharton, C. G. Bassa, S. Bogdanov, F. Camilo, F. Crawford, J. Deneva, J. van Leeuwen, R. Lynch, E. C. Madsen, M. A.

McLaughlin, M. Mickaliger, E. Parent, C. Patel, S. M. Ransom, A. Seymour, I. H. Stairs, B. W. Stappers, and S. P. Tendulkar. The Repeating Fast Radio Burst FRB 121102: Multi-wavelength Observations and Additional Bursts. *ApJ*, 833:177, December 2016.

[17] C. J. Law, M. W. Abruzzo, C. G. Bassa, G. C. Bower, S. Burke-Spolaor, B. J. Butler, T. Cantwell, S. H. Carey, S. Chatterjee, J. M. Cordes, P. Demorest, J. Dowell, R. Fender, K. Gourdji, K. Grainge, J. W. T. Hessels, J. Hickish, V. M. Kaspi, T. J. W. Lazio, M. A. McLaughlin, D. Michilli, K. Mooley, Y. C. Perrott, S. M. Ransom, N. Razavi-Ghods, M. Rupen, A. Scaife, P. Scott, P. Scholz, A. Seymour, L. G. Spitler, K. Stovall, S. P. Tendulkar, D. Titterington, R. S. Wharton, and P. K. G. Williams. A Multi-telescope Campaign on FRB 121102: Implications for the FRB Population. *ApJ*, 850:76, November 2017.

[18] J. Luan and P. Goldreich. Physical Constraints on Fast Radio Bursts. *ApJL*, 785:L26, April 2014.

[19] K. Masui, H.-H. Lin, J. Sievers, C. J. Anderson, T.-C. Chang, X. Chen, A. Ganguly, M. Jarvis, C.-Y. Kuo, Y.-C. Li, Y.-W. Liao, M. McLaughlin, U.-L. Pen, J. B. Peterson, A. Roman, P. T. Timbie, T. Voytek, and J. K. Yadav. Dense magnetized plasma associated with a fast radio burst. *Nature*, 528:523–525, December 2015.

[20] J. M. Cordes, R. S. Wharton, L. G. Spitler, S. Chatterjee, and I. Wasserman. Radio Wave Propagation and the Provenance of Fast Radio

Bursts. *ArXiv e-prints*, May 2016.

[21] S. Xu and B. Zhang. On the Origin of the Scatter Broadening of Fast Radio Burst Pulses and Astrophysical Implications. *ApJ*, 832:199, December 2016.

[22] V. Ravi. The observed properties of Fast Radio Bursts. *ArXiv e-prints*, October 2017.

[23] J.-P. Macquart and J. Y. Koay. Temporal Smearing of Transient Radio Sources by the Intergalactic Medium. *ApJ*, 776:125, October 2013.

[24] E. Petroff, E. D. Barr, A. Jameson, E. F. Keane, M. Bailes, M. Kramer, V. Morello, D. Tabbara, and W. van Straten. FRBCAT: The Fast Radio Burst Catalogue. *PASA*, 33:e045, September 2016.

[25] W. Lu and P. Kumar. A universal EDF for repeating fast radio bursts? *MNRAS*, 461:L122–L126, September 2016.

[26] J. van Leeuwen. ARTS – the Apertif Radio Transient System. In P. R. Wozniak, M. J. Graham, A. A. Mahabal, and R. Seaman, editors, *The Third Hot-wiring the Transient Universe Workshop*, pages 79–79, 2014.

[27] L. C. Oostrum, J. van Leeuwen, J. Attema, W. van Cappellen, L. Connor, B. Hut, Y. Maan, T. A. Oosterloo, E. Petroff, D. van der Schuur, A. Sclocco, and M. A. W. Verheijen. Detection of a bright burst from FRB 121102 with Apertif at the Westerbork Synthesis Radio Telescope. *The Astronomer's Telegram*, 10693, September 2017.

[28] P. Madau and M. Dickinson. Cosmic Star-Formation History. *ARA&A*, 52:415–486, August 2014.

[29] D. B. Melrose. Coherent emission mechanisms in astrophysical plasmas. *Reviews of Modern Plasma Physics*, 1:5, December 2017.

[30] T. Totani. Cosmological Fast Radio Bursts from Binary Neutron Star Mergers. *PASJ*, 65:L12, October 2013.

[31] K. Kashiyama, K. Ioka, and P. Mészáros. Cosmological Fast Radio Bursts from Binary White Dwarf Mergers. *ApJL*, 776:L39, October 2013.

[32] H. Falcke and L. Rezzolla. Fast radio bursts: the last sign of supramassive neutron stars. *A&A*, 562:A137, February 2014.

[33] B. Zhang. A Possible Connection between Fast Radio Bursts and Gamma-Ray Bursts. *ApJL*, 780:L21, January 2014.

[34] J. Fuller and C. D. Ott. Dark matter-induced collapse of neutron stars: a possible link between fast radio bursts and the missing pulsar problem. *MNRAS*, 450:L71–L75, June 2015.

[35] J. M. Cordes and I. Wasserman. Supergiant pulses from extragalactic neutron stars. *MNRAS*, 457:232–257, March 2016.

[36] R. M. Quimby, F. Yuan, C. Akerlof, and J. C. Wheeler. Rates of superluminous supernovae at z 0.2. *MNRAS*, 431:912–922, May 2013.

[37] D. Wanderman and T. Piran. The luminosity function and the rate of Swift's gamma-ray bursts. *MNRAS*, 406:1944–1958, August 2010.

[38] M. Nicholl, P. K. G. Williams, E. Berger, V. A. Villar, K. D. Alexander, T. Eftekhari, and B. D. Metzger. Empirical Constraints on the Origin of Fast Radio Bursts: Volumetric Rates and Host Galaxy Demographics as a Test of Millisecond Magnetar Connection. *ApJ*, 843:84, July 2017.

[39] W.-M. Gu, Y.-Z. Dong, T. Liu, R. Ma, and J. Wang. A Neutron Star-White Dwarf Binary Model for Repeating Fast Radio Burst 121102. *ApJL*, 823:L28, June 2016.

[40] G. E. Romero, M. V. del Valle, and F. L. Vieyro. Mechanism for fast radio bursts. *Phys. Rev. D*, 93(2):023001, January 2016.

[41] J. I. Katz. FRB as products of accretion disc funnels. *MNRAS*, 471:L92–L95, October 2017.

[42] N. Opperman and U.-L. Pen. On the non-Poissonian repetition pattern of FRB121102. *ArXiv e-prints*, May 2017.

[43] A. Spitkovsky. Time-dependent Force-free Pulsar Magnetospheres: Axisymmetric and Oblique Rotators. *ApJL*, 648:L51–L54, September 2006.

[44] J. I. Katz. Are fast radio bursts markers of dark core collapse? *MNRAS*, 469:L104–L107, July 2017.

[45] A. L. Piro. The Impact of a Supernova Remnant on Fast Radio Bursts. *ApJL*, 824:L32, June 2016.

[46] K. Murase, K. Kashiyama, and P. Mészáros. A burst in a wind bubble and the impact on baryonic ejecta: high-energy gamma-ray flashes and afterglows from fast radio bursts and pulsar-driven supernova remnants. *MNRAS*, 461:1498–1511, September 2016.

[47] J. I. Katz. Fast radio bursts – A brief review: Some questions, fewer answers. *Modern Physics Letters A*, 31:1630013, April 2016.

[48] U.-L. Pen and L. Connor. Local Circumnuclear Magnetar Solution to Extragalactic Fast Radio Bursts. *ApJ*, 807:179, July 2015.

[49] M. Lyutikov, L. Burzawa, and S. B. Popov. Fast radio bursts as giant pulses from young rapidly rotating pulsars. *MNRAS*, 462:941–950, October 2016.

[50] S. B. Popov and K. A. Postnov. Hyperflares of SGRs as an engine for millisecond extragalactic radio bursts. In H. A. Harutyunian, A. M. Mickaelian, and Y. Terzian, editors, *Evolution of Cosmic Objects through their Physical Activity*, pages 129–132, November 2010.

[51] J. I. Katz. How Soft Gamma Repeaters Might Make Fast Radio Bursts. *ApJ*, 826:226, August 2016.

[52] J. J. Geng and Y. F. Huang. Fast Radio Bursts: Collisions between Neutron Stars and Asteroids/Comets. *ApJ*, 809:24, August 2015.

[53] Z. G. Dai, J. S. Wang, X. F. Wu, and Y. F. Huang. Repeating Fast Radio Bursts from Highly Magnetized Pulsars Traveling through Asteroid Belts. *ApJ*, 829:27, September 2016.

[54] B. Zhang. A Cosmic Comb Model of Fast Radio Bursts. *ApJL*, 836:L32, February 2017.

[55] P. Kumar, W. Lu, and M. Bhattacharya. Fast radio burst source properties and curvature radiation model. *MNRAS*, 468:2726–2739, July 2017.

[56] Y. Lyubarsky. A model for fast extragalactic radio bursts. *MNRAS*, 442:L9–L13, July 2014.

[57] E. Waxman. On the Origin of Fast Radio Bursts (FRBs). *ApJ*, 842:34, June 2017.

[58] A. M. Beloborodov. A Flaring Magnetar in FRB 121102? *ApJL*, 843:L26, July 2017.

[59] J. A. Eilek and T. H. Hankins. Radio emission physics in the Crab pulsar. *Journal of Plasma Physics*, 82(3):635820302, June 2016.

[60] V. L. Ginzburg, V. V. Zheleznyakov, and V. V. Zaitsev. Coherent Mechanisms of Radio Emission and Magnetic Models of Pulsars. *Ap&SS*, 4:464–504, August 1969.

[61] G. Ghisellini and R. Svensson. The synchrotron and cyclo-synchrotron absorption cross-section. *MNRAS*, 252:313–318, October 1991.

[62] M. A. Ruderman and P. G. Sutherland. Theory of pulsars - Polar caps, sparks, and coherent microwave radiation. *ApJ*, 196:51–72, February 1975.

[63] G. A. Mourou, T. Tajima, and S. V. Bulanov. Optics in the relativistic regime. *Reviews of Modern Physics*, 78:309–371, April 2006.

[64] P. Goldreich and W. H. Julian. Pulsar Electrodynamics. *ApJ*, 157:869, August 1969.

[65] P. A. Sturrock. A Model of Pulsars. *ApJ*, 164:529, March 1971.

[66] J. Arons and E. T. Scharlemann. Pair formation above pulsar polar caps - Structure of the low altitude acceleration zone. *ApJ*, 231:854–879, August 1979.

[67] F. C. Michel. Theory of pulsar magnetospheres. *Reviews of Modern Physics*, 54:1–66, January 1982.

[68] C. Thompson, M. Lyutikov, and S. R. Kulkarni. Electrodynamics of Magnetars: Implications for the Persistent X-Ray Emission and Spin-down of the Soft Gamma Repeaters and Anomalous X-Ray Pulsars. *ApJ*, 574:332–355, July 2002.

[69] A. K. Harding and D. Lai. Physics of strongly magnetized neutron stars. *Reports on Progress in Physics*, 69:2631–2708, September 2006.

[70] J. A. Hibschman and J. Arons. Pair Multiplicities and Pulsar Death. *ApJ*, 554:624–635, June 2001.

[71] Z. Medin and D. Lai. Pair cascades in the magnetospheres of strongly magnetized neutron stars. *MNRAS*, 406:1379–1404, August 2010.

[72] T. H. Hankins and J. A. Eilek. Radio Emission Signatures in the Crab Pulsar. *ApJ*, 670:693–701, November 2007.

[73] A. M. Beloborodov and C. Thompson. Corona of Magnetars. *ApJ*, 657:967–993, March 2007.

[74] V. M. Kaspi and A. M. Beloborodov. Magnetars. *ARA&A*, 55:261–301, August 2017.

[75] M. Lyutikov. Magnetar giant flares and afterglows as relativistic magnetized explosions. *MNRAS*, 367:1594–1602, April 2006.

[76] M. Lyutikov, G. Machabeli, and R. Blandford. Cherenkov-Curvature Radiation and Pulsar Radio Emission Generation. *ApJ*, 512:804–826, February 1999.

[77] M. Lyutikov. Waves in a one-dimensional magnetized relativistic pair plasma. *MNRAS*, 293:447, February 1998.

[78] D. B. Melrose, M. E. Gedalin, M. P. Kennett, and C. S. Fletcher. Dispersion in an intrinsically relativistic, one-dimensional, strongly magnetized pair plasma. *Journal of Plasma Physics*, 62:233–248, August 1999.

[79] M. Gedalin, E. Gruman, and D. B. Melrose. Low-frequency waves in asymmetric magnetized relativistic pair plasma. *MNRAS*, 325:715–725, August 2001.

[80] J. J. Barnard and J. Arons. Wave propagation in pulsar magnetospheres - Refraction of rays in the open flux zone. *ApJ*, 302:138–162, March 1986.

[81] Q. Luo and D. B. Melrose. Curvature maser emission due to field line torsion in pulsar magnetospheres. *MNRAS*, 276:372–382, September 1995.

[82] G. Ghisellini. Synchrotron masers and fast radio bursts. *MNRAS*, 465:L30–L33, February 2017.

[83] J. D. Jackson. Classical Electrodynamics. *New York: Wiley*, 1975.

[84] G. B. Rybicki and A. P. Lightman. *Radiative processes in astrophysics*. 1979.

[85] R. D. Blandford. Amplification of radiation by relativistic particles in a strong magnetic field. *MNRAS*, 170:551–557, March 1975.

[86] Q. Luo and D. B. Melrose. Coherent curvature emission and radio pulsars. *MNRAS*, 258:616–620, October 1992.

[87] J. K. Daugherty and A. K. Harding. Electromagnetic cascades in pulsars. *ApJ*, 252:337–347, January 1982.

[88] A. N. Timokhin and A. K. Harding. On the Polar Cap Cascade Pair Multiplicity of Young Pulsars. *ApJ*, 810:144, September 2015.

[89] C. F. Kennel and F. V. Coroniti. Magnetohydrodynamic model of Crab nebula radiation. *ApJ*, 283:710–730, August 1984.

[90] A. M. Atoyan and F. A. Aharonian. On the mechanisms of gamma radiation in the Crab Nebula. *MNRAS*, 278:525–541, January 1996.

[91] O. C. de Jager, A. K. Harding, P. F. Michelson, H. I. Nel, P. L. Nolan, P. Sreekumar, and D. J. Thompson. Gamma-Ray Observations of the Crab Nebula: A Study of the Synchro-Compton Spectrum. *ApJ*, 457:253, January 1996.

[92] M. J. Rees and J. E. Gunn. The origin of the magnetic field and relativistic particles in the Crab Nebula. *MNRAS*, 167:1–12, April 1974.

[93] J. Arons. Pulsar Wind Nebulae as Cosmic Pevatrons: A Current Sheet's Tale. *Space Sci. Rev.*, 173:341–367, November 2012.

[94] A. M. Atoyan. Radio spectrum of the Crab nebula as an evidence for fast initial spin of its pulsar. *A&A*, 346:L49–L52, June 1999.

[95] S. S. Komissarov. Magnetic dissipation in the Crab nebula. *MNRAS*, 428:2459–2466, January 2013.

[96] S. J. Tanaka and K. Asano. On the Radio-emitting Particles of the Crab Nebula: Stochastic Acceleration Model. *ApJ*, 841:78, June 2017.

[97] P. A. Robinson. Nonlinear wave collapse and strong turbulence. *Reviews of Modern Physics*, 69:507–573, April 1997.

[98] P. Scholz, S. Bogdanov, J. W. T. Hessels, R. S. Lynch, L. G. Spitler, C. G. Bassa, G. C. Bower, S. Burke-Spolaor, B. J. Butler, S. Chatterjee, J. M. Cordes, K. Gourdji, V. M. Kaspi, C. J. Law, B. Marcote, M. A. McLaughlin, D. Michilli, Z. Paragi, S. M. Ransom, A. Seymour, S. P. Tendulkar, and R. S. Wharton. Simultaneous X-Ray, Gamma-Ray, and Radio Observations of the Repeating Fast Radio Burst FRB 121102. *ApJ*, 846:80, September 2017.

[99] D. Alsop and J. Arons. Relativistic magnetosonic solitons with reflected particles in electron-positron plasmas. *Physics of Fluids*, 31:839–847, April 1988.

[100] Y. A. Gallant, M. Hoshino, A. B. Langdon, J. Arons, and C. E. Max. Relativistic, perpendicular shocks in electron-positron plasmas. *ApJ*, 391:73–101, May 1992.

[101] M. Hoshino, J. Arons, Y. A. Gallant, and A. B. Langdon. Relativistic magnetosonic shock waves in synchrotron sources - Shock structure and nonthermal acceleration of positrons. *ApJ*, 390:454–479, May 1992.

[102] A. Sagiv and E. Waxman. Collective Processes in Relativistic Plasma and Their Implications for Gamma-Ray Burst Afterglows. *ApJ*, 574:861–872, August 2002.

[103] V. Gajjar, A. P. V. Siemion, D. H. E. MacMahon, S. Croft, G. Hellbourg, H. Isaacson, J. E. Enriquez, D. C. Price, M. Lebofsky, D. DeBoer, D. Werthimer, J. Hickish, C. Brinkman, S. Chatterjee, and S. Ransom. FRB 121102: Detection at 4 - 8 GHz band with Breakthrough Listen backend at Green Bank. *The Astronomer's Telegram*, 10675, August 2017.

[104] A. Panaitescu and P. Kumar. Fundamental Physical Parameters of Collimated Gamma-Ray Burst Afterglows. *ApJL*, 560:L49–L53, October 2001.

[105] L. Sironi, U. Keshet, and M. Lemoine. Relativistic Shocks: Particle Acceleration and Magnetization. *Space Sci. Rev.*, 191:519–544, October 2015.

[106] A. B. Langdon, J. Arons, and C. E. Max. Structure of relativistic magnetosonic shocks in electron-positron plasmas. *Physical Review Letters*, 61:779–782, August 1988.

[107] L. Sironi and A. Spitkovsky. Particle Acceleration in Relativistic Magnetized Collisionless Pair Shocks: Dependence of Shock Acceleration on Magnetic Obliquity. *ApJ*, 698:1523–1549, June 2009.

[108] M. Iwamoto, T. Amano, M. Hoshino, and Y. Matsumoto. Persistence of Precursor Waves in Two-dimensional Relativistic Shocks. *ApJ*, 840:52, May 2017.

[109] D. B. Melrose. Maser pulse emission mechanisms. In W. Sieber and R. Wielebinski, editors, *Pulsars: 13 Years of Research on Neutron Stars*, volume 95 of *IAU Symposium*, pages 133–139, 1981.

[110] A. F. Cheng and M. A. Ruderman. Bunching mechanism for coherent curvature radiation in pulsar magnetospheres. *ApJ*, 212:800–806, March 1977.

[111] V. V. Usov. On two-stream instability in pulsar magnetospheres. *ApJ*, 320:333–335, September 1987.

[112] Y. E. Lyubarskii. Possible mechanism of pulsar radio emission. *A&A*, 265:L33–L36, November 1992.

[113] G. Benford and R. Buschauer. Coherent pulsar radio radiation by antenna mechanisms - General theory. *MNRAS*, 179:189–207, April 1977.

[114] D. B. Melrose and M. E. Gedalin. Relativistic Plasma Emission and Pulsar Radio Emission: A Critique. *ApJ*, 521:351–361, August 1999.

[115] V. I. Karpman, C. A. Norman, D. Ter Haar, and V. N. Tsytovich. Relativistic solitons and pulsars. *Physica Scripta*, 11:271–274, May 1975.

[116] P. K. Shukla, N. N. Rao, M. Y. Yu, and N. L. Tsintsadze. Relativistic nonlinear effects in plasmas. *Physics Reports*, 138:1–149, May 1986.

[117] E. Asseo, G. Pelletier, and H. Sol. A non-linear radio pulsar emission mechanism. *MNRAS*, 247:529–548, December 1990.

[118] G. I. Melikidze, J. A. Gil, and A. D. Pataraya. The Spark-associated Soliton Model for Pulsar Radio Emission. *ApJ*, 544:1081–1096, December 2000.

[119] P. Goldreich and D. A. Keeley. Coherent Synchrotron Radiation. *ApJ*, 170:463, December 1971.

[120] D. B. Melrose. Amplified linear acceleration emission applied to pulsars. *ApJ*, 225:557–573, October 1978.

[121] M. Caleb, C. Flynn, M. Bailes, E. D. Barr, T. Bateman, S. Bhandari, D. Campbell-Wilson, W. Farah, A. J. Green, R. W. Hunstead, A. Jameson, F. Jankowski, E. F. Keane, A. Parthasarathy, V. Ravi, P. A. Rosado, W. van Straten, and V. Venkatraman Krishnan. The first interferometric detections of fast radio bursts. *MNRAS*, 468:3746–3756, July 2017.

[122] Y. Maan and J. van Leeuwen. Real-time searches for fast transients with Apertif and LOFAR. *ArXiv e-prints*, September 2017.

[123] C. Ng, K. Vanderlinde, A. Paradise, P. Klages, K. Masui, K. Smith, K. Bandura, P. J. Boyle, M. Dobbs, V. Kaspi, A. Renard, J. R. Shaw, I. Stairs, and I. Tretyakov. CHIME FRB: An application of FFT beamforming for a radio telescope. *ArXiv e-prints*, February 2017.

[124] T. M. Colegate and N. Clarke. Searching for Fast Radio Transients with SKA Phase 1. *PASA*, 28:299–316, November 2011.

[125] K. W. Bannister, R. M. Shannon, J.-P. Macquart, C. Flynn, P. G. Edwards, M. O'Neill, S. Osłowski, M. Bailes, B. Zackay, N. Clarke, L. R. D'Addario, R. Dodson, P. J. Hall, A. Jameson, D. Jones, R. Navarro, J. T. Trinh, J. Allison, C. S. Anderson, M. Bell, A. P. Chippendale, J. D. Collier, G. Heald, I. Heywood, A. W. Hotan, K. Lee-Waddell, J. P. Madrid, J. Marvil, D. McConnell, A. Popping, M. A. Voronkov, M. T. Whiting, G. R. Allen, D. C.-J. Bock, D. P. Brodrick, F. Cooray, D. R. DeBoer, P. J. Diamond, R. Ekers, R. G. Gough, G. A. Hampson, L. Harvey-Smith, S. G. Hay, D. B. Hayman, C. A. Jackson, S. Johnston, B. S. Koribalski, N. M. McClure-Griffiths, P. Mirtschin, A. Ng, R. P. Norris, S. E. Pearce, C. J. Phillips, D. N. Roxby, E. R. Troup, and T. Westmeier. The Detection of an Extremely Bright Fast Radio Burst in a Phased Array Feed Survey. *ApJL*, 841:L12, May 2017.

[126] V. S. Beskin, A. V. Gurevich, and I. N. Istomin. Theory of the radio emission of pulsars. *Ap&SS*, 146:205–281, July 1988.

[127] R. D. Blandford and C. F. McKee. Fluid dynamics of relativistic blast waves. *Physics of Fluids*, 19:1130–1138, August 1976.

[128] J. M. Cordes, N. D. R. Bhat, T. H. Hankins, M. A. McLaughlin, and J. Kern. The Brightest Pulses in the Universe: Multifrequency Observations of the Crab Pulsar's Giant Pulses. *ApJ*, 612:375–388, September 2004.

[129] B. B. Godfrey, W. R. Shanahan, and L. E. Thode. Linear theory of a cold relativistic beam propagating along an external magnetic field. *Physics of Fluids*, 18:346–355, March 1975.

[130] L. K. Hardy, V. S. Dhillon, L. G. Spitler, S. P. Littlefair, R. P. Ashley, A. De Cia, M. J. Green, P. Jaroenjittichai, E. F. Keane, P. Kerry, M. Kramer, D. Malesani, T. R. Marsh, S. G. Parsons, A. Possenti, S. Rattanasoon, and D. I. Sahman. A search for optical bursts from the repeating fast radio burst FRB 121102. *MNRAS*, 472:2800–2807, December 2017.

[131] M. Lyutikov. On the nature of eclipses in binary pulsar J0737-3039. *MNRAS*, 353:1095–1106, October 2004.

[132] M. Lyutikov and C. Thompson. Magnetospheric Eclipses in the Double Pulsar System PSR J0737-3039. *ApJ*, 634:1223–1241, December 2005.

[133] V. Ravi, R. M. Shannon, M. Bailes, K. Bannister, S. Bhandari, N. D. R. Bhat, S. Burke-Spolaor, M. Caleb, C. Flynn, A. Jameson, S. Johnston,

E. F. Keane, M. Kerr, C. Tiburzi, A. V. Tuntsov, and H. K. Vedantham. The magnetic field and turbulence of the cosmic web measured using a brilliant fast radio burst. *Science*, 354:1249–1252, December 2016.

[134] S. P. Tendulkar, V. M. Kaspi, and C. Patel. Radio Nondetection of the SGR 1806-20 Giant Flare and Implications for Fast Radio Bursts. *ApJ*, 827:59, August 2016.

[135] D. B. Wilson. Induced compton scattering in radiative transfer. *MNRAS*, 200:881–906, September 1982.

Vita

Wenbin Lu was born in Chongqing, China in 1990. He received the Bachelor of Science degree in Physics from Yuanpei College, Peking University (PKU) in the spring of 2013. The Yuanpei Program, named after PKU's most revered president, Mr. Yuanpei Cai, allows students to freely choose their field of study. Wenbin got interested in astrophysics from a casual discussion on cosmic rays with Prof. Zhuo Li, who later became his undergraduate advisor. Wenbin enrolled in the graduate program in the Department of Astronomy at the University of Texas at Austin in the fall of 2013. Since that time, under the supervision of Prof. Pawan Kumar, he has been trying to understand the key physics behind various high-energy transient phenomena, including tidal disruption events, fast radio bursts, gamma-ray bursts, and mergers of double neutron stars/black holes.

In the summer of 2018, Wenbin will take up the Burke Prize Fellowship as a postdoctoral fellow in the Astronomy Department at the California Institute of Technology.

This dissertation was typeset with LaTeXby the author.